

Structural Study of Hydra Nematocyst Wall Assembly

Inauguraldissertation

zur

Erlangung der Würde eines Doktors der Philosophie

vorgelegt

der Philosophisch-Naturwissenschaftlichen Fakultät

der Universität Basel

von

Elena Pokidysheva

aus Russland

Basel, Switzerland 2004

**Genehmigt von der Philosophisch-Naturwissenschaftlichen Fakultät auf Antrag von
Prof. Dr. Jürgen Engel und Prof. Thomas Kiefhaber**

Basel, den 06.07.2004

Prof. Dr. Marcel Tanner

Dekan .

Contents:

<u>Preface</u>	1
<u>Summary</u>	4
<u>General Introduction</u>	
Part 1.	
Nematocysts of Cnidaria. Morphogenesis of nematocyst capsule.	7
<i>Nematocysts Morphology</i>	8
<i>Nematocyst ultrafast exocytosis</i>	10
<i>Nematocyst morphogenesis</i>	12
<i>References</i>	16
Part 2.	
Domain organization of NOWA and minicollagen.	
Structural variety of the cysteine rich peptides.	18
<i>Domain organization of NOWA and minicollagen</i>	19
<i>Disulfide dependent protein folding pathways</i>	21
<i>Cystine knot containing growth factors family</i>	22
<i>Inhibitor cystine knot family or “Knottins”</i>	23
<i>Cystine stabilized α-helix structural motif</i>	27
<i>References</i>	29
<u>Chapter 1</u>	
Self-assembly of NOWA.	
Calcium dependent aggregation of assembled NOWA globules.	31
<i>Introduction</i>	32
<i>Materials and Methods</i>	34
<i>Results and Discussion</i>	36
<i>References</i>	42
<u>Chapter 2</u>	
NOWA membrane binding.	43
<i>Abstract</i>	44

<i>Introduction</i>	45
<i>Materials and Methods</i>	47
<i>Results and Discussion</i>	54
<i>References</i>	63

Chapter 3

The structure of the Cys-rich terminal domain of Hydra minicollagen, which is involved in disulfide networks of the nematocyst wall 64

<i>Abstract</i>	65
<i>Introduction</i>	66
<i>Experimental procedures</i>	69
<i>Results</i>	72
<i>Discussion</i>	76
<i>Acknowledgements</i>	80
<i>References</i>	81

Chapter 4

The structure of the first repeat of NOWA octad cysteine-rich domain.

Fluorescence study of oxidative refolding 84

<i>Abstract</i>	85
<i>Introduction</i>	86
<i>Materials and Methods</i>	89
<i>Results and Discussion</i>	92
<i>References</i>	98

Acknowledgements 99

Curriculum Vitae 100

Publications 102

Preface

The scope of this thesis is a structural investigation of the Hydra nematocyst capsule wall on the molecular level along with few steps forward in order to understand its assembly mechanism. The nematocyst is a unique organelle of the nematocytes, a special cell type of all *Cnidarians*. The nematocyst serves the functions of prey capture and defense in Hydra, jellyfish, corals, and other *Cnidarians*. It exhibits one of the fastest known cellular processes by its exocytosis (1). The nematocyst was studied in many different ways during the past four decades (1-15). The complexity of functions, assembly, and structure makes it a very intriguing object for zoologists, cell biologists and structural biologists. The capsule wall of this organelle persists very high osmotic pressures of about 150 bars gained by poly- γ -glutamic acid (3), being at the same time very elastic as it changes its volume considerably during discharge. This poses the problem of how a structure of sufficient stability may be assembled.

There were several steps already made in order to reveal the structure of the nematocyst wall. The aims of the present thesis were to extend the existing knowledge and recognize the structural basis of the nematocyst wall on the molecular level. Two proteins have been identified as major components of the wall: minicollagens (16) and NOWA (13). These proteins were found to compose recently identified structural building block of the nematocyst capsule wall termed “capsulomer” (17). Chapter 1 of the thesis is dedicated to the investigation of recombinant NOWA assembly and clustering that provides few insights into certain events of nematocyst morphogenesis. A permanent player of the nematocyst development and functioning is a membrane of Golgi vesicle. Previously made in vivo observations indicating close relations of the nematocyst and membrane (18,19) were accomplished by the in vitro studies of NOWA – membrane interaction in this thesis (see “Chapter 2”). Minicollagen and NOWA exhibit special domain organization sharing the Cys-rich domains which are meant to be used for intermolecular disulfide reshuffling. The minicollagens found in nematocysts are the shortest collagens currently known. The presence of the cysteine rich domains at both sides of the collagen molecule implies the ability to undergo the disulfide isomerization in order to accomplish regular collagen network elasticity by the very high strength. From the other hand NOWA, that has eight times repeated cysteine rich domain with the cysteine pattern identical to that in mini-collagen, has to be fitted to the collagen

network. Three-dimensional structure of this particular domain, which is presumably the most important feature of the nematocyst wall assembly, provides an insight into a mechanism of this assembly and reveals an interesting example of unusual cystine stabilized fold (see Chapter 3 and Chapter 4).

The overall organization of the nematocyst capsule wall serves us with a general model of the structures of very high tensile strength and provides with an excellent naturally designed tool for advanced materials elaboration.

References.

1. Holstein, T., and Tardent, P. (1984) *Science* **223**, 830-833
2. Wilby, O. K. (1976) *Nature* **262**, 387-388
3. Weber, J. (1990) *J Biol Chem* **265**, 9664-9669
4. Wang, W., Omori, M., Hayashibara, T., Shimoike, K., Hatta, M., Sugiyama, T., and Fujisawa, T. (1995) *Gene* **152**, 195-200
5. Phelan, M. A., and Blanquet, R. S. (1985) *Comp Biochem Physiol B* **81**, 661-666
6. Ozbek, S., Pertz, O., Schwager, M., Lustig, A., Holstein, T., and Engel, J. (2002) *J Biol Chem* **277**, 49200-49204
7. Ozbek, S., Engel, U., and Engel, J. (2002) *J Struct Biol* **137**, 11-14
8. Nagai, H., Oshiro, N., Takuwa-Kuroda, K., Iwanaga, S., Nozaki, M., and Nakajima, T. (2002) *Biosci Biotechnol Biochem* **66**, 2621-2625
9. Lubbock, R., Gupta, B. L., and Hall, T. A. (1981) *Proc Natl Acad Sci U S A* **78**, 3624-3628
10. Lenhoff, H. M., and Bovaird, J. (1961) *Dev Biol* **3**, 227-240
11. Koch, A. W., Holstein, T. W., Mala, C., Kurz, E., Engel, J., and David, C. N. (1998) *J Cell Sci* **111** (Pt 11), 1545-1554
12. Goodwin, M. H., and Telford, M. (1971) *Biol Bull* **140**, 389-399
13. Engel, U., Ozbek, S., Streitwolf-Engel, R., Petri, B., Lottspeich, F., Holstein, T. W., Ozbek, S., and Engel, R. (2002) *J Cell Sci* **115**, 3923-3934
14. Endean, R. (1987) *Toxicon* **25**, 483-492
15. Anderluh, G., Podlesek, Z., and Macek, P. (2000) *Biochim Biophys Acta* **1476**, 372-376
16. Kurz, E. M., Holstein, T. W., Petri, B. M., Engel, J., and David, C. N. (1991) *J Cell Biol* **115**, 1159-1169
17. Ozbek, S., Pokidysheva, E., Schwager, M., Schulthess, T., Tariq, N., Barth, D., Milbradt, A., Moroder, L., Engel, J., and Holstein, T. (2004) **submitted**
18. Holstein, T. (1981) *J. Ultrastruct. Res.* **75**, 276-290
19. Golz, R. (1994) *J. Morphol* **222**, 49-59

Summary

The present thesis includes four parts. All of them are devoted to the investigation of the nematocyst capsule wall structure and assembly. The nematocyst wall is unique in its resistance to high pressures accomplished by a pronounced elasticity. The capsule develops inside a Golgi vesicle using the vesicular membrane as a substrate. Recent studies demonstrated that the mature nematocyst capsule wall is a compact structure of several closely arranged layers of globular building units termed “capsulomers”. These globules have slightly heterogeneous size distribution of 20 nm average diameter. Capsulomers were shown to be heterooligomers of NOWA and minicollagens which are crosslinked by disulfide bonds. In addition capsulomer precursors composed of NOWA alone were identified at the certain step of the nematocyst capsule development.

Minicollagens and NOWA share similar cysteine rich domain that is presumably responsible for the disulfide dependent capsulomer formation and further covalent cross-linking of the capsulomers. However exact mechanism of the highly ordered intra- to inter- disulfide isomerization leading to the formation of the capsule wall remains unclear. The structure of the common cysteine rich domain was not known also.

(Chapter 1) In order to investigate whether NOWA alone assembles to capsulomer-like structures the full-length protein was expressed in mammalian cells, purified and investigated by various techniques. Mammalian expression system was chosen to provide post-translational modifications of the protein and correct disulfide connectivity. Monomeric and oligomeric fractions of the recombinantly expressed protein were isolated and studied by transmission electron microscopy. NOWA monomers revealed compact globular structures. Oligomeric fraction of protein was found to be self-assembled capsulomer-like globules of the average diameter similar to that of native wall capsulomers. The capsulomer-like structures have melted upon reduction. Similar experiments were performed with the recombinantly expressed NOWA fragment containing eight Cys-rich domains (ONCRD). This construct was shown to assemble into ring-like structures rather than spherical particles. Small ring-like structures were further associated in chains of different curvature. Thus assembly of the recombinant NOWA to capsulomer-like structures was concluded to be a feature of its cysteine rich domain although other protein domains needed to provide

a control of disulfide isomerization. Furthermore capsulomer-like structures exhibited calcium dependent clusterization. This property of the recombinant protein was discussed to explain natural behavior of the capsulomer precursors during nematocyst development.

(Chapter 2) Nematocyst wall maintains close contact with the membrane of the Golgi vesicle during capsule development as well as in mature form. To investigate whether NOWA is able to interact with the membrane surfaces recombinantly expressed protein was studied by several techniques. NOWA binding to the model lipid monolayers and bilayers was directly visualized by electron microscopy. Surface plasmon resonance kinetic studies revealed high affinity of the capsulomer-like structures to the negatively charged surface of lipid bilayer ($K_D \sim 100$ nM). Calcium induced clusters of the NOWA capsulomers exhibited ten times lower membrane affinity. This provides an explanation for *in vivo* dissociation of the capsulomer precursor clusters. Two parts of NOWA involved in the membrane binding were identified: C-type lectin domain and basic C-terminal sequence. The cysteine rich domain of the protein had shown no membrane affinity.

(Chapter 3) The minicollagen and NOWA cysteine-rich domains (MCRDs and NCRDs respectively) are believed to function in a switch of the disulfide connectivity from intra- to intermolecular bonds during maturation of the capsule wall. The N- and the C-terminal MCRDs as well as 8 cysteine rich domains of NOWA are homologous and share the cysteine pattern CXXX(X₃)CXXXCXPXCXXXCC. The peptide comprising the last 24 residues of the minicollagen-1 was produced synthetically and successfully refolded by oxidation under low protein concentration. The solution structure of the C-terminal MCRD was determined by ¹H NMR technique. Disulfide connections Cys2-Cys18, Cys6-Cys14, Cys10-Cys19 were found that constrained the structure into a compact new fold.

(Chapter 4) The solution structure of the first cysteine rich domain of Hydra nematocyst wall protein NOWA (NCRD1) has been determined using homonuclear and heteronuclear NMR techniques at natural abundance. The elucidated peptide composing 25 amino acids was produced synthetically and oxidized. The NCRD1 has revealed the disulfide pattern identical to that of the MCRD. Moreover NOWA domain exhibited overall structure topology similar to the topology of minicollagen domain structure. Despite the differences in the N-terminal structures two peptides

revealed the same structural fold defined by conserved cysteines connection and β -turns.

The MCRD and NCRD1 both have single tyrosine in their sequences. Tyrosine fluorescence quenching by disulfide bonds was observed in both peptides. The oxidative refolding of MCRD and NCRD1 has been monitored by tyrosine fluorescence. Resulting kinetics were fitted with mono-exponentials suggesting a simple kinetic mechanism that arises from the quenching by only one particular disulfide bond in each case. The Cys2-Cys18 bond in case of MCRD and Cys6-Cys14 in case of NCRD1 are discussed to be responsible for fluorescence quenching effect. Oxidative refolding rate constants related to the formation of indicated bonds were determined.

General Introduction

Part 1

Nematocysts of Cnidarians

Morphogenesis of the nematocyst capsule

General Introduction

Nematocyst Morphology

Nematocysts are one of the cnidae (2-4) which are highly specialized, secretory, subcellular organelles serving as offensive and defensive structures (5) typical of cnidarians. Remarkable in their structural and functional complexity, nematocysts serve as a fascinating model for different research directions. Cnidae have been distinguished into three broad classes: nematocysts, spirocysts and ptychocysts (6). Spirocysts and ptychocysts are found only in anthozoans (7-11). Nematocysts are found in hydroids, jellyfish, sea anemones, and corals. The presented thesis is focused on the nematocysts of Hydra. Mature nematocysts are primarily localized in tentacles but precursor forms are found mounted in ectodermal epithelial cells throughout the animal. A large number of different morphological types of nematocyst capsules are found within the Cnidaria. Individual species, however, have only a small number of different nematocyst types. The fresh water polyp *Hydra vulgaris* has four morphological types of nematocysts: stenoteles, desmonemes, atrichous and holotrichous isorhizas. Morphological differences among these types are easily noticed from the figures 1, 2, and 3.

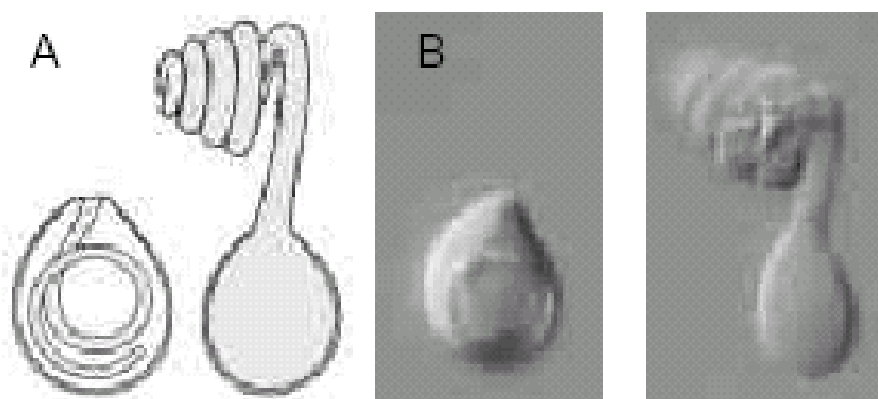


Figure 1.

Desmonemes of Hydra. Schematic representation (A) and light microscopy pictures of the intact and discharged capsule (B).

Figure 2.

Stenotele of Hydra.
Electron microscopy picture of the intact capsule (A), bar is 5 μ m.

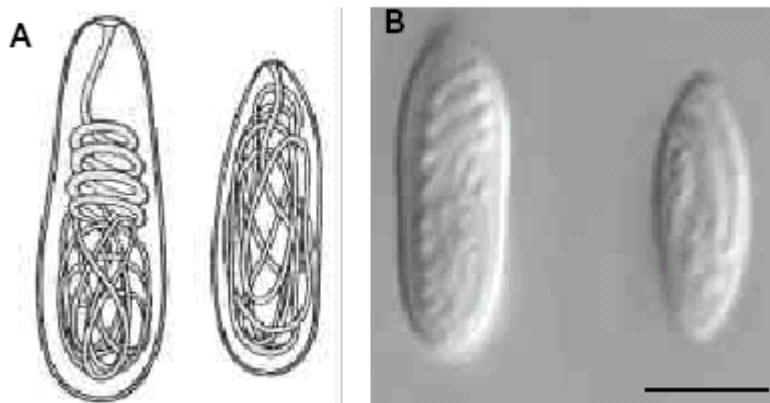
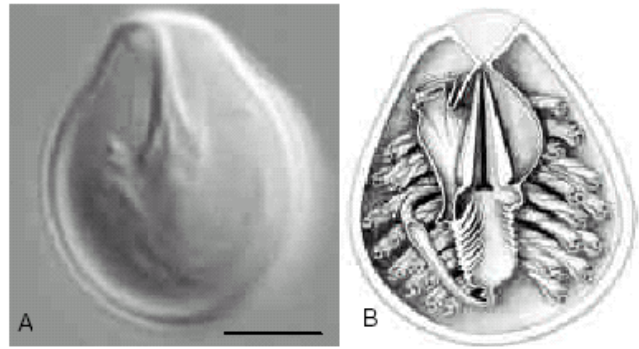


Figure 3.

Atrichous and holotrichous isorhizas. Schematic representation (A) and electron microscopy picture of the intact capsule (B).

Figures 1, 2 are adapted from (5). Fig.3 is from (12).

This study is focused on the structural assembly of the Hydra nematocyst capsule. All capsule-related experiments described below were performed preferentially with the stenoteles of *Hydra vulgaris*. Nematocyst capsules are formed in clusters of differentiating nematocytes (13) in the body column of Hydra polyps. Once capsule differentiation is completed these clusters break up into single cells that migrate to tentacles and become mounted in specialized tentacle epithelial cells, called battery cells (Fig.4). One nematocyst capsule is formed per cell in a differentiating nematocyte (14).

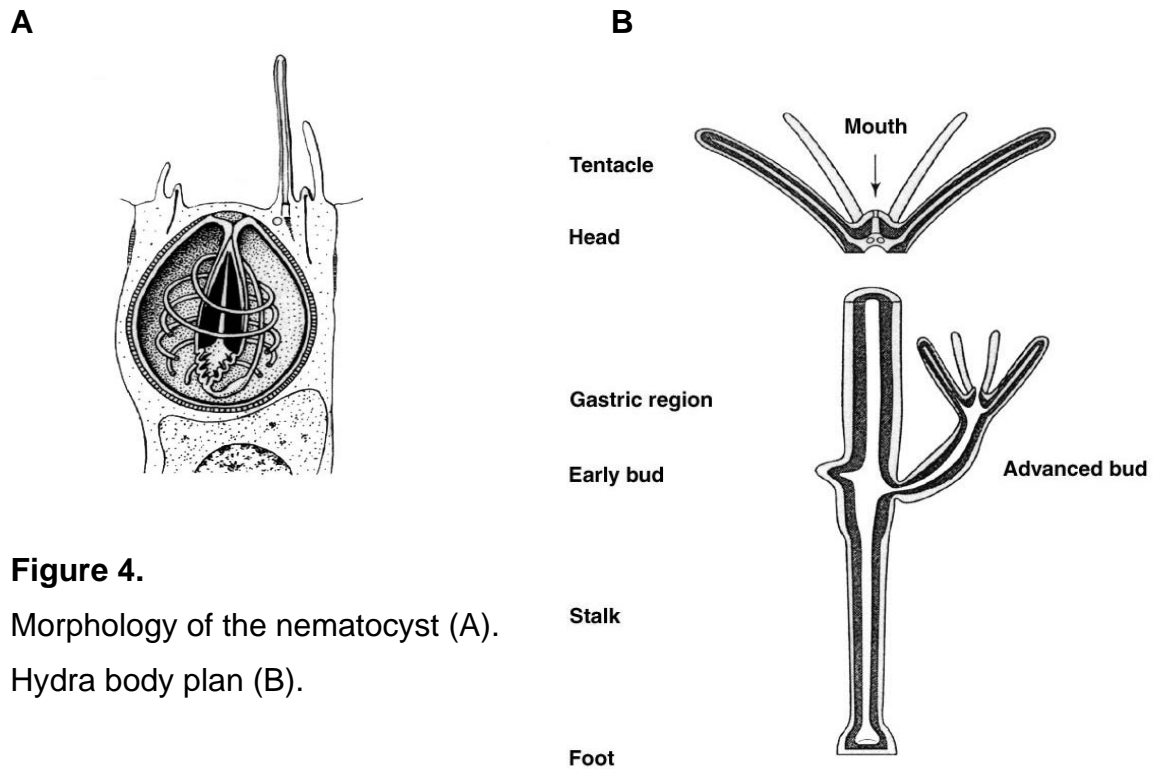


Figure 4.
Morphology of the nematocyst (A).
Hydra body plan (B).

Extensive EM investigations have documented the morphology and differentiation of capsules (15). Capsules have a strong outer wall surrounding an inverted tubule.

Nematocyst ultrafast exocytosis.

It has been realized for over 10 years ago that a high internal osmotic pressure develops inside the nematocyst capsule by the synthesis of poly- γ -glutamate at the late stages of capsule development (1, 16). The maximum pressure reaches 150 atmospheres which is unusually high for biological systems. The ability of the capsule to withstand such pressure immediately poses the intriguing question for its molecular composition and assembly. The present thesis work is devoted to this question.

The time course of the rapid process of nematocyst discharge has been visualized in *Hydra vulgaris* by *Holstein and Tardent* in 1984 (17). Discharge was triggered by an extracellular electrical stimulus. Using high-speed microcinematography, an initial increase of the stenotele volume (phase a) can be demonstrated during the interval between the onset of the electrical stimulus and the opening of the operculum. After about 100 μ s the capsule's cover is

opened and the stylets are ejected in less than 10 μs (phase b). Discharge is then arrested for approximately 150 μs (phase c), presumably in order to allow withdrawal of the stylets from the opening created in the prey's integument. Then the long (0.5 mm) and slender (0.8 μm) tubule evaginates at a velocity of about 0.3 m/s into the prey's body. Figure 5 shows a schematic representation of the events during nematocyst exocytosis as a function of time.

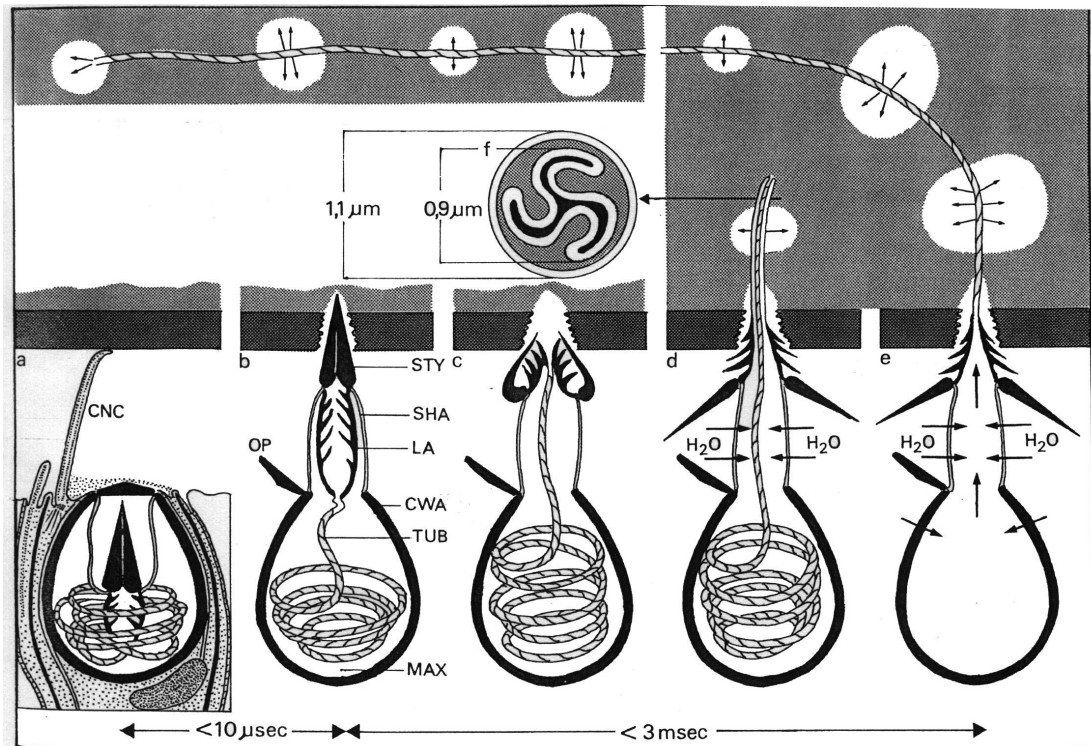


Figure 5

Schematic representation of the stenotele nematocyst discharge as a function of time. Five discrete phases are indicated: a, b, c, d and e. In phase "a" the nematocyst capsule is intact but dramatic decrease of body volume is observed. In phase "b" operculum opens (OP) and stylet (STY) with shaft (SHA) and lamellae (LA) is ejected. The tubule (TUB) is still inside the capsule. CWA indicates capsule wall. Phase "c" is a retention phase when capsule volume slowly decreases. In phase "d" stylets open and discharge observed. Phase "e" represents continuous discharge when tubule is completely exerted. Time scale is indicated on the low part of the figure. CNC

The figure is adapted from Tardent et.al.(18).

Nematocyst morphogenesis

The nematocyst is produced during a highly ordered secretion and assembly process of proteins inside a giant post-Golgi vesicle of the nematocytes (19). Nematocyst morphogenesis can be subdivided into five stages (15):

1. An early growth phase during which the capsule primordium forms and grows by addition of new vesicles to the vesicle harboring the capsule.
2. A late growth phase during which a tubule forms outside the capsule by addition of more vesicles; capsule and tubule wall form a continuous structure.
3. Invagination of the long external tubule into the capsule.
4. An early maturation phase leading to the formation of spines by condensation of the protein spinalin (20) inside the invaginated tubule.
5. A final late maturation step during which poly- γ -glutamate is synthesized in the matrix of the capsule (1). At this point the wall structure 'hardens' (i.e. is no longer deformed when tissue is fixed) and the capsule swells to its final size.

Two proteins have been identified as major constituents of the nematocyst capsule wall: NOWA (Nematocyst Outer Wall Antigen) (21) and mini-collagens (22). Mini-collagens are a family of unusually short collagens (22). They comprise a central collagen triple helix with 12-16 Gly-X-Y repeats flanked by polyproline stretches and terminal cysteine-rich domains (MCRDs). Minicollagens are trimeric molecules that are expressed as soluble precursors, which during nematocyst maturation polymerize probably by a switch in the disulfide linkage from intra- to intermolecular connections (19). This process is accompanied by a loss of minicollagen antibody reactivity in the head and tentacles regions of Hydra in mature nematocysts (19).

NOWA is a 90 kDa glycoprotein that has been described to be associated with the globular structure of the nematocyst outer surface (21). Interestingly, the molecular architecture of NOWA comprises a C-terminal octad repeat of a cysteine-rich domain homologous to that of minicollagen, suggesting a disulfide-dependent heteroassembly of minicollagens and NOWA. These two proteins are

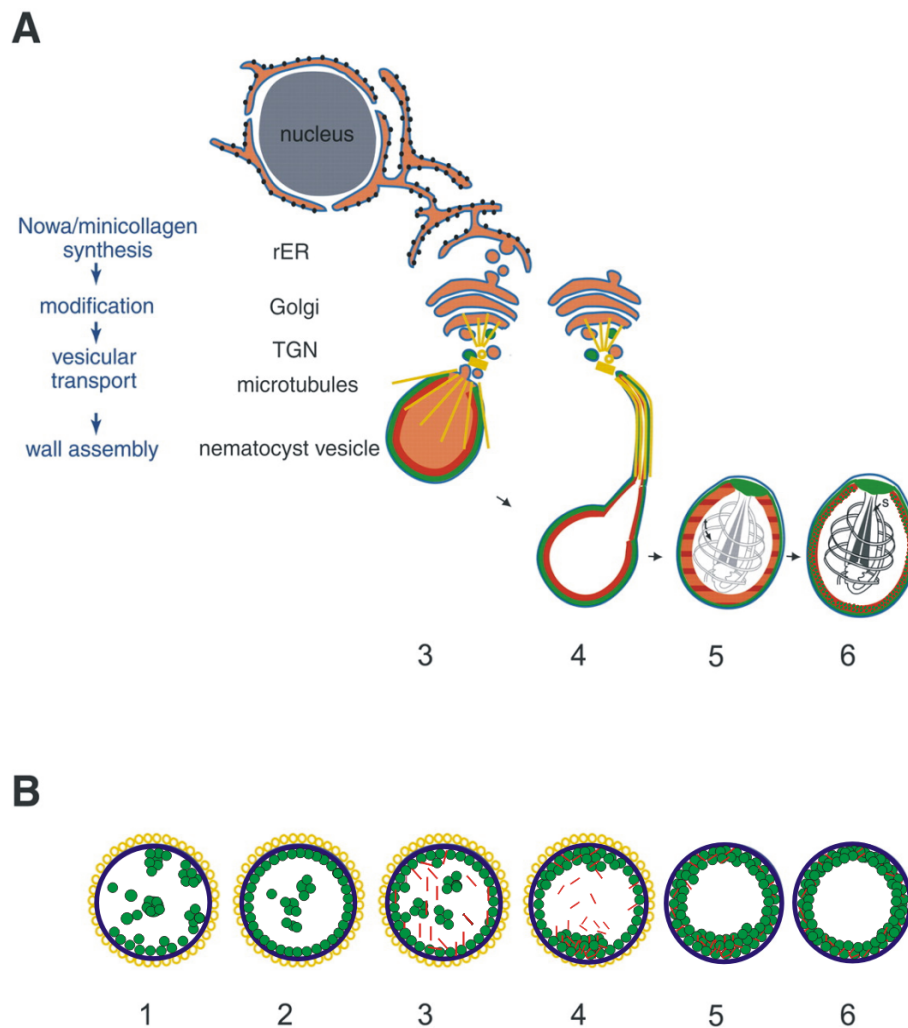


Figure 6

Scheme is originally adapted from Engel et.al (23) and has been modified according to the recent findings. Formation of the nematocyst capsule wall from Nowa (green) and minicollagen (red). (A) Protein sorting and transport as detected by minicollagen antibody and mAb H22, Ab MCCR; Ab CTLD and Ab. Minicollagen and Nowa synthesized in the ER are transported in separate vesicles to the nematocyst vesicle. Nowa is detected by three antibodies: mAb H22 (against glycosylation), Ab CTLD and Ab MCCR. MTs (yellow) are organized in a scaffold around the growing part of the nematocyst, the MTOC is localized between the Golgi apparatus and the growing apex of the nematocyst. Minicollagen first accumulates in the capsule matrix and is then sorted to the wall to form the wall together with NOWA (3). By further transport of protein-filled vesicles, the outer tubule forms (4). It is subsequently invaginated into the cyst, and spines (s) are formed in the tubule lumen (5). Finally, minicollagen crosslinkage leads to a compaction of the wall structure (6). (B) Model of nematocyst patterning by the MT cytoskeleton. The growing part of the nematocyst vesicle is shown in a schematic cross-section. MTs form a cage around the vesicle and determine its shape (1). The initial stage includes binding of NOWA to the membrane. At the same time NOWA accumulates inside the capsule (2). Membrane bound NOWA is used as template for minicollagen assembly. Soluble minicollagen trimers aggregate on the outer wall to continue formation of the wall (3-5) via intermolecular disulfide crosslinking. Finally Nowa and minicollagen are crosslinked by disulfide bonds to stabilize the structure (6).

expressed at the early stages of the nematocyst development. The general scheme of the nematocyst morphogenesis includes five described stages and detailed view of the wall assembly from NOWA and minicollagen is represented in Fig.6.

It has been described previously that the nematocyst capsule wall is composed of two distinct layers. NOWA was associated with the outer layer when mini-collagen was thought to compose a dense and elastic “inner” wall. These observations have been made by Holstein *et al.* using atomic force microscopy (17). Immunofluorescence analysis of the developing nematocyst capsule is consistent with a two-layer structure although immunofluorescent staining has only limited resolution (19). The immunostaining analysis has been done using the antibodies raised against glycosylated NOWA and the one against recombinantly expressed mini-collagen-1. The data clearly demonstrated a two layered structure of the wall. However, recent ultrastructural investigation of the ruptured capsule using scanning electron microscopy (23) suggests a uniform composition of the wall with a density gradient decreasing from the inner to the outer side. To visualize the fine structure of the nematocyst wall in profile isolated non-discharged capsules were sonicated to induce wall ruptures. Scanning electron microscopy (SEM) was then performed with carbon or platinum-covered samples fixed on glass covers. Most of the nematocysts were still intact after a short (2 minutes) ultrasound treatment but several showed a rupture predominantly perpendicular to the length axis of the capsule body where the tubule had then discharged without eversion. Figure 7A shows a total view of a stenotele displaying a typical rupture. The operculum at its narrow end, which opens to release the tubule when nematocyst discharge is triggered, is still closed and the stylet apparatus used for puncturing the cuticle of a prey organism is folded back inside the capsule body and wrapped by the base of the tubule. A high resolution imaging of the wall surfaces by platinum covering revealed a composition of the wall profile consisting of several layers (6-7) of the globular building units termed capsulomers (Fig. 7B). The thickness of the wall is about 150 nm and in contrast to the two-layer model a homogeneous globular appearance throughout the whole cross-section was observed. The two-layer appearance observed earlier can be explained by the density gradient from the outer to the inner side of the wall. Immunofluorescence studies (24) performed

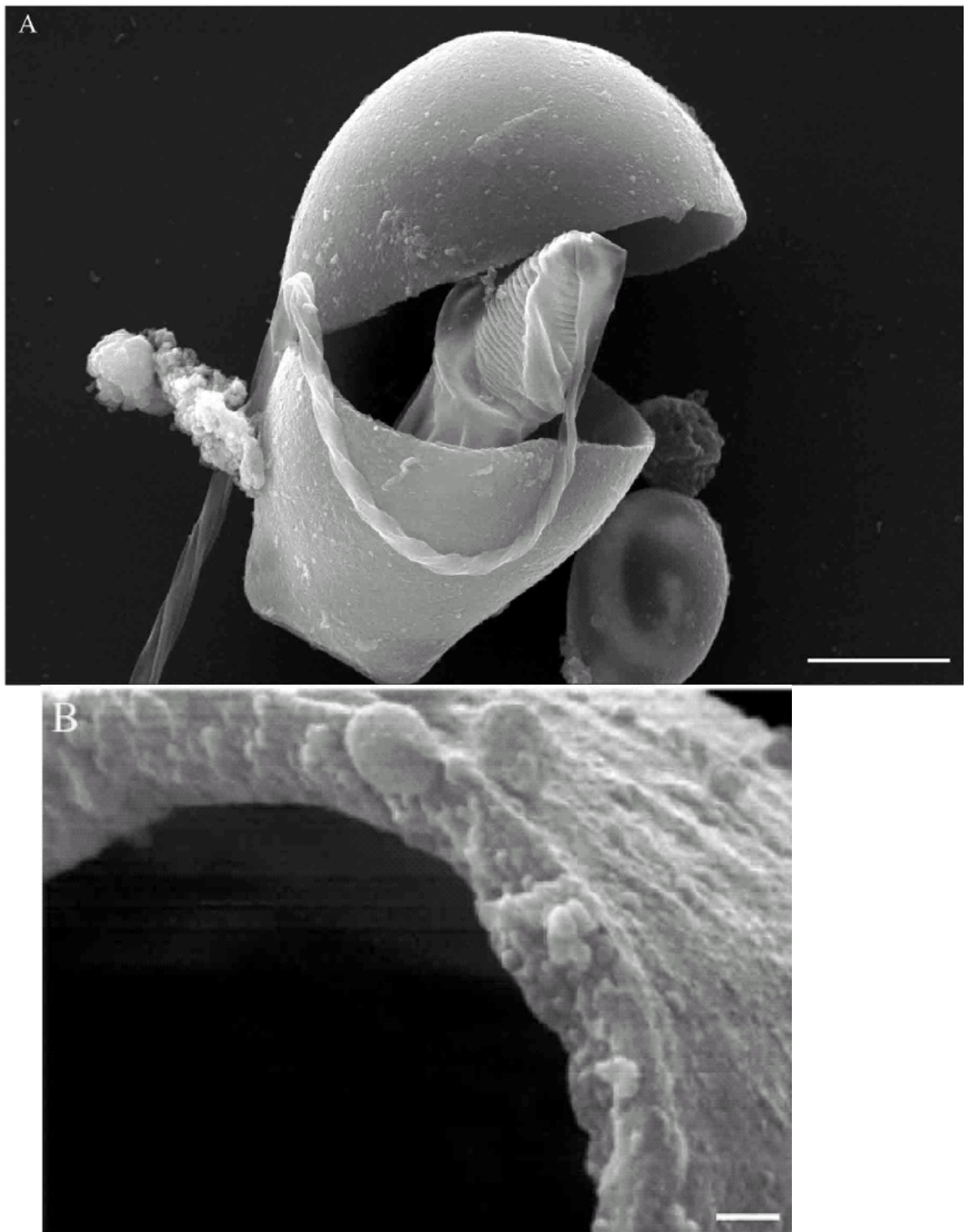


Figure 7.

Field Emission Scanning Electron Microscopy (FESEM) analysis of sonicated capsules with carbon (A) or platinum shadowing (B). A, Total view of a stenotele with a characteristic wall rupture induced by ultrasound treatment. Bar = 3 μ m. B, Profile of ruptured wall shown at high magnification. Bar = 100 nm. Figure is adapted from *Özbek et.al.*

with the antibodies against different domains of NOWA changes the picture of the NOWA appearance and localization during capsule development that was reported before (19). On the Fig. 8A developing nematocyst capsules are stained with three different antibodies: Anti-NOWA-ONCRD (raised against 8 folded cysteine rich domain), Anti-NOWA-CTLD (raised against C-type lectin domain) and Anti-H22 (raised against NOWA). It is obvious from the figures that localization of NOWA restricted to the wall is only observable by the anti-H22. The polyclonal antibodies raised against recombinantly expressed NOWA domains show identical staining of NOWA accumulated in huge aggregates inside the capsule. Thin section electron microscopy of the developing nematocyst shows that inside NOWA aggregates are composed of globular particles (Fig. 8B). These globules are precursors of the capsulomers and only contain NOWA. Staining with minicollagen antibody at this stage of the nematocyst development showed diffused homogeneous pattern throughout the capsule. Colocalization of NOWA and minicollagen staining unambiguously showed that compact globular appearances in the matrix contain exclusively NOWA protein (24). This observation is in agreement with the *in vitro* study of NOWA self-association and subsequent aggregation (see results of chapter 1). Upon maturation of the capsule the conglomerates melt or dissociate but no wall staining appears. In the mature nematocyst both NOWA domain antibodies only stain invaginated tubule when anti-H22 still stains the outer side of the capsule wall. Scanning electron microscopy analysis shows that the tubule is uniformly covered by loosely attached capsulomers (23). The following hypothesis can be proposed to explain such differences in staining patterns. One can assume that two types of NOWA protein exist. These types differ in a way of post-translational modifications. In this frame one type of NOWA is expressed as a soluble material and positioned directly on the membrane forming so called outer wall. The wall-related staining pattern observed with the H22 antibody is must therefore be assigned to this form of NOWA. Another form of the protein, most probably lacking some glycosylation, is initially accumulated in the capsule body as described above. These conglomerates melt at a certain point and dissociate towards the wall in a form of single globular particles. The absence of wall staining pattern with antibodies against NOWA domains is most probably due to the high compactness of the wall at this time. The dissociation of NOWA from

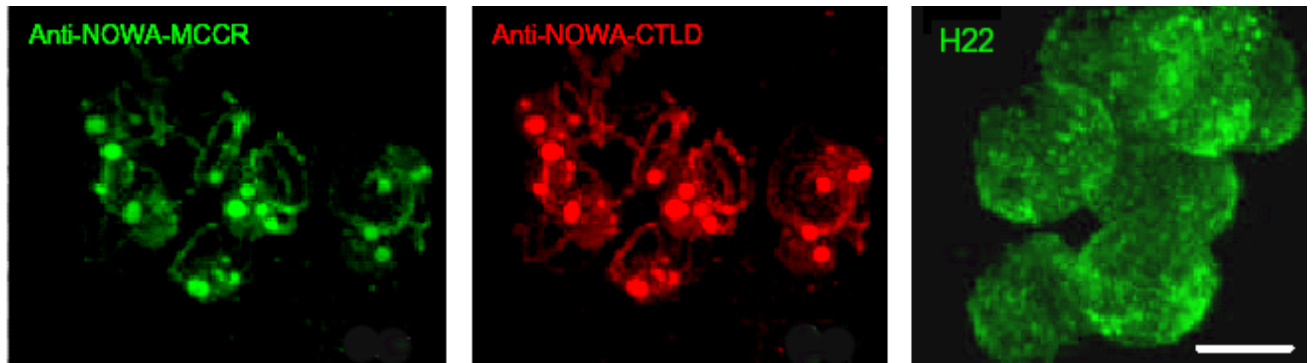
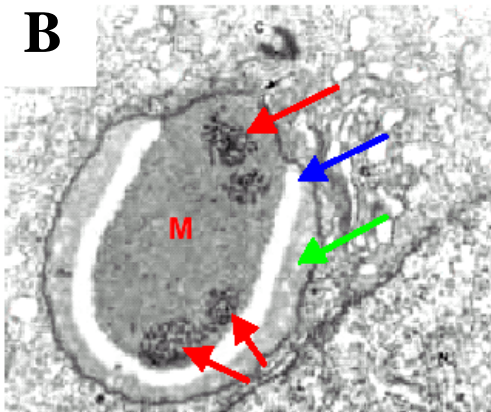
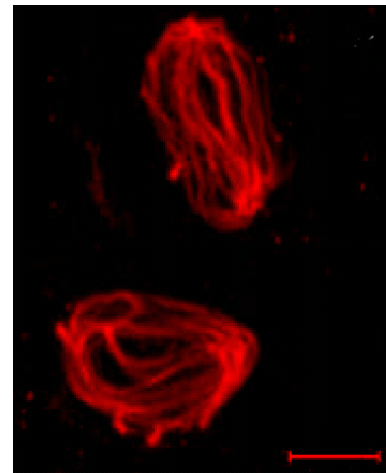
A**B****C**

Figure 8.

A, Immunofluorescent staining of developing nematocyst capsules using three different antibodies: Anti-NOWA-MCCR (raised against 8 fold cysteine rich domain), Anti-NOWA-CTLD (raised against C-type lectin domain) and Anti-H22 (raised against glycosylated NOWA). **B**, Transmission electron microscopy picture thin section of the developing capsule. Red arrows indicate globular particles identified as NOWA conglomerates. Bar indicated on the upper panel is 5 μm . **C**, Immunofluorescent staining of the late stage nematocyst development (Anti-NOWA-MCCR). Only invaginated wrapped tubule is stained. Bar is 5 μm . The data are adapted from the Diploma work thesis of Wurm C.

conglomerates to smaller units is most probably governed by Ca^{2+} ions. Poly- γ -glutamate (PG) synthesis starts in a late stage of nematocyst development after invagination of the external tubule (1). At the same time the staining for NOWA aggregates vanishes and the invaginated tubule is stained instead. It is known that poly- γ -glutamate binds calcium ions. Therefore parallel to the appearance of the PG the amount of calcium is supposed to decrease that leads to the dissociation of NOWA conglomerates to single capsulomers which associate with the wall. Calcium dependent aggregation of self-assembled recombinantly expressed NOWA will be demonstrated and discussed later in chapter 1.

References.

1. S. Szczepanek, M. Cikala, C. N. David, *J Cell Sci* **115**, 745-51 (Feb 15, 2002).
2. R. Blanquet, in *The biology of nematocysts* D. Hessinger, H. Lenhoff, Eds. (Academic, San Diego, 1988).
3. R. Mariscal, *Z Zellforsch Mikrosk Anat* **147**, 149-156 (1974).
4. J. Rifkin, R. Endean, *Cell Tissue Res* **233**, 563-577 (1983).
5. D. Hessinger, H. Lenhoff, *The biology of nematocysts*. (San Diego: Academic Press, 1988).
6. R. Mariscal, E. Conklin, C. Bigger, *Biol Bull Mar Biol Lab* **152**, 392-405 (1977).
7. J. A. Westfall, C. F. Elliott, R. W. Carlin, *J Morphol* **251**, 83-92 (Jan, 2002).
8. J. A. Westfall, D. D. Landers, J. D. McCallum, *J Morphol* **241**, 165-73 (Aug, 1999).
9. R. N. Mariscal, R. B. McLean, C. Hand, *Cell Tissue Res* **178**, 427-33 (Mar 24, 1977).
10. R. N. Mariscal, R. B. McLean, *Cell Tissue Res* **169**, 313-21 (Jun 28, 1976).
11. R. N. Mariscal, C. H. Bigger, R. B. McLean, *Cell Tissue Res* **168**, 465-74 (May 26, 1976).
12. D. L. Spector, R. D. Goldman, L. A. Leinwand, *Cells A LABORATORY MANUAL*, Light Microscopy and Cell Structure (Harbor Laboratory Press, Cold Spring, 1997), vol. 2.
13. C. N. David, A. Gierer, *J Cell Sci* **16**, 359-75 (Nov, 1974).
14. W. A. Mueller, *Trends Genet* **12**, 91-96 (1996).
15. T. Holstein, *J. Ultrastruct. Res.* **75**, 276-290 (1981).
16. J. Weber, *J Biol Chem* **265**, 9664-9 (Jun 15, 1990).
17. T. Holstein, P. Tardent, *Science* **223**, 830-3 (Feb 24, 1984).
18. P. Tardent, *Bioassays* **17**, 351-362 (1996).
19. U. Engel et al., *Embo J* **20**, 3063-73 (Jun 15, 2001).
20. A. W. Koch et al., *J Cell Sci* **111** (Pt 11), 1545-54 (Jun, 1998).
21. U. Engel et al., *J Cell Sci* **115**, 3923-34 (Oct 15, 2002).
22. E. M. Kurz, T. W. Holstein, B. M. Petri, J. Engel, C. N. David, *J Cell Biol* **115**, 1159-69 (Nov, 1991).
23. S. Oezbek et al., **submitted** (2004).
24. C. Wurm, TECHNISCHE UNIVERSITÄT Darmstadt (2003).

General Introduction

Part 2

Domain organization of NOWA and minicollagen

Structural variety of the cysteine-rich domains

Domain organization of NOWA and minicollagen.

As already mentioned two proteins composing a structure of the nematocyst capsule wall, NOWA (5) and minicollagen (7) have been identified. These proteins of completely different size and presumably different structural organization are suggested to form elastic and strong capsule wall via intermolecular disulfide isomerization.

Minicollagens of *Hydra* nematocysts are the shortest collagens known and at the same time are unique due to their unusual domain organization. The domain organization of the minicollagen molecule discussed by Engel et al (9) is presented in figure 1.

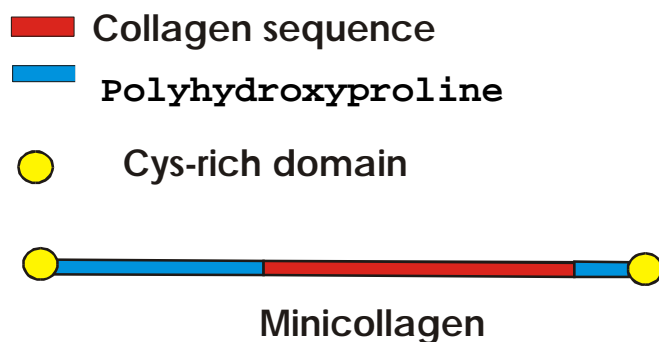


Figure 1.

Schematic representation of minicollagen domains. Yellow circles are the cysteine rich domains, which is a unique feature of nematocyst minicollagens.

The SMART database identifies two domains in the 90 kDa NOWA sequence: SCP and CTLD (Fig.2).

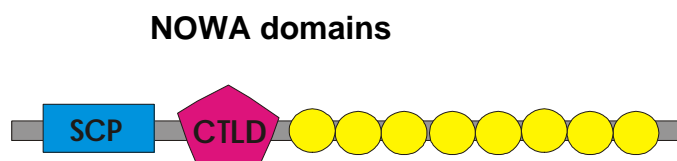


Figure 2.

NOWA domain organization identified by SMART and by homology to the minicollagen Cys-rich domain (yellow circles)

SCP (Sperm Coating Protein) domain found in the extracellular protein family. Human glioma pathogenesis-related protein GliPR and the plant pathogenesis-related protein both containing SCP domains represent functional links between plant

defense systems and human immune system. The function as well as 3D fold are not known for this domain.

The C-type lectin domain (CTLTD) is found in many different proteins predominantly but not exclusively in vertebrates. Many of these domains function as calcium-dependent carbohydrate binding modules. C-type-lectin-like domains were first identified as 110-140-residue-long carbohydrate recognition domains (CRDs) of group C of animal lectins, which bound carbohydrates in a Ca^{2+} -dependent manner (11). By comparing sequences of C-type lectins, a set of conserved positions was identified, which includes residues involved in Ca^{2+} - and carbohydrate-binding, and fold integrity maintenance (11, 13). Known CTLTD structures exhibit significant structural conservation despite the low sequence similarities. Structurally, CTLTDs were divided into two groups: *canonical* CTLTDs having a long loop region, and *compact* CTLTDs that lack it (4). Conserved structural folds for canonical and compact C-type lectins are shown on figure 3.

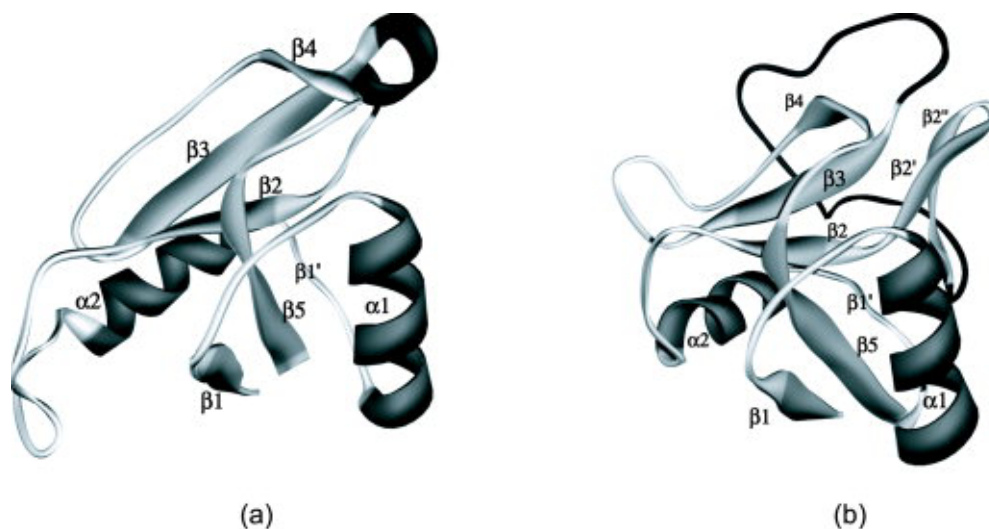


Figure 3

Ribbon diagrams of (a) compact (intimin, 1f00) and (b) canonical (E-selectin, 1g1t) CTLTD structures. The long loop region in E-selectin, and the short α -helix that replaces the LLR in compact CTLTDs, are shown in black. Secondary structure labels are according to the secondary structure element (SSE) naming scheme. This figure is adapted from Zelensky et. al. (4).

Besides the SCP and CTLD domains NOWA has eight cysteine-rich repeats similar to the two in minicollagen first described in (5). These repeats start after the CTLD and are followed by a basic C-terminal sequence. The presence of an identical cysteine pattern in these two proteins suggests a possibility to reshuffle disulfides from intra to intermolecular bonds during formation of the nematocyst capsule wall. Therefore covalently cross-linked wall structure can supply unusually high tensile stress resistance. It was demonstrated that minicollagen trimers are not covalently cross-linked. Consequently all disulfides must be closed within the domain (9). The cysteine-rich domain in minicollagen and NOWA has an unusual cysteine pattern which could not be assigned to any consensus pattern identified in known cysteine-rich domains. This poses the questions for cysteine connectivity and 3-D structure of this domain. Also an interesting problem is whether the separated Cys-rich domain is able to fold independently. In the present theses I have approached indicated problems and found that minicollagen and NOWA cysteine rich domains fold independently into a compact structure stabilized by disulfide bonds, which is in fact a new structural fold (see Chapter 3 and Chapter 4). Below a summary of the structural variety of the currently known cysteine-rich peptides is presented.

Disulfide dependent protein folding pathways.

Native disulfide bond formation is crucial for the proper folding of many proteins. Disulfide bond formation and formation of non-covalent interactions are coupled significantly during conversion of a conformationally unstable precursor to the stable native product. Two mechanisms for oxidative folding are described for monomeric proteins. In the folded-precursor mechanism, the precursor species first folds non-covalently into a state in which reactive thiol- groups are correctly positioned for the formation of native disulfide bonds. In contrast, in the quasi-stochastic mechanism, the disulfide formation occurs quasi-stochastically, i.e. reactive thiol groups encounter each other with a probability determined primarily by loop entropy, albeit modified by conformational biases in the unfolded state. In this case the incorrectly established disulfide bonds need to be reshuffled. It has been demonstrated that the quasi-stochastic mechanism is more plausible than the folded-precursor mechanism for most globular proteins (14). Oxidative folding of the minicollagen and NOWA cysteine rich domains is discussed in chapter 4.

Independently folded cysteine rich domains of proteins and bioactive cysteine rich peptides are of large structural and functional variety. It is difficult to classify them according to their cysteine patterns or three-dimensional structural folds. Nevertheless few classes could be identified.

Cystine knots containing growth factors family.

First of all cystine knots have to be described. These are fascinating structural motifs in which an embedded ring formed by two disulfide bonds and their connecting backbone segments is threaded by a third disulfide bond. Three related cystine knot containing families are distinguished today: growth factor cystine knots (GFCKs), inhibitor cystine knots (ICKs), and cyclic cystine knots (CCKs) (15). Few structural examples for each type of cystine knot will be given in the scope of this introduction. Polypeptide growth factors, a diverse group of regulatory agents, that controls cell survival, proliferation and differentiation. The determination of the crystal structure of dimeric Nerve Growth Factor (NGF) revealed a novel three-dimensional fold. Each subunit consist of predominantly β -strand secondary structure and an unusual clustering of three disulfide bridges (2).

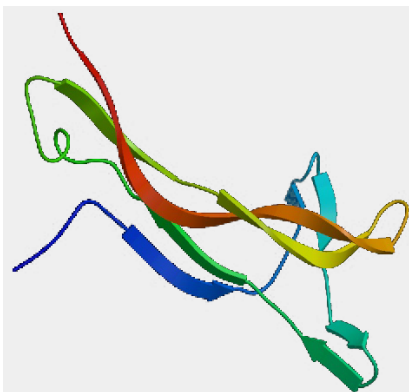


Figure 4.

Structure of the NGF monomer (2).

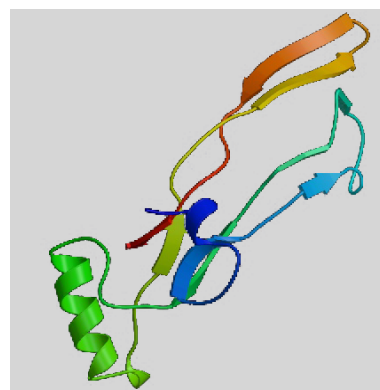


Figure 5.

Structure of the TGF β 2 monomer (1).

Subsequently the structure of TGF β 2 showed a tertiary fold similar to NGF. This observation has been confirmed by a structural comparison of the NGF and TGF β 2 molecules (1, 16-18). The structure of platelet derived growth factor (PDGF-BB) has provided another example of this structural fold (19).

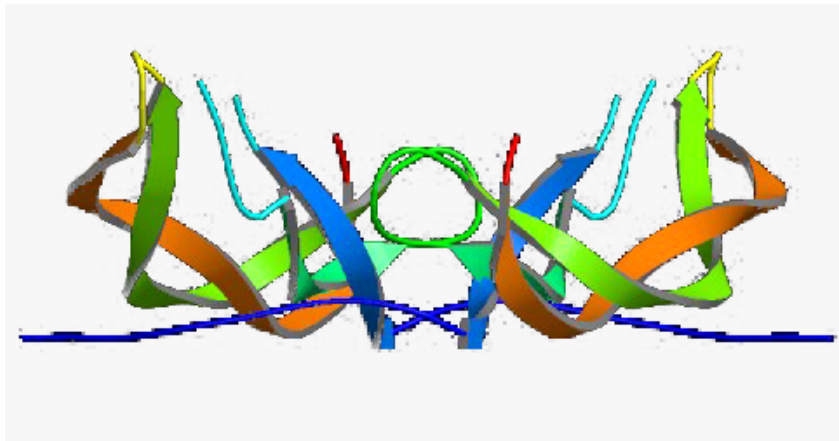


Figure 6. Crystal structure of the platelet derived growth factor BB dimer.

The six half-cystines are virtually the only conserved feature evident from the structural sequence alignment of NGF and TGF β 2. The long-range disulfide bond formation observed for this class of proteins and their consensus cysteine pattern can be represented by only four cysteines as CX_mC / CXC , where m is variable for different proteins. A general cystine knot containing growth factor fold is summarized by the scheme represented on figure 7.

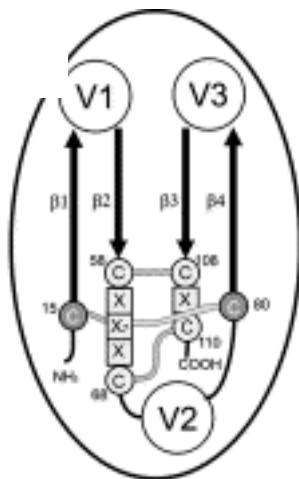


Figure 7.

General scheme representing a cystine knot containing growth factor super-family structural fold. Here V1, V2, V3 represent any structural feature. Cysteines connections indicated by white curves. The squared Xs indicate any amino acid in between the consensus cysteines.

Inhibitor cystine knots family or “knottins”.

A second family of the cystine knot containing proteins is inhibitor cystine knots family or “knottins”. The name “inhibitor cystine knot” has been introduced long time ago when the first knottins were identified. The first “knottins” were the potato

carboxypeptidase A inhibitor, the structure of which was solved already in 1982 (20) and the trypsin inhibitor identified in 1989 (21). Over the last two decades many other proteins were recognized as knottins. A previously mentioned third class of cystine knots, cyclic cystine knots, can be generally classified as knottins as well. They are separated into a distinct type only because of the cyclic backbone. All other sequential and structural features are preserved for this type of proteins. In the scope of this introduction cyclotides are considered as a member of knottins structural family. Currently the knottin structural family includes several unrelated functional protein families:

- Protease inhibitors from plants (trypsin inhibitors are the most abundant)
- Peptides from the *Rubiaceae* and the *Violaceae* plant families
- Toxins from cone snail, spider, bug, crab, scorpion
- Gurmarin-like peptides, human Agouti-related protein
- Antimicrobial peptides

Figure 8 shows representative 3-D structures of the proteins from each family.

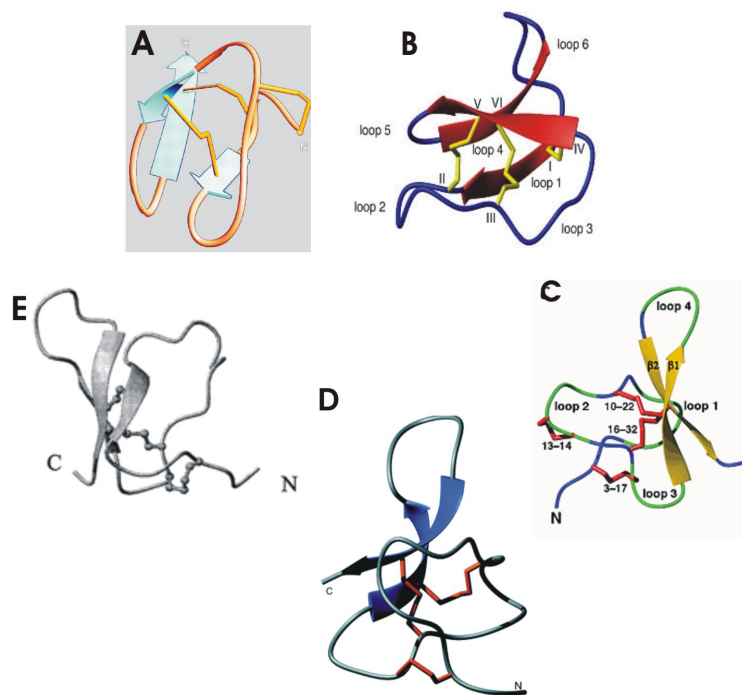


Figure 8.

Members of the Knottins structural family: **A**, α -amylase inhibitor from amaranth (1QFD) (3); **B**, cyclotide Kalata B1 (1K48) (6); **C**, insecticidal neurotoxin J-ACTX-Hv1c (1HP3) (8); **D**, gurmarin, a sweet-taste-suppressing plant polypeptide (1C4E) (10); **E**, tachystatin A, antimicrobial peptide (1CIX) (12). Each of these peptides represents a particular protein family as indicated above.

It becomes clear already from simple comparison of the structures that all these peptides constitute a structural family characterized by a number of β – strands connected by loops and stabilized to a compact tight structure by the cystine knot.

All “knottins” are found to be very stable but the most fascinating examples of stability are cyclotides. These peptides have an average unfolding temperature of 100° C and higher (22). However it has been noticed that knottins, that contain at least three disulfide bridges, are possibly built from an ancestral two-disulfide elementary motif. This motif has been termed the CSB (Cystine Stabilized β -sheet) motif (23). Figure 9 represents CSB elementary motif and the knottin structure built on its basis.

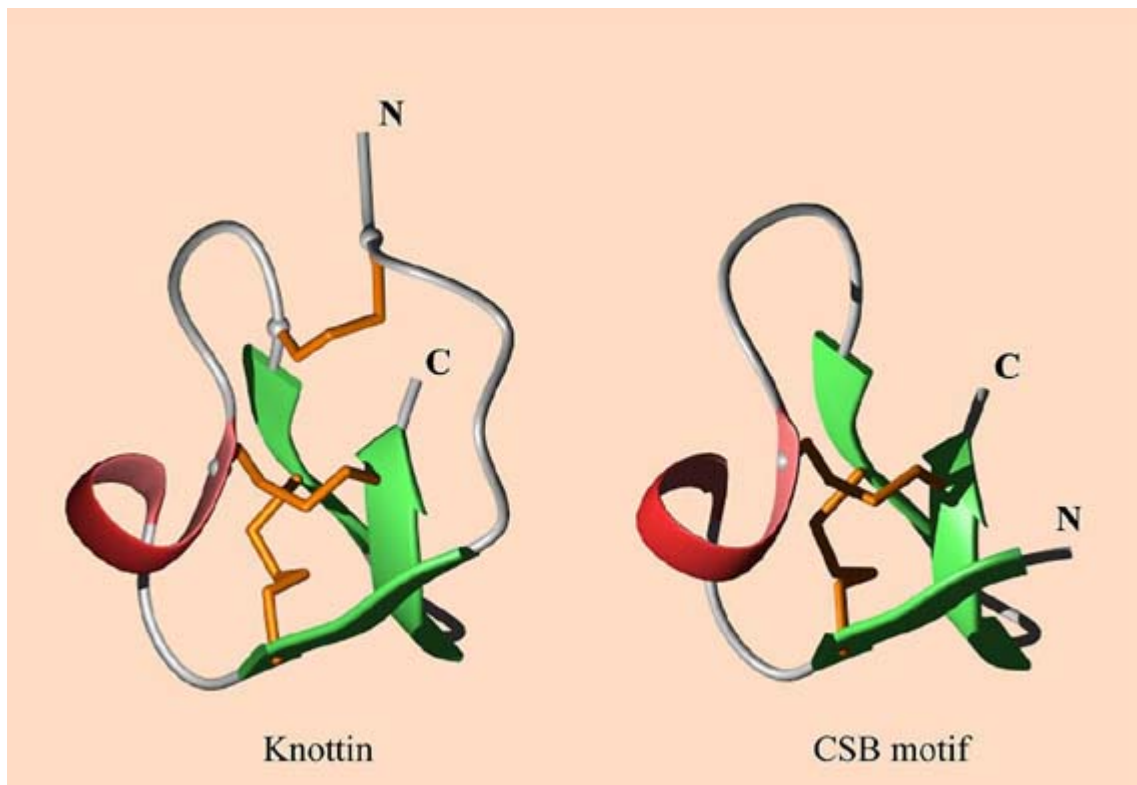


Figure 9. Cystine Stabilized β -sheet motif (right model) and knottin (left).

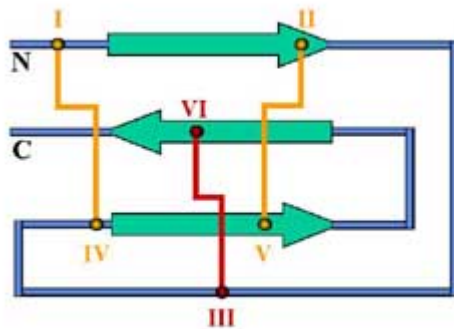
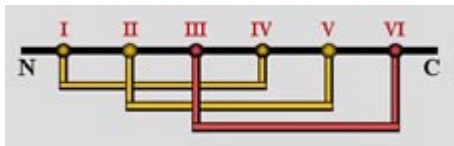
General classification of knottins is considered to be as following:

- ?? The knot implies that knottins contain at least 3 disulfide bridges;
- ?? The structural family of knottins has the disulfide between cysteines III and VI going through disulfides I-IV and II-V;

?? Cysteine IV is special because it is either adjacent to cysteine III (e.g. in spider toxins) or two positions before CYS V (e.g. in protease inhibitors), or three positions before CYS V in PCI.

A comparison of the knottins and the cystine knot containing growth factors is shown schematically in the figure 10.

Knottins



Growth Factor cystine knots

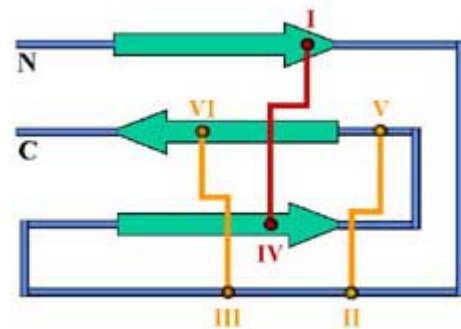
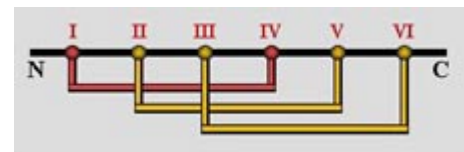


Figure 10.

Schematic comparison of the Knottins and Growth Factor Family. Both families have the same cystine pattern but the penetrating disulfide bridge is different, i.e. cystine knot is knotted in different ways. Lower panel shows schematic representation of the structural fold observed for these two families. This scheme is adapted from the knottin's website (<http://knottin.cbs.cnrs.fr>).

Along with the diverse natural biological activity knottins are currently considered to be a very promising scaffold for drug design due to their stability, small size and high sequence tolerance.

Cystine stabilized α -helix structural motif.

Although cystine knots framework is very abundant among the cysteine rich proteins this is not the only possibility of the disulfide bonds arrangement. Distinct structural motif among the large variety of the multiple cysteine-containing peptides was identified in 1991 by *Kobayashi et. al.* and named “cystine stabilized α -helix” (24). It consists of one pair of half-cystines in positions $i, i+4$, i.e. separated by an intervening tripeptide of no sequence homology, disulfide-linked to a second pair of half-cystines in positions $j, j+2$ of a second strand. Many peptides of different origins and functions are found to adopt this structural motif. All of them have a consensus cysteine framework that can be symbolized as Cys- X_1 -Cys/ Cys- X_3 -Cys. In this consensus representation “slash” represents any sequence in between the cysteines that may even contain additional disulfides. The proteins exhibiting CSH structural motif have been reviewed later in 1998 by *Tamaoki et. al.* (25) and revealed a large variety of families such as endothelins (26, 27), sarafotoxins (28), bee and scorpion venom toxins (24, 29). Representative 3D structures of the CSH folding motif are shown on the figure 11.

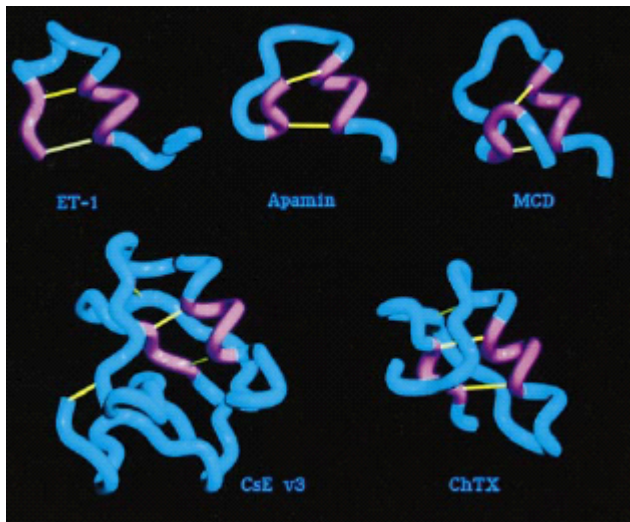


Figure 11.

Backbone structures of ET-1, apamin, MCD peptide, CsE v3 and ChTX with the portion of the CSH motif depicted in magenta and disulfide bridges in yellow. The figure is adapted from the review article by Tamaoki et. al.

Schematic drawing of the consensus structural motif is also adapted from the review article by Tamaoki et. al. (25) and shown on figure 9 below.



Figure 12.

Schematic drawing of the CSH motif with ball-and-stick models of two disulfide bonds. An α -helix spanning the Cys-(X)₃-Cys sequence portion is crosslinked by two disulfides to the sequence portion Cys-X-Cys, folded into an extended β -type structure.

Furthermore authors of the review made an attempt to extend classification of the cysteine patterns and considered the framework of Cys-X_m-Cys/ Cys-X_n-Cys where m/n can adopt numbers from 0 to 5. They found that CSH folding motif is predominantly found only in case of m/n = 1/3 as it was considered above. Nevertheless for the m/n = 3/3 they found several examples of the disulfide bonded connections of the anti-parallel α -helices (30) or anti-parallel β -strands (tachyplesin) (31). From the other hand several members of the previously described growth factors family satisfy the consensus framework of the CSH fold with two additional cysteines in the “slash” sequence. Tamaoki et. al. ascribe such proteins as a distinct portion inside the folding motif family with the α -helix replaced by β -strand.

The reviewed structures represent only small part of the currently known cysteine-rich peptides and stable domains. The large variety of different cysteine-rich structural motifs left out of the scope of this introduction because these structures can hardly be classified.

References

1. S. Daopin, K. A. Piez, Y. Ogawa, D. R. Davies, *Science* **257**, 369-73 (Jul 17, 1992).
2. N. Q. McDonald *et al.*, *Nature* **354**, 411-4 (Dec 5, 1991).
3. S. Lu *et al.*, *J Biol Chem* **274**, 20473-8 (Jul 16, 1999).
4. A. N. Zelensky, J. E. Gready, *Proteins* **52**, 466-77 (Aug 15, 2003).
5. U. Engel *et al.*, *J Cell Sci* **115**, 3923-34 (Oct 15, 2002).
6. L. Skjeldal, L. Gran, K. Sletten, B. F. Volkman, *Arch Biochem Biophys* **399**, 142-8 (Mar 15, 2002).
7. E. M. Kurz, T. W. Holstein, B. M. Petri, J. Engel, C. N. David, *J Cell Biol* **115**, 1159-69 (Nov, 1991).
8. X. H. Wang *et al.*, *J Biol Chem* **276**, 40306-12 (Oct 26, 2001).
9. U. Engel *et al.*, *Embo J* **20**, 3063-73 (Jun 15, 2001).
10. J. I. Fletcher *et al.*, *Eur J Biochem* **264**, 525-33 (Sep, 1999).
11. K. Drickamer, *J Biol Chem* **263**, 9557-60 (Jul 15, 1988).
12. N. Fujitani *et al.*, *J Biol Chem* **277**, 23651-7 (Jun 28, 2002).
13. K. Drickamer, *Prog Nucleic Acid Res Mol Biol* **45**, 207-32 (1993).
14. E. Welker, W. J. Wedemeyer, M. Narayan, H. A. Scheraga, *Biochemistry* **40**, 9059-64 (Aug 7, 2001).
15. D. J. Craik, N. L. Daly, C. Waine, *Toxicon* **39**, 43-60 (Jan, 2001).
16. M. P. Schlunegger, M. G. Grutter, *Nature* **358**, 430-4 (Jul 30, 1992).
17. A. G. Murzin, *Proteins* **14**, 191-201 (Oct, 1992).
18. M. B. Swindells, *Science* **258**, 1160-1; discussion 1161-2 (Nov 13, 1992).
19. C. Oefner, A. D'Arcy, F. K. Winkler, B. Eggimann, M. Hosang, *Embo J* **11**, 3921-6 (Nov, 1992).
20. D. C. Rees, W. N. Lipscomb, *J Mol Biol* **160**, 475-98 (Sep 25, 1982).
21. W. Bode, H. J. Greyling, R. Huber, J. Otlewski, T. Wilusz, *FEBS Lett* **242**, 285-92 (Jan 2, 1989).
22. M. L. Colgrave, D. J. Craik, *Biochemistry* **43**, 5965-75 (May 25, 2004).
23. A. Heitz, D. Le-Nguyen, L. Chiche, *Biochemistry* **38**, 10615-25 (Aug 10, 1999).
24. Y. Kobayashi *et al.*, *Biopolymers* **31**, 1213-20 (Sep, 1991).
25. H. Tamaoki *et al.*, *Protein Eng* **11**, 649-59 (Aug, 1998).
26. M. D. Reily *et al.*, *FEBS Lett* **300**, 136-40 (Mar 30, 1992).

27. M. D. Reily, J. B. Dunbar, Jr., *Biochem Biophys Res Commun* **178**, 570-7 (Jul 31, 1991).
28. A. Aumelas *et al.*, *Int J Pept Protein Res* **37**, 315-24 (Apr, 1991).
29. M. Bruix *et al.*, *Biochemistry* **32**, 715-24 (Jan 19, 1993).
30. K. H. Han *et al.*, *Biochem J* **313 (Pt 3)**, 885-92 (Feb 1, 1996).
31. H. Tamamura *et al.*, *Biochim Biophys Acta* **1163**, 209-16 (May 13, 1993).

Chapter 1*

Self-assembly of NOWA.

Calcium dependent aggregation of assembled NOWA globules.

* This work was performed in collaboration with Suat Oezbek.

Introduction

The nematocyst capsule wall is composed of the globular building units that we termed “capsulomers” (Fig. 6 B of General Introduction) (1). It was shown recently that capsulomers consist of both NOWA and mini-collagens (1). In the referred article authors showed as well that in the capsulomers of the wall polymer NOWA and minicollagens form disulfide-linked hetero-oligomers. This was demonstrated by treatment of the nematocysts with mild sonication preserving native complexes and subsequent size exclusion chromatography followed by biochemical and microscopy studies of the separated capsulomers. The high molecular weight peak corresponded to the capsulomers was collected and analyzed with the negative staining transmission electron microscopy (TEM). The same sample was analyzed by Western blotting under reducing conditions with the antibodies against mini-collagen1 and anti-NOWA-CTLD and showed the presence of both proteins. Visualization of the isolated capsulomer peak via electron microscopy revealed the presence of capsulomers with rather heterogeneous distribution. The observed heterogeneity of isolated capsulomers was due to the naturally occurring capsulomer size distribution and additionally due to the aggregation on the column.

It has been shown in several publications that the capsule architecture is highly sensitive to reducing agents and that *Hydra* minicollagens are only solubilized by reduction (2); (3), (4, 5). It was also demonstrated that polymerization of recombinantly expressed minicollagen-1 can be triggered in vitro by oxidative reshuffling of the initially soluble collagen trimers (6). As cysteine residues are constricted to the short terminal domains of the minicollagen molecules a model may be proposed in which the cysteine-rich domains function as linkers of a collagen polymer by an intermolecular exchange of disulfide linkage. NOWA contains homologous cysteine-rich domains as a C-terminal octad repeat suggesting a similar assembly process and a possibility to link to minicollagens.

As discussed in the general introduction conglomerates found inside the capsule body during early stages of nematocyst morphodogenesis are composed of globular structures and contain NOWA only. This fact suggests the possibility of capsulomer-like globules formation out of isolated NOWA molecules with no mini-

collagens involved. Since mature capsulomers assemble via formation of intermolecular disulfide bonds between NOWA and minicollagen molecules assembly of capsulomer precursors may be also achieved by disulfide isomerization.

In order to elucidate whether NOWA alone assembles to capsulomer – like structures I expressed the full-length protein in mammalian cells and followed its assembly by various techniques. In addition similar experiments were performed with the recombinantly expressed fragment containing the 8 Cys-rich domains.

Materials and Methods

cDNA constructs, expression and purification of recombinant proteins.

Sequences for full length NOWA and its C-terminal cysteine-rich domain comprising residues 464-749 were amplified by PCR using the NOWA pBluescript vector as a template. NheI and BamHI sites were introduced in the 5'- and 3'- primers, respectively, to enable convenient cloning into the corresponding sites of the mammalian expression vector pCEP-Pu. Primers used were:

5'-TGC GGC TAG CCA GAT CCT CAA CAG TAT GGT TGT TTT TAG CG-3', 5'-CGG GAT CCT TAG GCT TTA CTT TGC TTT TTT CTT ACG GGA GG-3' for the full length NOWA.

5'-TGC GGC TAG CCC AAA TTA CTG GAA CAT GTC C-3' and

5'-TTT GGA TCC TTA CAT TCG TCC AAG ACT AC-3'

for the cysteine-rich domain. For stable transfection, 293 EBNA cells were kept in Dulbecco's modified Eagle's medium F12 supplemented with 10% fetal bovine serum, 1% Gln, and PenStrep. Cells were grown to 80% confluence in 6-well plates and transfected overnight with 1 mg of vector DNA using 5 ml of Lipofectamine reagent. The selection of positive clones was performed by culturing transfected cells with 2 mg/ml puromycin with frequent changes of medium until a resistant population appeared. All reagents were purchased from Invitrogen. For expression, stably transfected EBNA 293 cells were grown to high density in 125-ml cell culture flasks using complete medium and then switched to serum-free expression medium. Cell supernatants were harvested several times until the cells detached, pooled and filtered. Filtered expression medium was dialyzed against binding buffer (20 mM Tris; 300 mM NaCl; 5mM Imidazol) before loading on the column. Recombinant proteins were then purified in native conditions using nickel-Sepharose chromatography according to the manufacturer's instructions (QIAGEN). Eluted fractions were analyzed by SDS-PAGE and dialyzed against 50 mM Tris-HCl, pH 8.0, and 150 mM NaCl.

SDS-PAGE, Silver stain and Western blot analysis.

Samples were incubated in Laemmli buffer with or without β -mercaptoethanol or DTT and separated on 12% SDS-gels. For resolving higher aggregates gradient

gels (3-10%) were applied with 2.5% stacker gels. Samples were always duplicated for subsequent Silver staining and Western blotting. The following protocol for Silver staining was used:

1. Fixation - Soak gel for 30 min in 50ml MeOH + 10ml Acetic Acid + 40ml MQ-H₂O
2. Briefly rinse in MQ-H₂O;
3. Reduce for 30 min in 30% Ethanol, 100mM Na Acetate pH 6;
4. Rinse in MQ-H₂O 3 times for 10 min.
5. Staining for 30 min in 0.1 % of Silver Nitrate;
6. Briefly rinse in H₂O;
7. Developer solution : 2.5% Na₂CO₃.

Western blot analysis was performed using mouse antibody directed against His-tag and polyclonal rabbit antibody raised against Cys-rich octad repeat domain of NOWA. Primary antibody (1:1000) was detected using an anti-rabbit-horseradish peroxidase conjugate antibody (1:2000) and the ECL chemoluminescence system (Amersham Biosciences).

Antibody production.

Polyclonal antibody directed against the recombinantly expressed eight folded cysteine rich domain of NOWA was generated in rabbits by Eurogentec (Herstal, Belgium). Immunization was carried out following a standard protocol using 100 µg of purified protein in PBS.

Transmission electron microscopy.

The negative staining of purified NOWA was performed as described elsewhere (7). The 300 mesh electron microscopy grids coated with carbon were glow discharged. Protein sample was allowed to adsorb on the grid surface for 1-2 minutes, then blotted, washed by distilled water, blotted again, and stained either by 2% Uranil Acetate or 2% Phosphotungstic acid adjusted to pH 7 by sodium hydroxide. After staining for 2 minutes samples were washed by water again blotted and allowed to air dry completely before insertion into the microscope.

Results and Discussion.

Disulfide-dependent self-assembly of NOWA leads to the formation of capsulomer – like structures.

The proposed self-assembly of NOWA was analyzed by recombinant expression of the full-length protein and the isolated cysteine-rich octad repeat domain in 293 cells. Both recombinant constructs were designed with N-terminal polyhistidine-tag for purification via Nickel-Sepharose chromatography (Fig. 1). I introduce the name NCRD for single cysteine-rich domain in NOWA and octad NCRD (ONCRD) for the repeat with 8 cysteine rich domains.

Full-length NOWA was expressed in mammalian cells and purified via Nickel chromatography under native conditions. In order to examine the oligomerization state of recombinantly expressed protein purified NOWA was analyzed on the SDS page by Silver staining under reducing and non-reducing and reducing conditions. As it is shown on figure 2A non-reduced material did not enter the 12% SDS page suggesting the high degree of oligomerization. The same sample at the reducing conditions showed single band corresponded to the NOWA monomer size. To verify that absence of protein band under non-reducing conditions is due to the oligomerization gradient SDS page followed by Western blotting was performed. This experiment revealed a protein band recognized by NOWA specific antibody of about 1 MDa (Fig. 2B). Treated with mild reduction (1 mM of DTT) oligomerized protein turned into the ladder of bands corresponding to monomers (of 93 kDa apparent size), dimers and higher oligomers of NOWA (Fig. 2B). These biochemical data show the presence of disulfide bonded oligomers of NOWA immediately after purification.

To examine whether observed oligomerization is a result of the self-assembly process the experiments described below were performed.

Although the oligomerization was always observed purified batches of NOWA varied in extend of assembly to high oligomers so that rarely a small fraction of the material was found to be in monomeric state under non-reducing conditions. A monomer-rich sample was analyzed with size exclusion chromatography. This experiment revealed two distinct peaks assigned to monomeric and highly oligomerized NOWA (Fig 3A). Fractions of both peaks

MRSSTVWLFLALLSVALSTEVKDLDAVDEQSTKRDPVPTVAVGVPPTLDDEGKLTN
 VTMKLLSETNRYRLMHGVTPLGSCPVCSEAAQKHADEIAASGVAKPDHNSKYGQ
 IIFSSKDPEDINQGADYFGTLVPARIYNQIKNFDFVKDAFKENAADFSQLWEGS
 EVVGFASKKAGDTVYVVMYFNPAGNNELSFYDNVHRVTGSGDMQQKIK
 CPDGWKANNNGNCYKLFEEEMAWADAVDHCNVLKS SLFSGESVEEGAF LK TMLVGR
 SSPSWIGMSDMAAKGGFQFVDGTPYVYSDWSRESQQLVIDLWNTKKETVKNQCIT
 ASYEGWNYKDCFKKLPFVCK
 MRPNGMTSYSLDLYFPSSFTDDLYDINSQRYATMKGVITKAFNESYGKDIWVFG
 STFYQFMSRENGDVAASTLLRFAPDVRAPVDPI TKLRDYLRGQTDLKILSVRLIPGSGRGLLPN

QITGTCPSG CSGDCYPECKPGCCGQVNLNAPVQP
 SGYTACSQYPN CGLSCQSSCSQSCCQONPYQPSVMSGTIVIQP
 NEQSVCPQHPG CSQHCAPRCSPQCCQQSMNSLYQP
 PQMSACPQFPS CSPTCAPQCSQLCCQQSSMPLQM
 PQMPSCPQFPS CSASCAPQCSQQCCQQPSMSIQP
 LQISSCPQFPS CSPSCAPQCSQQCCQQPSMPIQL
 PLMGS CSQMPG CSASCAPLCSQQCCQQQSM LQQSIMQQPMM
 MAQNP CSLQQPG CSSACAPACRLSCCSLGRMNLGRKRSHVHHK LKASRKKKQSKA

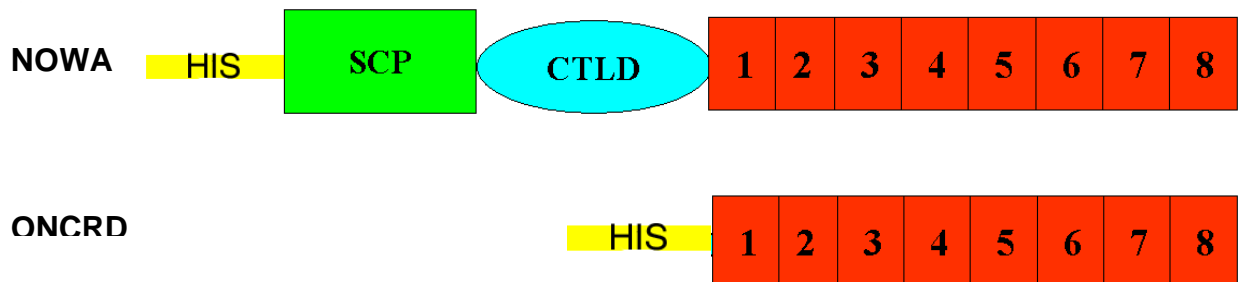


Figure 1.

The sequence of full length NOWA. Domains organization of recombinantly expressed NOWA and ONCRD – eight folded cysteine rich domain of NOWA. Full length NOWA has two ONCRD and two additional domains: SCP (green) and CTLD (aquamarine) Red squares 1-8 are eight times repeated cysteine rich domain altogether called ONCRD. Green and blue colors of the amino acid sequence correspond to the domain colors in the schematic representation. In the ONCRD part of the sequence aligned cysteines colored in red. Both constructs have 6-His-tag for purification purposes.

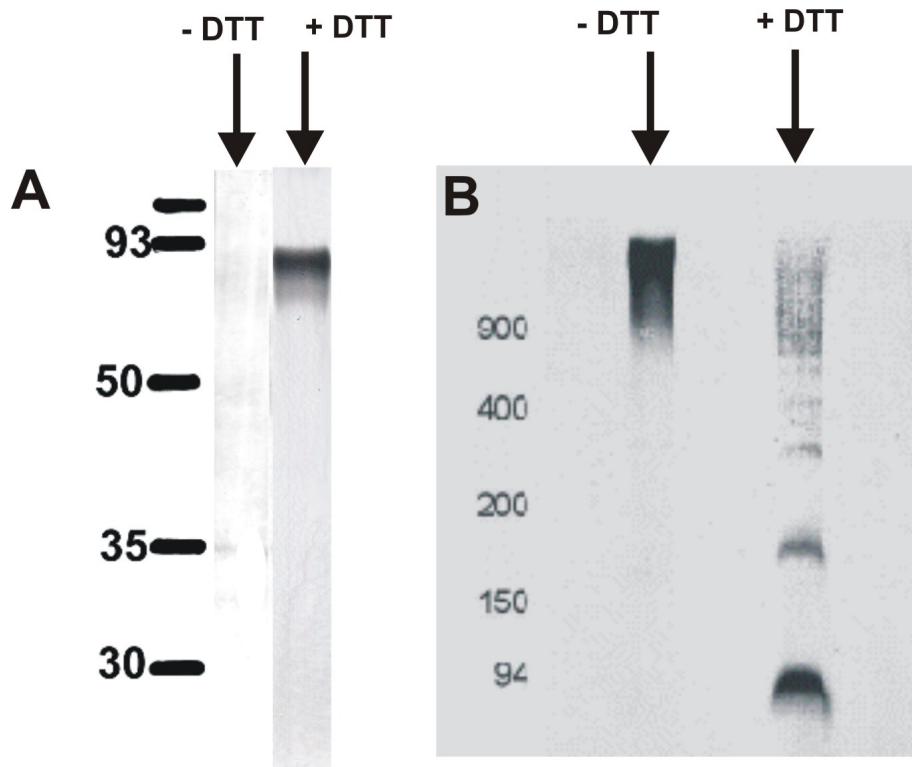


Figure 2.

Expression and purification of full-length NOWA.

A, Silver staining of the purified NOWA under non-reducing and reducing conditions; Reduced band corresponds to the expected monomer size. Non-reduced material did not enter the gel.

B, Gradient SDS page followed by Western blotting analysis of the full length NOWA under nonreducing and mild reducing conditions.

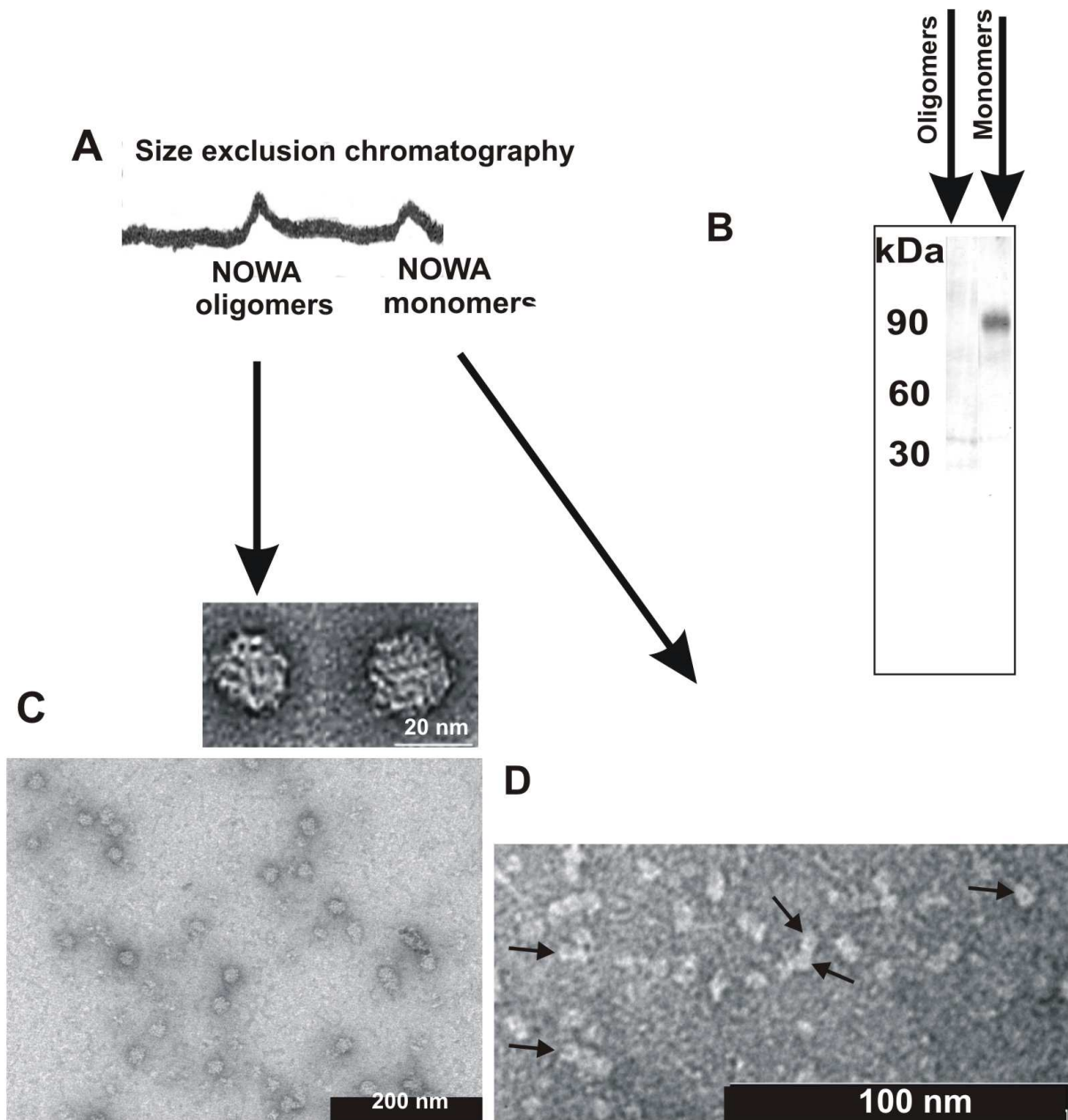


Figure 3.

A, Size exclusion chromatography of recombinantly expressed NOWA. Two peaks are found and subsequently analyzed by 12 % SDS page Silver staining (**B**) and negatively staining transmission electron microscopy (**C**, **D**). **C**, Insert is a magnified view of NOWA capsulomer – like structures. **D**, Arrows are pointing on the ring-like molecules. Bars are indicated on pictures.

were collected and analyzed by Silver staining on the SDS page under non-reducing conditions (Fig. 3B). Expected monomeric band was observed for lower mass peak. High molecular weight NOWA oligomers did not enter 12% SDS gel. Both samples were analyzed with negative staining transmission electron microscopy (Fig 3 C and D).

The oligomers of NOWA protein appeared as globular particles with a size distribution of 17 to 25 nm in diameter. The average diameter of these particles was estimated to be 20 nm that is very similar to the diameter of naturally occurring capsulomers (Fig 3C) (1). Therefore electron microscopy analysis clearly shows that oligomerized form of NOWA has defined shape and thus is most probably a result of the ordered self-association process.

Electron micrograph of NOWA monomers revealed particles of 6-7 nm diameters with a tendency of lateral association. Sometimes ring-like structures were indicated (Fig 3D). In general, assuming the partial specific volume of the protein $v = 0.73\text{cm}^3/\text{g}$, one can calculate the volume occupied by a protein of mass M as follows:

$$V = v * N_A * M = 108 \text{ nm}^3 \text{ for } 90 \text{ kDa NOWA monomer}$$

Assuming that protein is a single globular domain, the radius, R_{\min} , of the smallest spherical particle that could contain a protein of a given mass can be estimated. Using the following equation we can calculate the minimum radius for a spherical equivalent of the 90 kDa monomeric NOWA protein.

$$R_{\min} = (3 V / 4 \pi)^{1/3} = 2.95 \text{ nm}$$

Consequently the minimum diameter of such molecule is 5.9 nm. This matches the electron microscopically observed size of the NOWA monomer (6-7 nm) suggesting a very compact globular fold of the molecule. Nevertheless limitations of the applied method have to be considered. For example, the negative staining procedure can lead to some decrease in the observed radius meaning that size of the molecules observed with this method can be underestimated. In order to

estimate the upper limit of the monomer diameter we performed rotary shadowing transmission electron microscopy of NOWA monomeric fraction. These images are presented on the figure 4B (upper panel) and show roughly 9-10 nm. Rotary shadowed pictures have to be normally corrected for the decoration with metal by subtraction of 2.5 nm. Accordingly an average diameter of monomers revealed by rotary shadowing is about 7.5 nm which is almost identical to that observed with negative staining. Consequently NOWA monomer is in fact very compact globular structure.

Relaying on the same logic as was used for the monomer radius calculations we can estimate maximum number of monomers composing single capsulomer-like structure. Assuming spherical shape of NOWA oligomers its volume ($V = 4/3 \pi r^3$) calculated for average 20 nm spheres equals **4187 nm³**. On the other hand the volume of hypothetical spherical monomer of 2.95nm radius was calculated to be 108 nm³. This is minimal possible volume consequently the maximum number of monomers composing single average capsulomer will be:

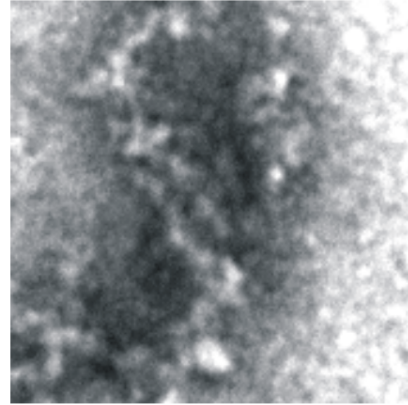
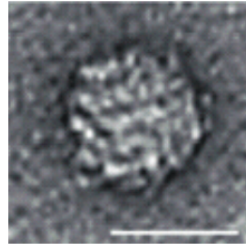
$$\mathbf{N = V \text{ of oligomeric sphere} / V \text{ of monomeric sphere} = 38}$$

In reality this number should decrease due to less compact state of the particle. Accordingly the biggest NOWA oligomer (25 nm in diameter) can consist of maximum **72** monomers and the smallest one (17 nm) can be hypothetically composed of **23** monomeric units. The distribution in the number of monomers composing single capsulomer-like structure (23 - 72) makes impossible estimation of the average molecular mass by ultracentrifugation.

To assess whether capsulomer-like structures composed of recombinant NOWA and compact globular structural fold of monomeric NOWA are disulfide dependent features direct electron microscopy visualization of the native and reduced states of the monomeric and oligomeric protein fractions was applied (Fig. 4). Compact spherical structure of single capsulomer-like globule at the native conditions (Fig. 4A left) abolished completely upon addition of the reducing agent (1mM DTT) (Fig. 4A right). Reduced sample revealed randomly aggregated molecules.

Figure 4 B shows rotary shadowing of the selected NOWA monomers at the native conditions (upper panel) in comparison with the reduced monomers (lower panel). Round shaped molecules unwrapped at the reducing conditions and

A



B

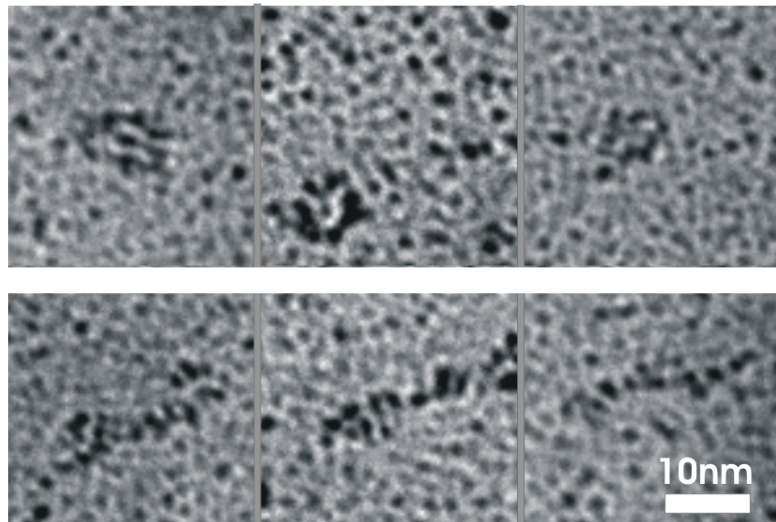


Figure 4.

A, Negative staining transmission electron microscopy images of folded capsulomer-like globule made of recombinantly expressed full length NOWA. Samples were kept at the following conditions before adsorption on the EM grid: 20mM Tris 50 mM NaCl pH 7.5 (left image); 20mM Tris 50 mM NaCl 1mM DTT (right image). On the right panel disordered aggregates are observed after reduction.

B, Rotary shadowing transmission electron microscopy analysis of NOWA monomers in the native form (upper panel) and those upon reduction with 1mM DTT.

exhibit the length approximately equal to their circumference. Thus folding of NOWA monomers and further self-assembly of monomers into the capsulomer-like globules are disulfide dependent processes. Presumably cysteine rich domain of the protein (ONCRD) is particularly responsible for this.

In order to investigate whether cysteine rich domain of NOWA exhibits behaviour similar to that of the full length protein the ONCRD construct was expressed in mammalian cells. After expression and purification ONCRD was analysed with the same set of experiments applied to the full length NOWA. Silver staining analysis of purified product revealed a single band of 45 kDa protein (calculated mass 35 kDa) under reducing conditions (Fig. 5A). The apparent mass was higher than expected but mass spectrometry revealed 35.5 kDa mass. Unlike the full-length NOWA the ONCRD under non-reducing conditions did not show high oligomeric band on the gradient (3% - 10 %) gel although reduction led to the monomer appearance (Fig 5B). Monomeric fraction was sometimes (but very rarely) observed on the non-reduced SDS page. However Isolation of ONCRD monomers by size exclusion chromatography failed because of the low extinction coefficient accompanied by little amount of the material. Thus instead of separate analysis of monomeric and oligomeric fractions crude purified ONCRD was subjected for electron microscopy negative staining. Results represented on figure 5 C and D. ONCRD oligomers appeared as globular particles of 10 – 13 nm in diameter which are often connected to each other. Close view of the ONCRD globules showed pronounced ring appearance (Fig. 5D). These rings are presumably composed of ONCRD monomers that are disulfide interlinked and sometimes seem to undergo further cyclization process (Fig 5C). Summarizing observed features of the ONCRD in comparison with full length NOWA behaviour one can speculate that cysteine rich domain induces self-assembly by a cyclization process. This process is unlimited and rather 2-dimensional in case of ONCRD when in case of the full-length NOWA assembly is controlled and able to proceed in all directions. Probably other domains of NOWA contribute to self-assembly by providing non-covalent interactions and on the other hand by restriction of assembly process to a certain extent as the octad repeat domain alone appears to form larger polymers.

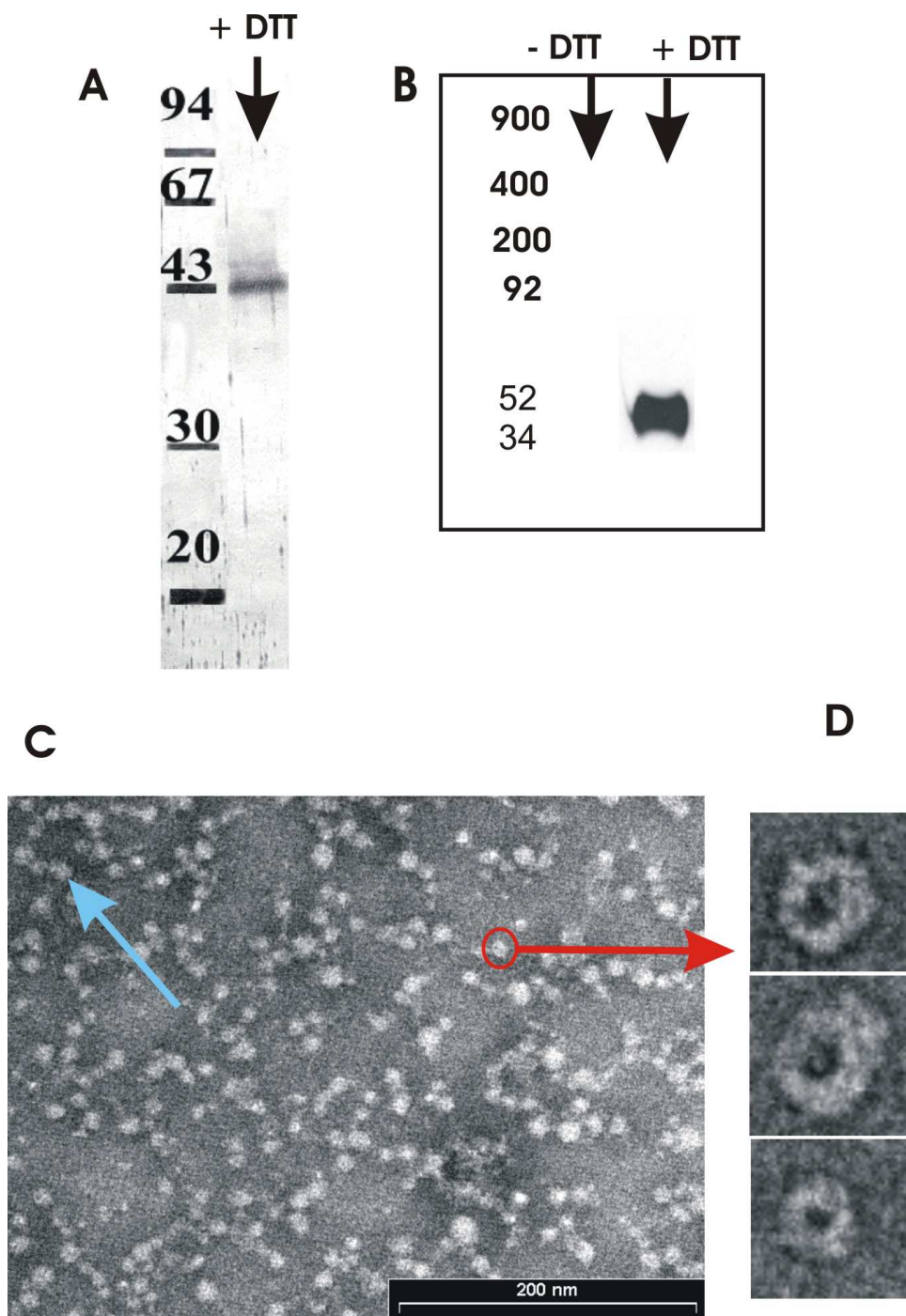


Figure 5.

A, Silver staining analysis of the recombinant purified ONCRD under reducing conditions. **B**, Western blotting of the same sample reduced and non-reduced. **C**, Electron microscopy negative staining micrograph of the purified ONCRD. Red arrow indicate close view of the round particle (**D**). Aquamarine arrow shows cyclization of the round particles. Round structures are in fact rings as seen from the higher magnification picture (**D**).

Thus self-assembly of NOWA is spontaneously happening *in vitro* with the recombinant product. It is a disulfide-dependent process that is predominantly a feature of NOWA cysteine-rich domain. The recombinant ONCRD forms ring structures instead of NOWA capsulomer-like globules.

Calcium dependent aggregation of NOWA capsulomer-like globules.

On the figure 6 A and B we represent the data extracted from the fixed angle rotary shadowing and neutral staining transmission electron microscopy analysis of recombinant NOWA at the 5 mM Ca^{2+} concentration. Globular capsulomer-like particles discussed above are obviously associated into the clusters. These clusters are of different size and shape. Represented TEM images allow to distinguish single capsulomers as building units of bulky conglomerates. Shadows indicate the height of the individual globules as well as the whole clusters on the Fig. 6A. This association is a calcium dependent process. Figure 6C visualizes the same batch of recombinantly expressed NOWA as on figure 6A but in the absence of divalent ions (5mM of EDTA was added after purification and dialysis against 20 mM Tris buffer). Clearly there are no aggregates higher than capsulomers exist under these conditions.

Calcium dependent aggregation of NOWA capsulomers is an important observation in terms of nematocyst morphogenesis. It was described in the part 1 of General Introduction that clusters composed of NOWA were found in the body of developing nematocyst. At the certain time of capsule morphogenesis these clusters dissociate towards the capsule wall. Comparison of the *in vivo* findings with the observed calcium dependent aggregation of recombinant NOWA proposes that *in vivo* “melting” of the NOWA clusters is as well calcium dependent process.

Calcium dependent cluster formation does not happen to the rings formed by recombinant cysteine rich domain of NOWA. As evident from the EM study the degree of ONCRD polymerization is not dependent on the presence of calcium (data not shown). Consequently, one of the two other domains of NOWA must be responsible for calcium aggregation. We assign this property to the C-type lectin domain of protein. This domain is known to bind carbohydrates and other ligands in calcium dependent manner in many proteins (8). It is also found to have very

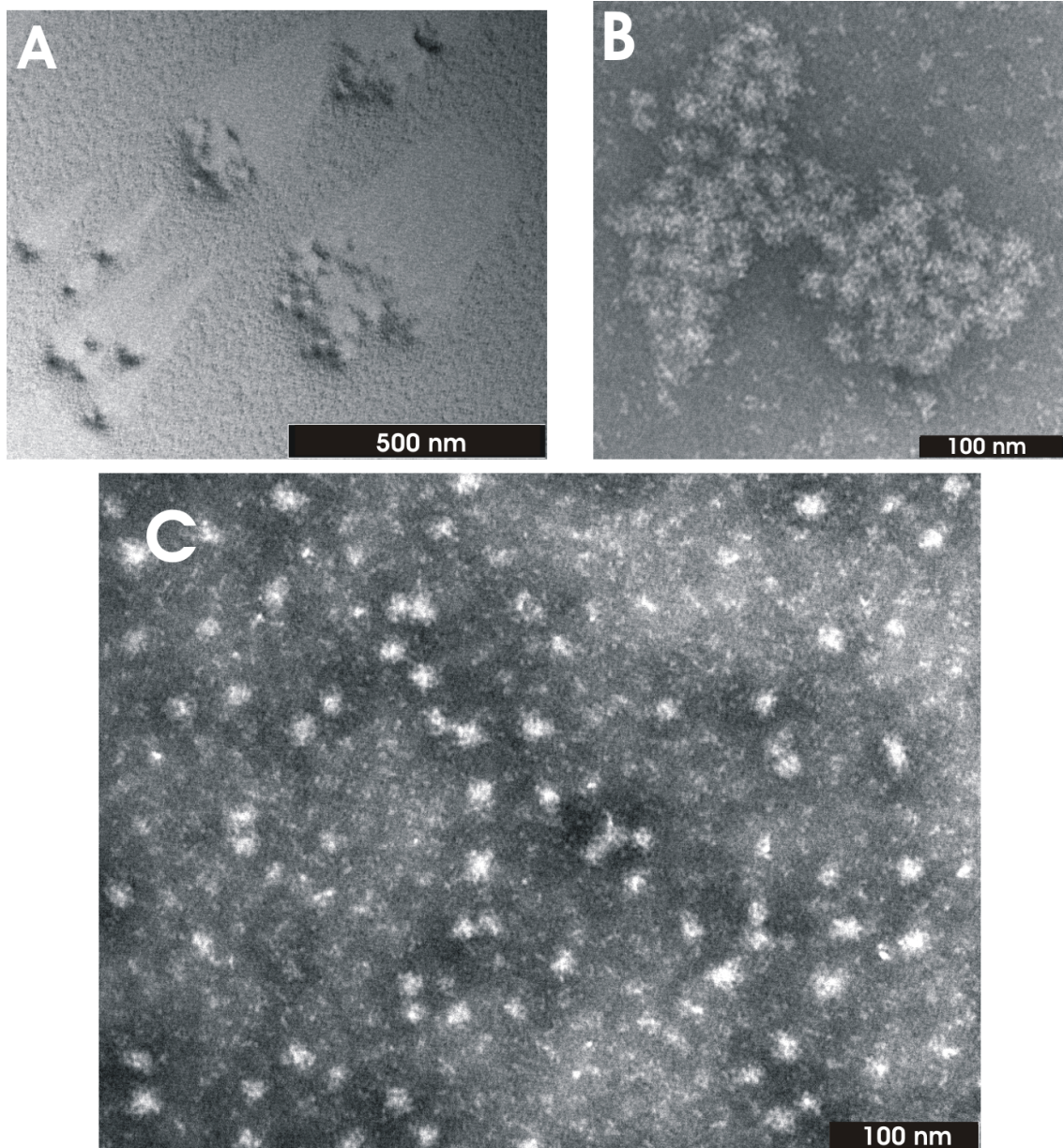


Figure 6.

Transmission electron microscopy analysis with fixed angle rotary shadowing technique (A) and neutral staining (B) of recombinantly expressed full length NOWA at different content of CaCl_2 . Figures A and B represent conditions at 5 mM calcium. C – 5 mM EDTA (no divalent ions present in the protein solution).

high tendency to dimerize. Taking these facts into account one can think of similar mechanisms of NOWA capsulomers aggregation *i.e.* exposed CTLDs can potentially either undergo dimerization with the same domain of different capsulomer precursor or bind its glyco- residues. As was mentioned earlier NOWA is a glycosilated protein. In both scenarios binding mechanism would be calcium dependent process. Alignment of NOWA C-type lectin domain against other members of the super family gives reasonable similarity. Circular dichroism spectra of this domain showing the presence of both helices and betta-sheets in the secondary structure, though exhibiting no change with calcium content variation. All known CTLDs are shown to have very similar structure fold including two alfa-helices and several β – strands independently of their degree of sequence similarity (8). The only significant difference among all these domains is presence or absence of the loop, which is usually but not necessarily responsible for the calcium binding. We have no structural evidence for the presence of such loop in NOWA C-type lectin domain but still this domain is the most prominent one in terms of calcium dependent aggregation of NOWA.

References

1. S. Oezbek *et al.*, **submitted** (2004).
2. U. Engel *et al.*, *Embo J* **20**, 3063-73 (Jun 15, 2001).
3. R. Blanquet, H. M. Lenhoff, *Science* **154**, 152-3 (Oct 7, 1966).
4. H. M. Lenhoff, E. S. Kline, R. Hurley, *Biochim Biophys Acta* **26**, 204-5 (Oct, 1957).
5. R. N. Mariscal, H. M. Lenhoff, *Experientia* **25**, 330-1 (Mar 15, 1969).
6. S. Ozbek, U. Engel, J. Engel, *J Struct Biol* **137**, 11-4 (Jan-Feb, 2002).
7. U. Aebi *et al.*, *Introduction to practical light- and electron microscopy* (1998).
8. A. N. Zelensky, J. E. Gready, *Proteins* **52**, 466-77 (Aug 15, 2003).

Chapter 2

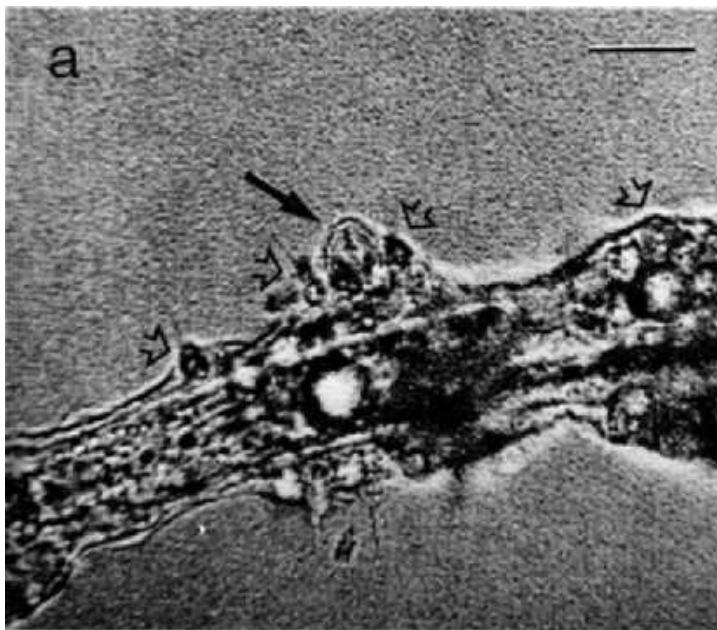
NOWA membrane binding

Abstract

Nematocyst capsule wall formation is happening inside the Golgi vesicle. Membrane serves as a substrate for the developing capsule at the early stages of nematocyst morphogenesis. Moreover as shown by transmission electron microscopy (1), the nematocyst is completely enclosed by a vesicular membrane in the mature form. We discussed in the general introduction that NOWA found in two states during capsule morphogenesis one of which is located inside the capsule body in a clusters form and the other is colocalized with the membrane of Golgi vesicle. The membrane associated form of NOWA protein is already identified at the very early stages of capsule formation. Consequently it has been proposed that NOWA is able to interact with the Golgi vesicle membrane. The mechanism of such interaction is an interesting feature in terms of understanding of the nematocyst capsule wall assembly and structure. In order to demonstrate and investigate NOWA - membrane interaction *in vitro* we have applied several independent qualitative and quantitative approaches. By these methods the ability of NOWA to interact with the model negatively charged (75% POPC : 25% POPG) phospholipid bilayer as well as with monolayer of the same composition was demonstrated. Binding of NOWA to the model membrane composed of 100% POPC was found to be negligible. Kinetic surface plasmon resonance studies allowed us to determine the binding constants in the presence and absence of calcium. In order to map a protein sequence responsible for the membrane association we investigated separate NOWA domains interaction with the model membranes. Two likely candidates were identified: C-type lectin domain and basic terminal sequence of the protein.

Introduction.

Nematocyst outer wall antigen (NOWA) was identified initially as a protein composing the outer wall of the nematocyst capsule wall. Further studies revealed rather homogeneous structure of the wall and presence of NOWA along with minicollagen in the wall structural building units “capsulomers”. However during the morphogenesis of the nematocyst capsule NOWA was found in two distinct forms: a cluster form accumulated inside the developing capsule body and a form associated with the membrane of the Golgi vesicle already at the very early stages of the capsule development. Later on cluster form of the protein has melted and dissociated toward the wall of the future nematocyst (2). This phenomenon was discussed to be a feature of the calcium dependent aggregation of NOWA (see chapter 1). At all time of the nematocyst development Golgi membrane serves as a substrate for the capsule wall formation (3). A mature nematocyst is found to be completely enclosed by a vesicular membrane as it is evident from the electron



microscopy study (figure below adapted from Golz, 1994) (1). In its basolateral portion, this membrane is separated from the cell membrane by a more than 0.5 μm thick cytoplasmic layer containing other intracellular membranes and a complex cytoskeleton. At its apical

part, however, the nematocyst membrane is closely apposed to the cell membrane of the opercular region, forming a putative contact region of up to 1 μm^2 . Here are vesicular and cell membranes separated by a thin cytoplasmic lamella of less than 50 nm. Therefore the nematocyst wall is always in a close

contact with vesicular membrane suggesting an interaction of the wall proteins with this membrane.

In the present study we investigated the binding of the recombinantly expressed and self-assembled NOWA to the model phospholipid monolayers and bilayers. We found out that such binding does exist and membrane bound protein was shown to be in the capsulomer-like associated form. The mechanism of NOWA – membrane interaction was a second subject that we tried to approach in this chapter. To recognize the particular domain of the 90 kDa protein which is responsible for membrane affinity we investigated two recombinantly expressed NOWA domains: CTLD and ONCRD. The very C-terminal sequence of NOWA is enriched by positively charged Lys residues and is expected to be flexible. Regions with clusters of lysines are often found to be membrane associated or even penetrate the membranes. For instance so called cell penetrating peptides such as Tat or Penetratin contain preferentially arginines and lysines in their sequences (4). These peptides use electrostatic attraction to bind and consequently penetrate negatively charged membrane surfaces. We suggest that similar mechanism can be utilized by NOWA. In addition the data clearly indicated that CTLD (C-type lectin domain) of the protein plays a role in the membrane binding as well.

Materials and Methods.

Transmission electron microscopy.

The negative staining of purified NOWA was performed as described elsewhere. The 300 mesh electron microscopy grids coated with carbon were glow discharged to make the surface hydrophilic. Protein sample was allowed to adsorb on the grid surface for 1-2 minutes, then blotted, washed by distilled water, blotted, and stained either by 2% uranyl acetate or 2% phosphotungstic acid adjusted to pH 7 by sodium hydroxide. After staining for 2 minutes samples were washed by water again blotted and allowed to air dry completely before insertion into the microscope. Samples for protein - lipid monolayer interaction studies were prepared as illustrated on figure 1.

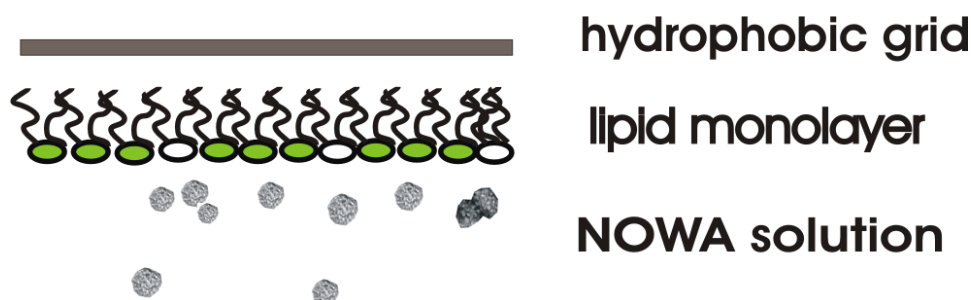
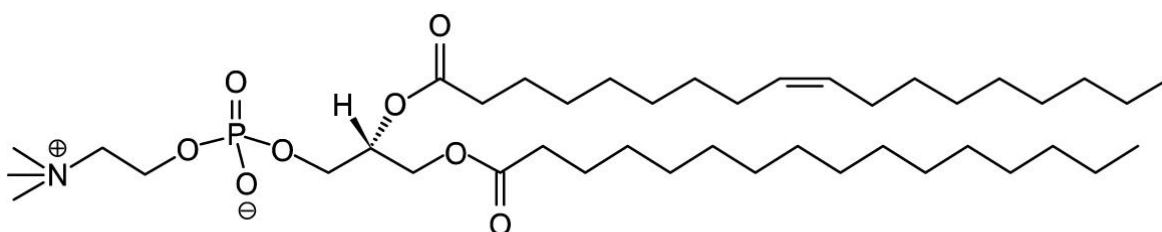


Figure 1. *Experimental set-up for deposition of phospholipid monolayer together with bound NOWA on the surface of hydrophobic carbon film (not glow discharged) of EM grid.*

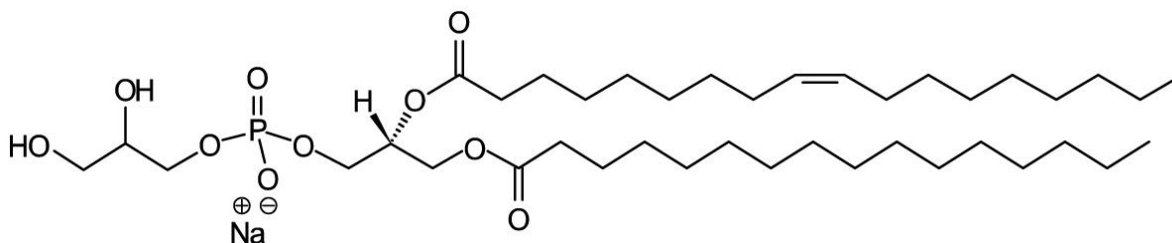
Briefly, 20 μ l of the protein solution in 10mM Tris 50mM NaCl buffer was placed in a Teflon trough (3 mm diameter, 0.5 mm deep). The surface of the solution was coated either with 1 μ l of the egg L- α -Phosphatidylcholine (PC) or lipid mixture of 75% PC and 25% of L- α -Phosphatidylglycerol (PG) at a final concentration of 0.5 mM in chloroform/hexane 1:1 (v/v). After evaporation of organic solvent the lipid monolayer is formed at the air/water interface. The trough was incubated for 30 minutes at room temperature in a closed humid chamber. The concentration of proteins (NOWA and 8 repeated MCRDC) was 50 μ g/ml. A 300 mesh carbon coated electron microscopy grid was placed on

top of the lipid monolayer, which was allowed to adsorb spontaneously on the hydrophobic surface of carbon film. Neutral negative staining of the monolayer-bound protein was performed and samples were analysed with transmission electron microscope. Schematic representation of described procedure shown on the figure 1. Electron microscopy of liposomes was performed using the same staining protocol (neutral negative stain). In all cases when samples contained lipids EM grids were not glow discharged to keep the surface of carbon grid hydrophobic and to avoid hydrophilic/hydrophobic mosaic. All phospholipids were purchased from **Avanti Lipids, Inc.**

Chemical formula of L- α -Phosphatidylcholine (PC):



For the L- α -Phosphatidylglycerol (PG):



Liposomes preparation.

SUV liposomes.

SUV (small unilamellar vesicles) were used for the immunofluorescent staining experiments as well as for the SPR (surface plasmon resonance) kinetic measurements (Biacore). Two types of liposome compositions were used: neutral 100% phosphatidylcholine (PC) and negatively charged 75% PC + 25% PG mixture. For preparation of SUVs lipids were dissolved and mixed (in case of PC/PG mixtures) in an organic solvent (chloroform : methanol mixture)

at the concentration of 50 mg lipid/ml organic solvent to assure a homogeneous mixture of lipids. Once the lipids are thoroughly mixed in the organic solvent, the solvent was evaporated using a dry nitrogen stream to yield a lipid film. The lipid film was thoroughly dried to remove residual organic solvent by placing the vial on a vacuum pump overnight. Hydration of the dry lipid film was accomplished simply by adding buffer (identical to the one used for protein solution) to the container of dry lipid and agitating. Typically the concentration of lipids in the hydration medium was 5mg/ml. The temperature of the hydrating medium was heated above the gel-liquid crystal transition temperature (T_c or T_m) of the lipid with the highest T_c before adding to the dry lipid. After addition of the hydrating medium, the lipid suspension was always maintained above the T_c during the hydration period. Hydration time was above 1 hour with vigorous shaking, mixing, or stirring. Once a stable, hydrated LMV (large multilamellar vesicles) suspension has been produced, the particles were downsized by sonication. Disruption of LMV suspensions using sonic energy (sonication) produced small, unilamellar vesicles (SUV) with diameters in the range of 15-50nm. Probe tip sonicator was used with high energies but careful temperature control (to avoid overheating). The sonication tip releases titanium particles into the lipid suspension which have been removed by centrifugation prior to use. Upon sonication the lipid suspension yielded a slightly hazy transparent solution. The haze is due to light scattering induced by residual large particles remaining in the suspension. These particles were removed by centrifugation to yield a clear suspension of SUV. The small unilamellar liposomes suspension was used for bilayer formation on surface of the Biacore chip L1 (5) or on the quartz slide soaked in Polyethyleneimine (PEI) (6).

Preparation of giant liposomes.

Gentle hydration method

Stock solutions of phospholipids (100% PC or 75% PC / 25% PG mixture) were made in chloroform. Lipid films were prepared as described above for SUV. The dry lipid mixtures were hydrated gently without agitation in pure

Millipore water (17.5 MW/cm) at 37°C (this temperature is above both phospholipid transition temperatures). A characteristic cloud containing giant liposomes was observed after several hours of incubation (12 to 36 hours) as previously described (7). Giant liposomes were examined under the light microscope. Typically size distribution of 0.3 - 3 μm was detected.

NOWA interaction with giant liposomes.

In order to study NOWA interaction with giant liposomes we used the following experimental procedure. Giant liposome solution of the desired lipid composition has been mixed with the recombinantly expressed and purified protein and incubated for several hours. For separation of the liposomes with the bound NOWA from unbound protein the solution mixture was centrifuge at 275000 g in a sucrose gradient. The visible liposome containing fraction was collected and used for transmission electron microscopy.

NOWA – bilayer interaction studied by fluorescent immunostaining.

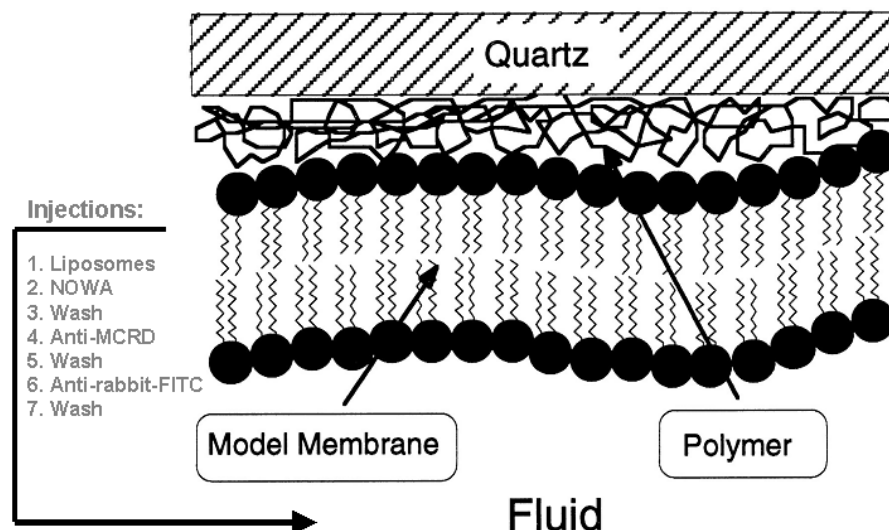


Figure 2. *Conceptual diagram of polymer-cushioned bilayer at the solid-solution interface. In our case the solid substrate was optically polished monocrystalline quartz slide. The arrows indicate polymer substrate for the model membrane deposition, model membrane and direction of liquid flow during injections.*

Special flow chamber demonstrated on figure 2 has been designed to perform immunofluorescent study of the NOWA - lipid bilayer interaction. For this study we used polymer cushioned phospholipid bilayer as a model membrane. The Polyethyleneimine PEI was used as a substrate for the PC/PG bilayer (6). The quartz slide was immersed in a 100ppm PEI solution of 0.5mM KNO₃/H₂O (Milli-Q water, pH ~7) for 15 minutes and allowed to dry for several hours. In the second step, the PEI-coated quartz was transferred into the flow cell filled with H₂O, and SUV vesicles of desired composition (100%PC or 75%PC/25%PG) were added from an aqueous stock suspension (1 mg/ml) to a final concentration of 0.14 mg/ml lipids. Bilayer formed spontaneously on the polymer substrate. To perform NOWA – membrane interaction study 50µg/ml of purified NOWA solution was injected and washed consequently by buffer 50mM Tris 100mM NaCl. To recognize NOWA bound to the bilayer the anti-MCRD (NOWA) polyclonal antibody, anti-rabbit secondary antibody labelled by FITC have been consequently injected. Each injection followed by washing with 50mM Tris 100mM NaCl buffer. The control experiment to ensure the absence of non-specific antibody membrane binding was performed. Control lacks the protein injection. Samples were examined by confocal microscopy.

Surface Plasmon Resonance principles.

To investigate the kinetics of NOWA – membrane, separate NOWA domains – membrane and C-terminal MCRD of mini-collagen – membrane interaction we applied surface plasmon resonance method utilized by Biacore technology. Surface plasmon resonance (SPR) arises when light is reflected under certain conditions from a conducting film at the interface between two media of different refractive index. In Biacore systems the media are the sample and the glass of the sensor chip, and the conducting film is a thin layer of gold on

the chip surface. SPR causes a reduction in the intensity of reflected light at a specific angle of reflection. This angle varies with the refractive index close to the surface on the side opposite from the reflected light (the sample side in Biacore). When molecules in the sample bind to the sensor surface, the concentration and therefore the refractive index at the surface changes and an SPR response is detected. Plotting the response against time during the course of an interaction provides a quantitative measure of the progress of the interaction. This plot is called a sensorgram. What Biacore actually measures is the angle of minimum reflected light intensity. The light is not absorbed by the sample: instead the light energy is dissipated through SPR in the gold film. Thus the light used to detect interaction processes never enters the sample. SPR response values are expressed in resonance units (RU). One RU represents a change of 0.0001° in the angle of the intensity minimum. For most proteins, this is roughly equivalent to a change in concentration of about 1 pg/mm^2 on the sensor surface. The exact conversion factor between RU and surface concentration depends on properties of the sensor surface and the nature of the molecule responsible for the concentration change. Figure 3 illustrates the Biacore technology described above. The figure is adapted from the Biacore website.

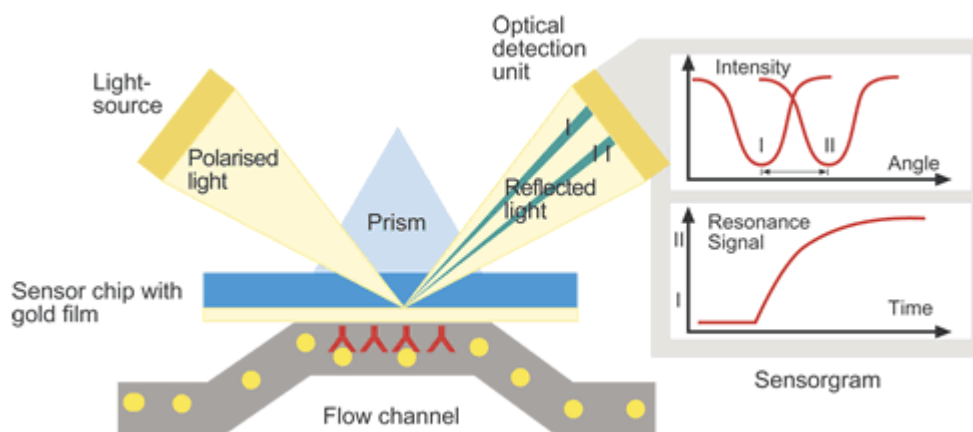


Figure 3. Illustration of the the Biacore technology principles. This figure is adapted from the Biacore website (www.biacore.com). Light passed through the prism is totally reflected. There are minimums in the intensity of the reflected light observed at the certain angles that are due to the surface

plasmon resonance. . This angle is a measure of the sample side media refractive index that change depending on mass bound to the ligand. The larger the angle the more mass is bound on the surface of the chip. As a result one can measure resonance signal time dependence.

Bilayer formation on the surface of L1 chip.

The surface of Biacore L1 chip consists of dextran modified with lipophilic compounds. These lipophilic compounds function the same way as previously described polymers for cushioned membranes. They allow the formation of lipid bilayer on the surface. Formation of such a bilayer was directly monitored by the SPR signal (RU) reflecting the amount of lipids on the surface. Figure 5 shows a characteristic sensogram of egg PC bilayer formation on the surface of L1 Biacore chip. from the injected unilamellar vesicles (see figure 4 below).

SDS-PAGE and Western blot analysis.

Samples were incubated in Laemmli buffer with or without b-mercaptoethanol and separated on 12% SDS-gels. Western blot analysis was performed using polyclonal antibody (rabbit) raised against Cys-rich octad repeat domain (ONCRD) of NOWA. Primary antibody (1:1000) was detected using an anti-rabbit-horseradish peroxidase conjugate antibody (1:2000) and the ECL chemoluminescence system (Amersham Biosciences).

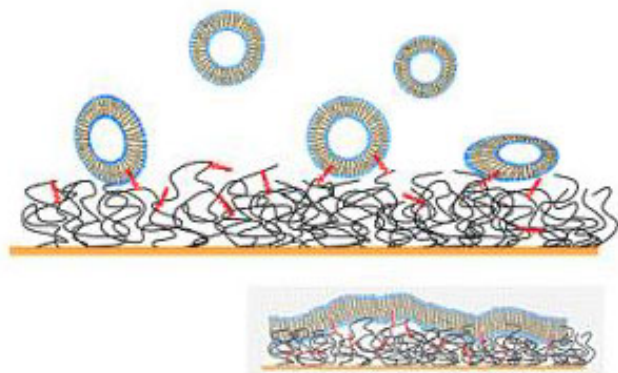


Figure 4.

Biacore chip L1 designed for liposomes capturing thus creating a bilayer on the substrate of lipophilic residues.

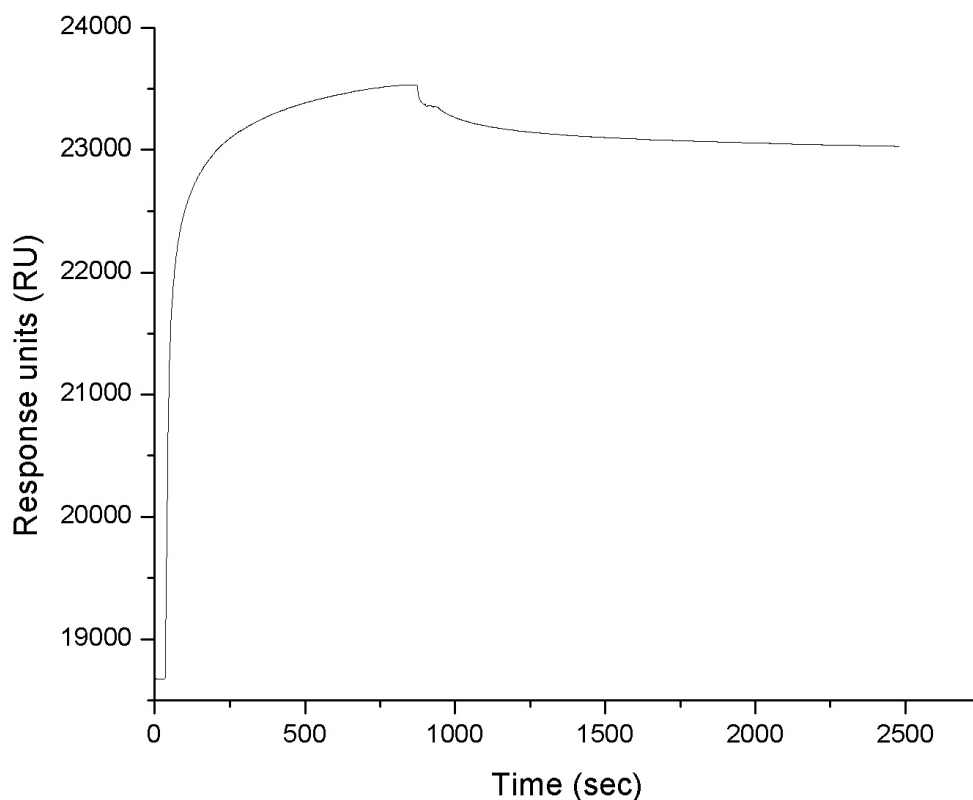


Figure 5.

Typical sensogram of PC phospholipids coupling to the Biacore chip L1. RU is a resonance units that reflect the mass bound to the surface of biosensor chip. The response was typically about 5000 RU. Liposomes capturing was performed at the low flow rate 5 $\mu\text{l}/\text{min}$ during 900 seconds (15 minutes) following by the buffer wash. Signal was stable for at least 24 hours. In order to investigate binding of NOWA to the model membrane proteins were injected over immobilized bilayer in different concentrations at the flow rate 10 $\mu\text{l}/\text{min}$.

Results and Discussion.

NOWA – lipid monolayer interaction.

Direct visualization of the NOWA binding to the model membrane has been done with neutral staining transmission electron microscopy. A technique commonly used for the two - dimensional protein crystallization was applied (8). Briefly this technique implies protein two - dimensional crystallization on the surface of the lipid monolayer. For the His-tagged soluble proteins lipid derivatized with a Ni²⁺-NTA head group molecule in 25% ratio was frequently used (8-11). Proteins at different concentrations were incubated with the lipid monolayer spontaneously created on the water/air interface. After certain incubation time lipid monolayer carrying bound protein was deposited on the non-discharged carbon EM grid, stained and analyzed with transmission electron microscopy in order to obtain 2D crystals. This approach allowed to observe proteins in certain predominant orientation even if two-dimensional crystal did not form. In order to study NOWA – monolayer interaction exactly the same procedure was applied but instead of Ni²⁺-NTA lipids either pure phosphatidylcholine (PC) or a mixture of 25% negatively charged phosphatidylglycerol (PG) and 75% PC were used. Experimental setup is shown on Fig. 1 and experimental procedure is described in details in the materials and methods section of this chapter. The idea of such setup is that only protein bound to the lipid monolayer can be visualized. If interaction did not exist we would observe nothing or lipid monolayer. In addition to qualitative control of the protein-membrane interaction this approach allows to see the preferential orientation of the bound molecules. Figure 6 represents transmission electron microscopy analysis of the recombinantly expressed full length NOWA protein bound to the surface of the lipid monolayer. Capsulomer-like structures are clearly connected to the negatively charged membrane (Fig. 6 A, C). Neutral PC phospholipid monolayer carried no bound protein as it is shown on figure 6 B. Figures A and B are presented at the same magnification. Figure C is a close view of A where the structure of phospholipid monolayer as well as well defined NOWA capsulomer-like globule are unambiguously observed. Regions of monolayer covered carbon film can be clearly distinguished from the non-covered carbon film. On the figure 6 the borders of such regions

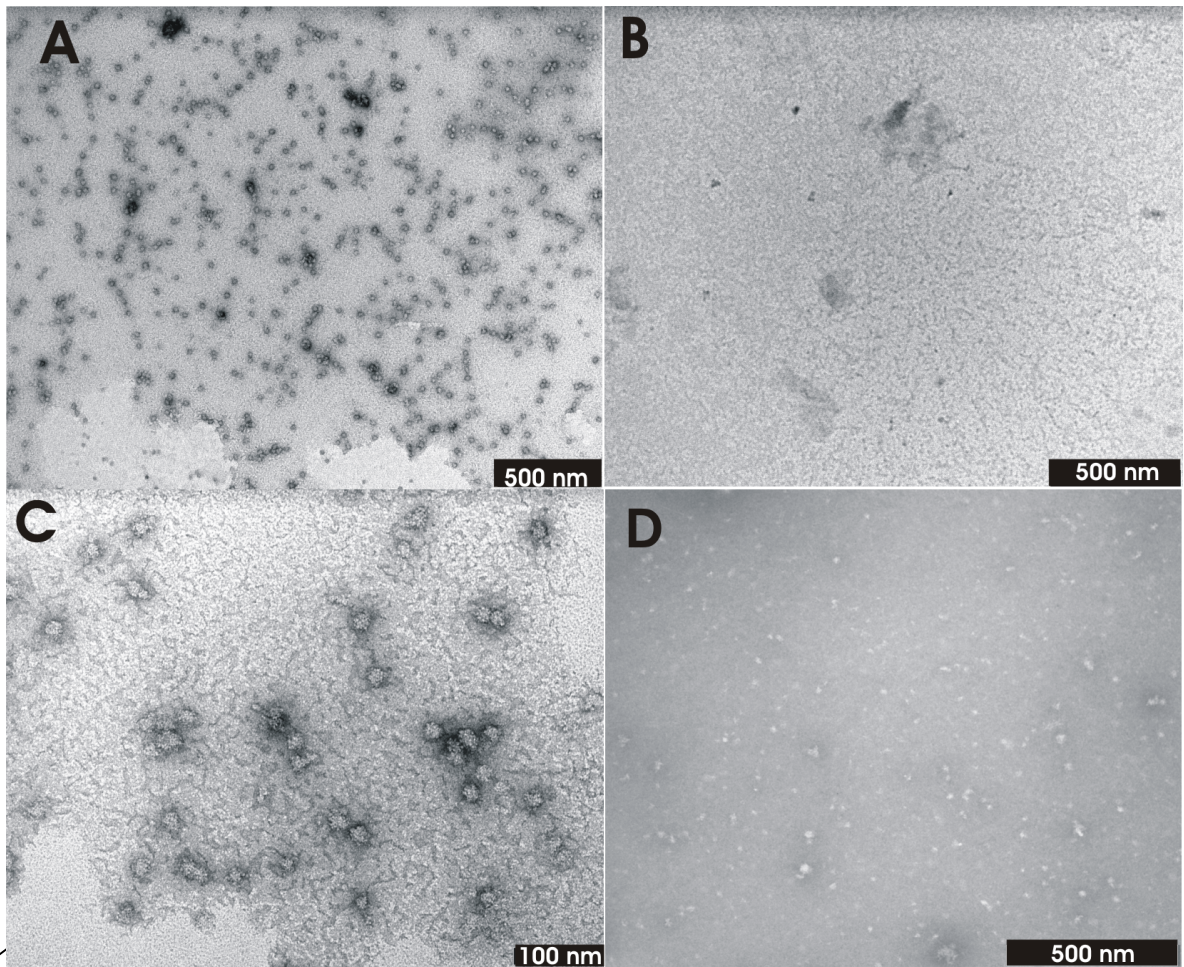


Figure 6

Transmission electron microscopy analysis of NOWA interaction with negatively charged (75% PC+25% PG) phospholipid monolayer (A, C). In contrast to the negatively charged monolayer the neutral 100% PC model membrane carrying no bound protein (B). Figures A and B are presented at the same low magnification. Figure C is a close view of A where the structure of phospholipid monolayer as well as well defined NOWA capsulomer precursors are unambiguously observed. Regions of monolayer covered carbon film can be clearly distinguished from the non-covered carbon film. The borders separating these regions are indicated by arrows. In comparison to the monolayer neutral negative staining of NOWA adsorbed on the surface of non-discharged carbon grid is represented on figure D.

indicated by arrows. Neutral negative staining of NOWA adsorbed on the surface of non-discharged carbon grid is represented on figure D.

NOWA – bilayer interaction.

Binding of NOWA to the giant liposomes.

Considering the fact that NOWA is a secreted protein and has no predicted transmembrane sequences we assumed that membrane affinity of this protein is due to its interaction with the surface of the membrane. Electron microscopy analysis qualitatively demonstrated NOWA – monolayer surface affinity is strongly supporting the above assumption. In general, transmembrane domain would need some space inside the membrane to be incorporated. Therefore lipid monolayer adsorbed on the EM carbon grid most likely could not supply enough space for incorporation of transmembrane protein. Nevertheless lipid bilayer is a better model of the real cellular membrane. Consequently we performed our further investigation of NOWA – membrane interaction including kinetic studies using bilayer as a model system. As a qualitative control we used transmission electron microscopy analysis of NOWA capsulomers binding to the “giant” liposomes. Giant liposomes were prepared by gentle hydration method as described in details in materials and methods section. Recombinantly expressed and purified NOWA was added into solution of the giant liposomes and incubated for several hours. Giant liposome fraction was separated via centrifugation and used for neutral negative staining TEM. On the figure 7 upper panel represents resulting liposomes with bound NOWA capsulomers. Lower panel of figure 7 shows magnified view of the capsulomer-like globules on the surface of liposome or at its border. The locations of magnified regions indicated by circles and arrows. Only negatively charged liposomes carried the protein. Liposomes composed of pure neutral phosphatidylcholine (PC) had normal shape but capsulomer precursors were not found on their surface (data not shown). These data clearly demonstrate the affinity of NOWA to the negatively charged phospholipid bilayer.

NOWA – bilayer interaction.

Immunofluorescent study.

In addition to electron microscopy analysis of the giant liposomes we performed immuno fluorescent staining of NOWA bound to the flat negatively charged bilayer.

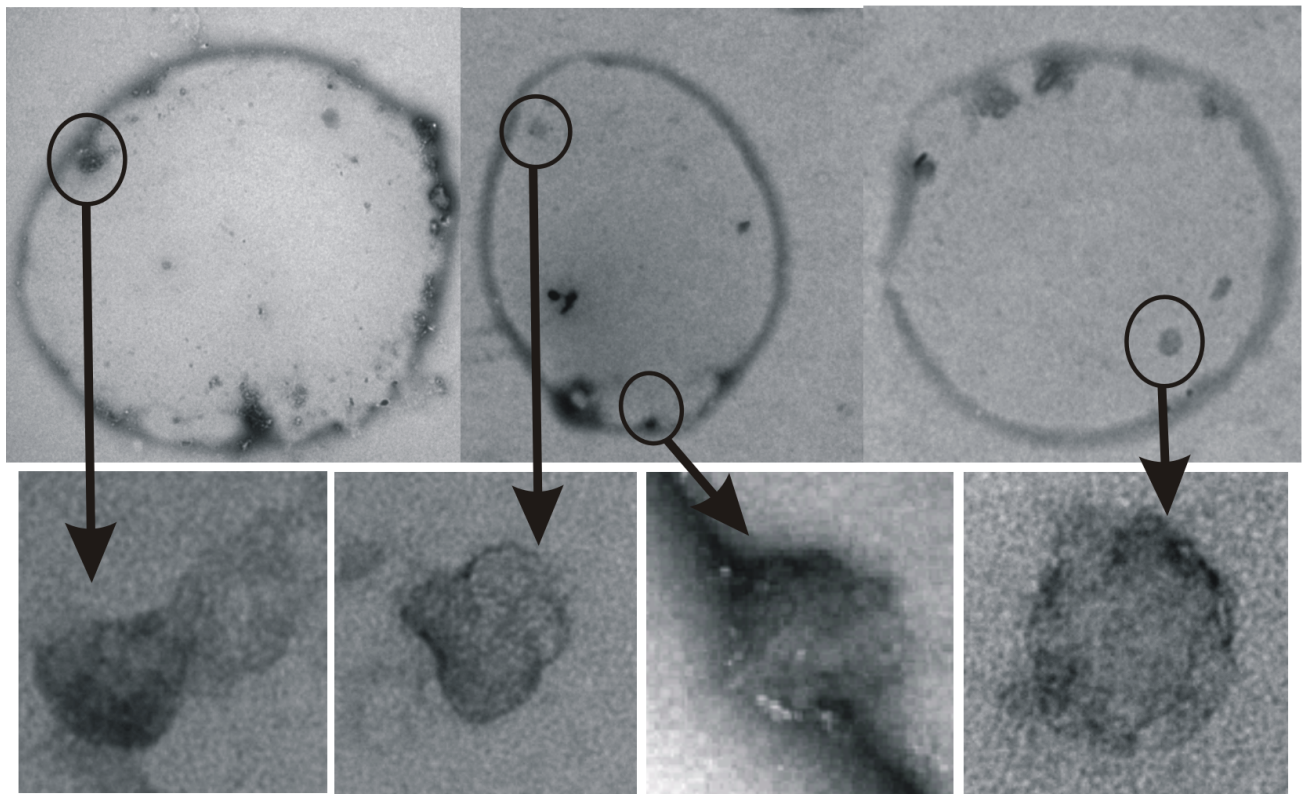


Figure 7.

Transmission electron microscopy analysis of NOWA capsulomers binding to the “giant” liposomes. Upper panel shows single liposomes stained with 2% Na Ph after incubation with recombinantly expressed NOWA and separation of liposome fraction from the unbound protein fraction. Lipid composition of liposomes was 75% POPC+25% POPG. Lower panel is a close view of the capsulomer precursors on the surface of liposome or at its border. Particular locations of the magnified regions are indicated by circles and arrows.

Special flow chamber has been constructed for this experiment. Figure 2 in the materials and methods section of this chapter demonstrates a conceptual diagram of polymer-cushioned bilayer at the solid-solution interface that coincides with the constructional principles of the designed flow chamber. In our case the solid substrate was optically polished monocrystalline quartz slide. Arrows shown on figure 2 indicate polymer substrate (polyetheleneimine) for the model membrane deposition, model membrane and direction of liquid flow during injections. This method of the model membrane deposition allows formation of defined lipid bilayer on the surface of polymer substrate (6). Injection of NOWA over lipid bilayer followed by injections of specific antibody, washing buffer, fluorescently labelled secondary (anti-rabbit) antibody and washing buffer accordingly. Results were observed with confocal microscope and are presented on the figure 8. Data from the described set of injections shown on figure 8A is compared to the control experiment where injection of NOWA has been omitted (Fig. 8B). Control experiment ensures the absence of non-specific antibodies - model membrane interaction. Positive experiment (Fig.8A) supplies another proof for the NOWA – negatively charged membrane interaction. Furthermore observable shape of the membrane bound protein is again spherical and some cluster formation of the NOWA capsulomers can be noticed. Summarizing qualitative protein-membrane binding experimental data we can now confirm the following thesis:

- recombinantly expressed NOWA binds to the model membrane systems of the 25% : 75% of negatively charged : neutral phospholipid composition;
- such binding happens with similar efficiency to the monolayer and bilayer of the same composition;
- neutral membrane systems do not bind the protein. Consequently electrostatic mechanism might be important for NOWA – membrane interaction;
- NOWA–membrane association does not interfere with capsulomer-like globules formation. NOWA capsulomers are able to form cluster of the membrane surface.

Nevertheless two questions are still open: how strong is the NOWA-membrane interaction and what protein sequence or domain is responsible for this association. In order to answer these questions quantitative kinetic study of the NOWA and its separate domains interaction with the charged bilayer have been performed.

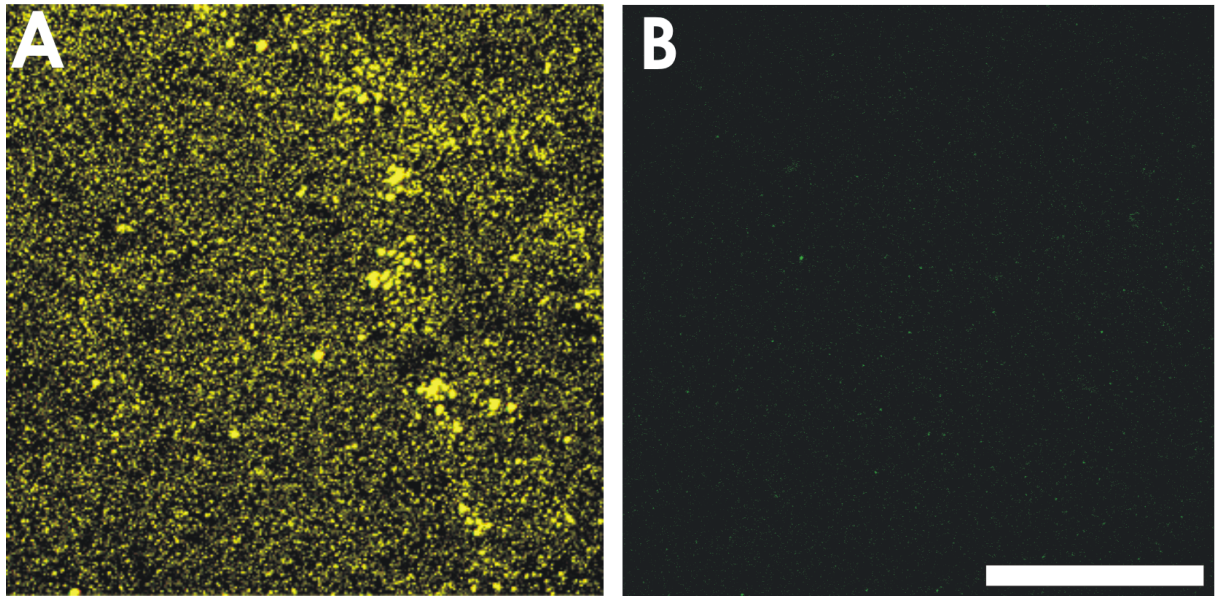


Figure 8

Immuno-fluorescent study of NOWA - membrane interaction. Figure represents confocal microscopy images of the positive NOWA – charged lipid bilayer interaction (A) and negative control (B). Experimental setup is described in materials and methods and shown on figure 2. Injections were as follows: A, NOWA, anti-OMCCR polyclonal antibody, washing buffer, anti-rabbit secondary antibody labelled by FITC, washing buffer consequently. Washing buffer composition was 50mM Tris 100mM NaCl pH 7. Control experiment was done with the same set of injections except injection of NOWA. Bar is 10 μ m. Figure A is a stereo image.

To investigate the kinetics of NOWA – membrane, separate NOWA domains – membrane and C-terminal mini-collagen cysteine rich domain (MCRD) – membrane interaction we applied surface plasmon resonance (SPR) method utilized by Biacore technology. The use of biosensors employing surface plasmon resonance (SPR) provides excellent instrumentation for a label-free, real-time investigation of biomolecular interactions. General principles of SPR technology described in the materials and methods section can be summarized in a following way. Surface plasmon resonance arises when light is reflected under certain conditions from a conducting film at the interface between two media of different refractive index. SPR causes a reduction in the intensity of the reflected light at a specific angle of reflection. This angle varies with the refractive index close to the surface on the side opposite from the reflected light i.e. sample side. Sample side refractive index changes depending on the mass bound on the surface of the chip. Therefore monitoring of the SPR angle directly corresponds to the mass change on the surface of biosensor chip. In our case the surface of the biosensor chip represented by the surface of model membrane immobilized on the Biacore L1 chip substrate. This biosensor chip has modified dextran matrix allowing the capture of the lipid vesicles and formation of a flexible phospholipid bilayer. Phospholipid liposomes composed of phosphatidylglycerol and phosphatidylcholine were injected onto the surface of a L1 biosensor chip. Because injection of 50 mM NaOH did not change the mass immobilized to the biosensor chip, it was concluded that a stable phospholipid bilayer had formed on the chip. Typical sensogram of the bilayer formation is shown on figure 5 of materials and methods section. The surface plasmon resonance signal from the immobilized bilayer was typically about 5000 RU. This signal was stable for at least 24 hours and was not changed upon washing with any of the incubation buffers (data not shown). The experiments comprising separate set (related to the particular specie at the certain conditions) were performed during the time of bilayer stability. To ensure the completeness of the chip coverage by the model membrane we used a short pulse of the 0.1 mg/ml serum albumin (BSA). It is known that BSA interacts with the L1 biosensor chip modified dextran matrix (about 400 RU) but does not interact with the lipid bilayers (20 RU). Response signal from the surface assembled model membrane has been corrected to zero for all kinetic curves. Flow

rate for all kinetic measurements was 10 $\mu\text{l}/\text{min}$ which allowed to avoid diffusion limited kinetic and to minimize the usage of protein at the same time.

In order to demonstrate the presence of NOWA protein on the surface of model membrane (25% PG) after injection of protein the experiment shown on figure 9 has been performed. At zero time NOWA solution has been injected over previously immobilized lipid membrane. Injection was stopped at 150 seconds and immediately followed by the injection of the antibody against C-type lectin domain of NOWA. Specific antibody – protein interaction unambiguously showed that NOWA was present on the lipid bilayer. Non-specific interaction of anti/NOWA/CTLD with the model membrane has been checked and found to be negligible compare to the protein – antibody recognition. Dissociation of the NOWA – antibody complexes started at 300 seconds (Fig.9 indicated by arrow). This dissociation kinetic coincides with the dissociation kinetic of NOWA from the membrane as will be demonstrated later in this chapter. Therefore described experiment clearly shows the possibility of quantitative kinetic analysis of the NOWA binding to the phospholipid bilayer.

In order to determine K_D value for NOWA – membrane association we measured concentration dependent kinetics and plotted the equilibrium response signal against logarithmic scale of the molar protein concentration. Corresponding dissociation constants were determined from the resulting equilibrium isotherm as a protein concentration at 50% saturation. NOWA – membrane association was found to be calcium dependent. Therefore two sets of concentration dependent kinetics were measured in the presence and absence of Ca^{2+} . These data are presented on the figure 10. According K_D values determined from the equilibrium isotherms are specified on the lower panel of figure 10. The isotherm plotted for the set of experiments with calcium did not reach the saturation consequently K_D value in this case could not be determined reliably by this approach. Measurements of the higher NOWA concentrations were not possible because of the protein precipitation in the solution. As we already seen from the qualitative binding experiments NOWA – membrane interaction is a complex process of capsulomer – like structures association in parallel with aggregation of protein on the surface and in solution. Thus binding constants determined by the equilibrium analysis are can not be considered reliable.

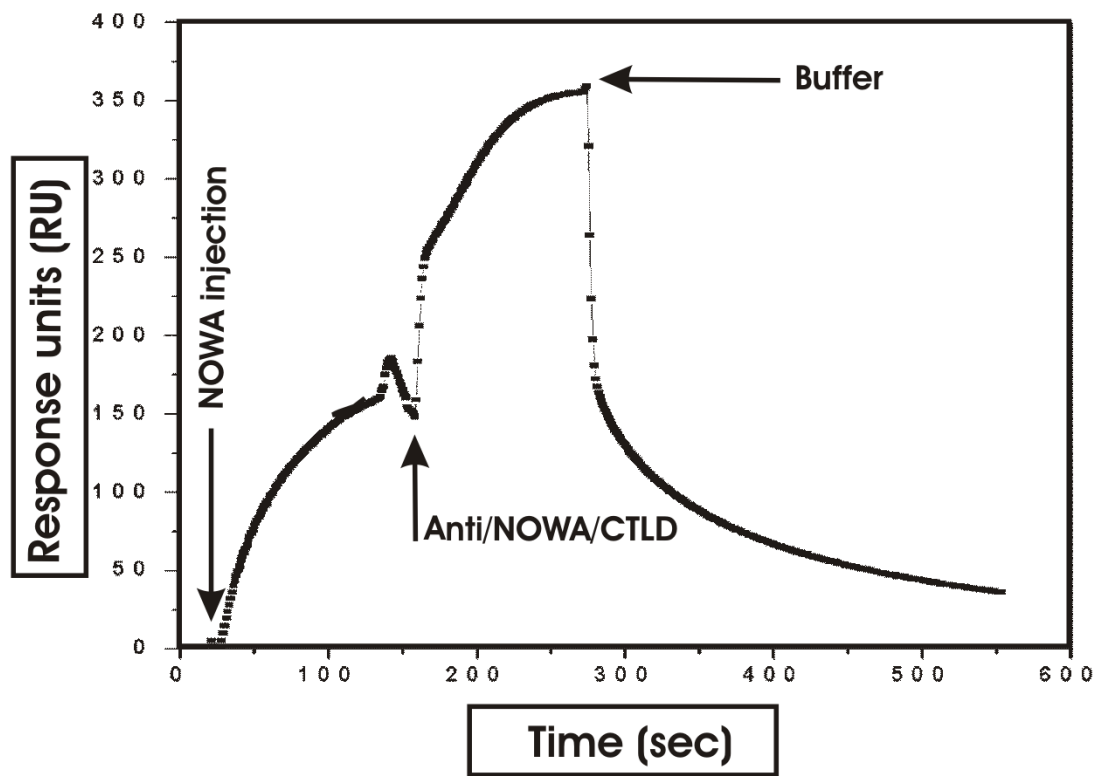


Figure 9.

Biacore study of the NOWA – negatively charged (25% PG : 75% PC) lipid bilayer interaction. Response signal from the surface assembled model membrane has been corrected to zero. Flow rate was 10 $\mu\text{l}/\text{min}$. At zero time NOWA in the concentration of 777 nM has been injected over lipid membrane. Injection was stopped at 150 seconds and immediately followed by the injection of the antibody against C-type lectin domain of NOWA. Dissociation of the NOWA – antibody complexes started at 300 seconds. At this time injected antibody solution was replaced by running buffer of the same composition as it was used for both protein and antibody (10 mM Tris, 50mM NaCl pH 7)..

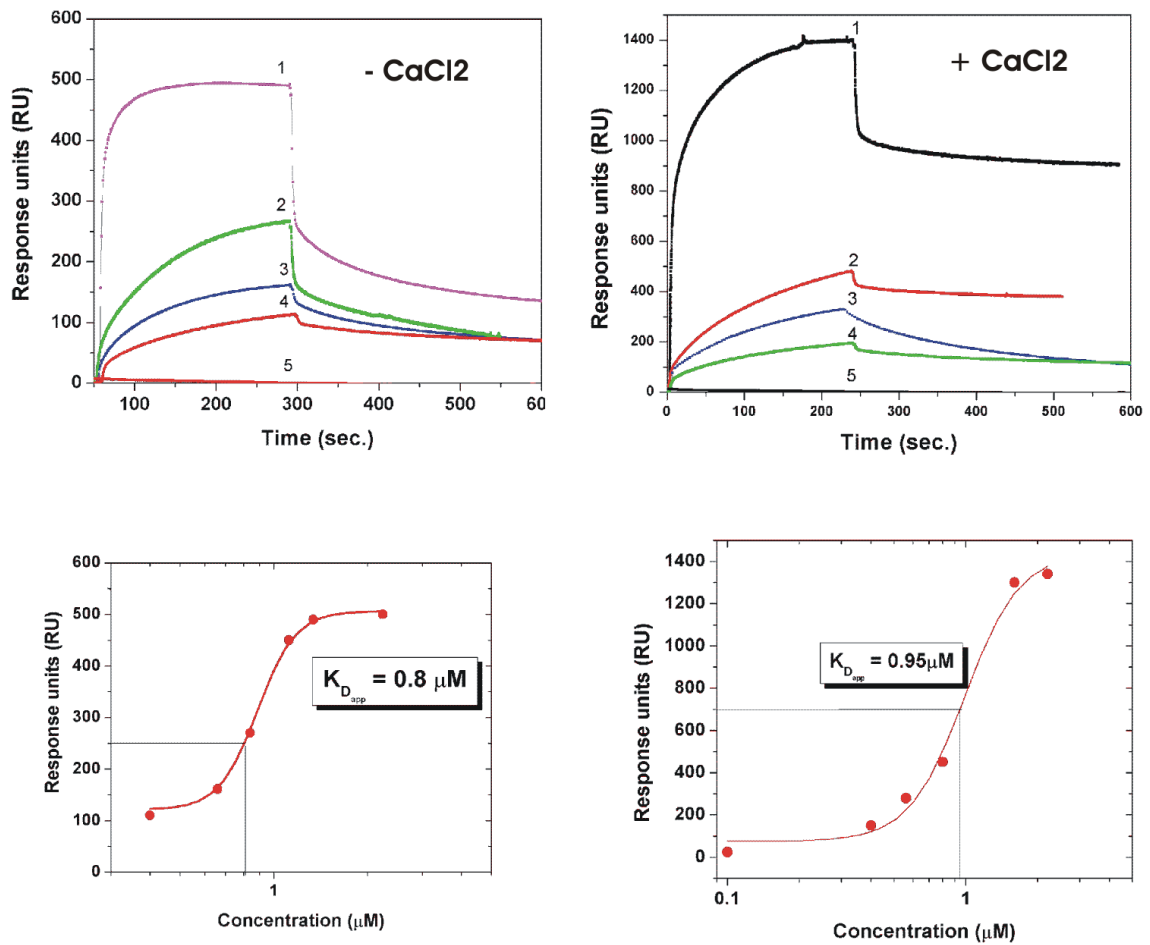


Figure 10.

Analysis of NOWA – lipid bilayer interaction. Association and dissociation kinetics of NOWA – model membrane have been measured by surface plasmon resonance at different protein concentrations. Composition of running buffers were 10 mM Tris, 50mM NaCl (A) and 10 mM Tris, 50mM NaCl, 10mM CaCl₂ (B). The equilibrium response signal was plotted against logarithmic scale of molar protein concentration C, D for both sets of experiments. Corresponding K_d values determined as a concentration at the half saturation indicated on figures.

In addition to the equilibrium isotherms analysis we applied kinetic analysis to determine association, dissociation rates and therefore kinetically derived binding constants. Due to the complex binding behaviour kinetic data could not be fitted by a simple model implying the binding of single specie to a single binding site, i.e $A + B = AB$ for association phase and $AB = A + B$ for dissociation. However a model assuming parallel dissociation of two different complexes applied to the dissociation phase fitted the curves with reasonable accuracy. This model can be described in the following terms: $A_i B_j = A_i + B_j$. By fitting the data to this model we have calculated the dissociation rate constants k_{d1} and k_{d2} for two complexes that are independently dissociate from the membrane surface. These two complexes are found to dissociate with the rates which differ ten times in the order of magnitude (table 1). In terms of our system two independent species as single capsulomer-like globules and aggregates of any size higher than single capsulomer. Cluster (aggregates) formation was found to be calcium dependent (see chapter 1). Although we performed the kinetic measurements in the absence of calcium chelating agents were not added in the solution implying the presence of some residual divalent ions. Consequently some clusters were present in protein solution as it was always seen by transmission electron microscopy. In addition to the existing solution aggregates there is an aggregation process happening on the surface of the model membrane. We assigned higher dissociation rate to the aggregates of NOWA capsulomers no matter of their origin (solution or surface aggregation). Single capsulomer precursors appeared to have very slow dissociation rate constant in the other words single NOWA capsulomers almost irreversibly bind to the negatively charged membrane surface. This was already obvious from the qualitative studies. In all qualitative experiments NOWA bound to the membrane was extensively washed out nevertheless every time protein stayed on the surface. Although some clusters were also present on the surface of lipid monolayer single capsulomer – like structures were found to be much more abundant. We assumed in our kinetic study that single capsulomer-like globules have higher affinity to the membrane surface and therefore higher association rate in addition to the slower dissociation rate. Using above assumptions we performed an analysis of the binding kinetics in the presence and absence of calcium. The curves were well fitted using Biaevaluation software supplied by Biacore. The resulting rate constants and according affinity constants are

Table 1.

Kinetic constants for binding of NOWA, C-type lectin domain of NOWA and C-terminal minicollagen cysteine rich domain to the model negatively charged (25% PG) membrane obtained from the evaluation of association and dissociation phases (I) and equilibrium binding data (II).

	$k_{d1} \text{ (s)}^{-1}$	$k_{d2} \text{ (s)}^{-1}$	$k_{a1} \text{ (M*s)}^{-1}$	$K_{D1} \text{ (M) (I)}$	$K_D \text{ (M) (II)}$	$K_{A1} \text{ (M)}^{-1} \text{ (I)}$
NOWA full length no CaCl₂	$(1.6 \pm 0.4) \times 10^{-3}$	$(3 \pm 1) \times 10^{-2}$	$(2.3 \pm 0.5) \times 10^4$	$(0.7 \pm 0.3) \times 10^{-7}$	$(0.8 \pm 0.2) \times 10^{-6}$	$(1.6 \pm 0.9) \times 10^7$
NOWA full length 10mM CaCl₂	$(5.6 \pm 0.4) \times 10^{-3}$	0.2 ± 0.1	$(3.2 \pm 0.8) \times 10^4$	$(1.8 \pm 0.5) \times 10^{-7}$	$(0.9 \pm 0.3) \times 10^{-6}$	$(0.6 \pm 0.3) \times 10^7$
CTLD (NOWA domain)	$(1.4 \pm 0.1) \times 10^{-2}$	n. a.	$(1.1 \pm 0.1) \times 10^4$	$(1.3 \pm 0.2) \times 10^{-6}$	$(1.1 \pm 0.3) \times 10^{-6}$	$(0.8 \pm 0.2) \times 10^6$
MCRD (C-terminal domain of minicollagen)	$(5.9 \pm 0.3) \times 10^{-4}$	n. a.	240 ± 50	$(2.1 \pm 0.6) \times 10^{-6}$	n. d.	$(0.4 \pm 0.2) \times 10^6$

summarized in the table 1. Kinetic analysis in the above assumptions revealed affinity of single NOWA capsulomers to the membrane of 100nM. At the same time K_D values calculated from the equilibrium isotherms were about 1 μ M. This contradiction is due to the presence of clusters that have much lower affinity to the membrane but much higher molecular mass reflected in the equilibrium SPR response signal. Consequently the affinity constants obtained from the equilibrium plots related rather to the strength of clusters – membrane association or surface clusters formation. At low initial protein concentrations (100 nM) either with or without calcium there are no high aggregates present in the solution and binding kinetics determined only by single capsulomers. Such curves were successfully fitted using a simple $A + B = AB$ consideration and revealed the rate constants identical to those present in the complex model. The difference in the membrane affinity for NOWA capsulomers and their clusters is in good agreement with the cluster melting and diffusion towards the membrane during nematocyst morphogenesis. Once calcium concentration is dropped (increase in poly- γ -glutamate concentration) the capsulomer precursor conglomerates melt, their membrane affinity rises ten times and they diffuse to the wall of the developing capsule. Another hypothesis arises from the diminished membrane affinity of NOWA conglomerates. One can speculate that cluster formation and membrane binding utilize the same protein domain thus aggregation process interferes with the capsulomer - membrane interaction. On the other hand once membrane surface is completely covered by capsulomers the same binding mechanism switched to the aggregation in order to add another wall layer. On this stage aggregation process must be accomplished by NOWA – mini-collagen disulfide isomerization. To specify the particular domain of NOWA responsible for the membrane binding we performed kinetic studies described below.

Binding of NOWA domains to phospholipid bilayer.

The membrane binding of two separate domains of NOWA – ONCRD (8 folded cysteine rich domain) and CTLD (C-type lectin domain) were examined by surface plasmon resonance. Both domains were shown to be structured after expression by CD in case of CTLD and electron microscopy in case of OMCCR. ONCRD recombinant construct was expressed without native C-terminal sequence of NOWA which carrying a strong positive charge. Figure 11 represents the results of

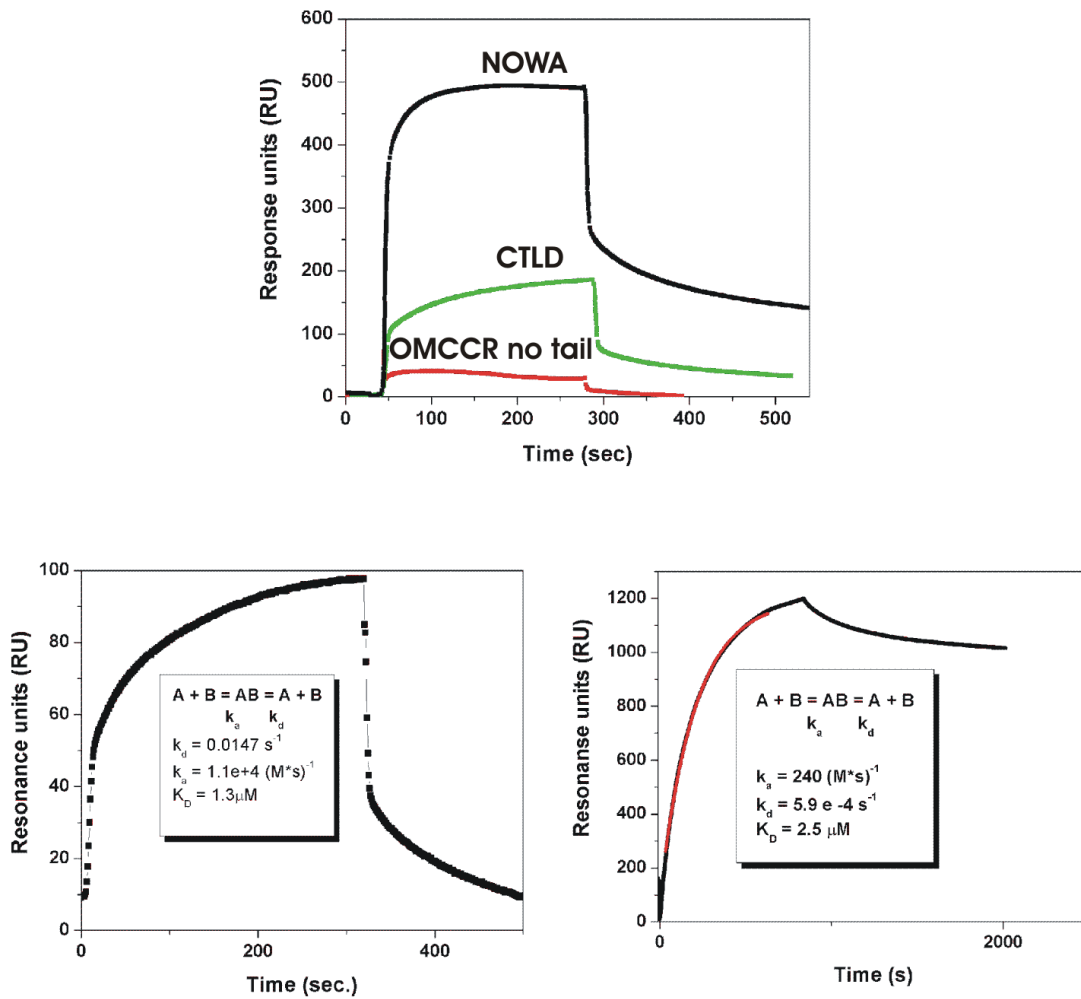


Figure 11

A. Kinetics of NOWA, CTLD, and OMCCR binding to the 25% PG containing membrane measured by surface plasmon resonance. Molar concentrations of proteins were 1.5 μM . OMCCR exhibits no binding. **B.** Kinetic constants calculated using one to one model for the CTLD – membrane interaction shown for the particular curve of 0.5 μM protein concentration. **C.** The C-terminal minicollagen cysteine rich domain (MCRD) – model membrane interaction. The peptide carrying a native charged tail was injected in concentration of 38 μM . Calculated kinetic constants are indicated on figure. Red colour curve represents the fitting of association phase.

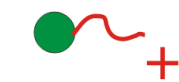
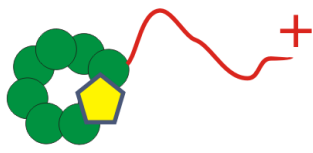
performed experiments with the domains binding to the lipid bilayers. Comparison of the association and dissociation kinetics of NOWA, CTLD and ONCRD to the 25% PG containing membrane measured by surface plasmon resonance is present on figure 11A. Molar concentrations of proteins were 1.5 μM equal for all samples. It is immediately obvious from the kinetics that CTLD binds to the membrane in contrast to the ONCRD exhibiting no binding. Kinetic constants for the NOWA CTLD – membrane binding determined using first order reaction model are summarized in the table 1. The membrane affinity of the C-type lectin domain is about 10 times smaller than that of NOWA. The association rate is slower and dissociation is more easily happening. Therefore one can conclude that CTLD even though contributing to the NOWA – membrane interaction does not take the whole responsibility. There must be additional mechanism involved. We assumed that higher affinity is due to the positively charged C-terminal sequence of NOWA which is most probably flexible and can lead to the electrostatic interaction of protein with the negatively charged membrane. The absence of ONCRD – membrane binding is a side evidence for this hypothesis. In order to check if charged tail – membrane interaction exist we performed the same type of experiments with the C-terminal cysteine rich domain of the minicollagen – 1 (MCRD). The structure of this domain was solved and will be discussed in details in the next chapter. We will also show in the following chapters that C-terminal MCRD revealed a new fold which is shared by NOWA cysteine rich domains. Therefore the MCRD can be considered as a model system for the last cysteine rich repeat of NOWA. We speculate here that the native C-terminal sequence of NOWA following the last cysteine rich repeat has structural and functional properties similar to those of the C-terminal tail of minicollagen. Direct use of the last NOWA cysteine rich repeat with the long native terminal sequence was more complicated because of the solubility problems. The MCRD of minicollagen showed strong binding to the model membrane as it was expected. Kinetic constants calculated from this experiment are also presented in table 1. Characteristic association/dissociation kinetic of MCRD to the 25% PG bilayer is shown on the figure 11C. In contrast to MCRD single NOWA cysteine rich domain had no membrane affinity though it has very similar structure including C-terminal flexible tail. The only difference between these two peptides is the charge of their tail residues: in case of NOWA peptide tail carries no charge. Schematic representation of NOWA

cysteine rich domain structural organization, summarized membrane binding properties of investigated molecules and alignment of the C-terminal sequences of NOWA and minicollagen – 1 are presented on the figure 12.

Concluding the results of this chapter we showed that recombinantly expressed NOWA exhibits binding to the negatively charged model lipid membranes. This binding is strong for single capsulomer-like NOWA globules and becomes weaker for higher aggregates. C-type lectin domain of NOWA was shown to participate in the membrane binding although additional mechanism is required to accomplish the strength of full-length protein interaction. This additional mechanism is proposed to be due to the electrostatic interaction of C-terminal positively charged NOWA sequence with negatively charged surface of lipid membrane.

A

NOWA composed of OMCCR(●) and CTLD(◊) with native charged tail

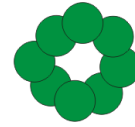


C-terminal MCRD

Membrane interaction



Recombinant OMCCR lacking native tail



First repeat of NOWA cysteine rich domain carrying non/charged tail

No membrane interaction



B

C-terminal of NOWA -

CSLQQPGCSSACAPACRLSCSLGRMNLRKRSHVHHKCLKASRKKKQSKA
CPPV CVAQCVPTCPQYCCPAKRK

C-terminal of Minicollagen-1

Figure 12.

- A.** Schematic drawing of the hypothetical domain organization of the NOWA cysteine rich domain and CTLD with and without positively charged C-terminal sequence. The scheme summarizes membrane binding properties found for the NOWA protein and for the domains of NOWA and minicollagen. We claim that NOWA – membrane interaction is due to both C-type lectin domain and charged C-terminal sequence of the protein.
- B.** Aligned sequences of the very C-terminal cysteine rich repeat of NOWA and C-terminal CRD of minicollagen. Positively charged residues colored in red and cysteines colored in green.

References.

1. R. Golz, *J. Morphol* **222**, 49-59 (1994).
2. C. Wurm, TECHNISCHE UNIVERSITÄT Darmstadt (2003).
3. U. Engel *et al.*, *Embo J* **20**, 3063-73 (Jun 15, 2001).
4. E. Vives, J. P. Richard, C. Rispal, B. Lebleu, *Curr Protein Pept Sci* **4**, 125-32 (Apr, 2003).
5. C. Williams, S. Cook, M. Knoppers, **BIAjournal** (2000).
6. J. Y. Wong *et al.*, *Biophys J* **77**, 1445-57 (Sep, 1999).
7. D. Needham, E. Evans, *Biochemistry* **27**, 8261-9 (Oct 18, 1988).
8. E. W. Kubalek, S. F. Le Grice, P. O. Brown, *J Struct Biol* **113**, 117-23 (Sep-Oct, 1994).
9. C. Venien-Bryan *et al.*, *J Mol Biol* **274**, 687-92 (Dec 19, 1997).
10. E. Barklis, J. McDermott, S. Wilkens, S. Fuller, D. Thompson, *J Biol Chem* **273**, 7177-80 (Mar 27, 1998).
11. E. Barklis *et al.*, *Embo J* **16**, 1199-213 (Mar 17, 1997).

Chapter 3**

The structure of the Cys-rich terminal domain of *Hydra* minicollagen, which is involved in disulfide networks of the nematocyst wall.

Elena Pokidysheva ^{1*}, Alexander G. Milbradt^{2*}, Sebastian Meier^{3*}, Christian Renner^{2#}, Daniel Häussinger³, Hans Peter Bächinger⁴, Luis Moroder², Stephan Grzesiek^{3#}, Thomas W. Holstein ⁵, Suat Özbek^{1#} and Jürgen Engel¹.

¹Department of Biophysical Chemistry, Biozentrum, University of Basel, Klingelbergstrasse 70, CH-4056 Basel, Switzerland

²Max-Planck-Institute for Biochemistry, D-82152 Martinsried, Germany

³Department of Structural Biology, Biozentrum, University of Basel, Klingelbergstrasse 70, CH-4056 Basel, Switzerland

⁴Shriners Hospital for Children and Department of Biochemistry and Molecular Biology, Oregon Health & Science University, Portland, OR 97239, USA

⁵Institute of Zoology, Technical University of Darmstadt, Schnittpahnstrasse 10, D -64287 Darmstadt, Germany

*Note: these authors contributed equally to this work

**Note: This work is published in Journal of Biological Chemistry

Abstract

The minicollagens found in the nematocysts of *Hydra* constitute a family of invertebrate collagens with unusual properties. They share a common modular architecture with a central collagen sequence ranging from 14-16 Gly-X-Y repeats flanked by polyproline / hydroxyproline stretches and short terminal domains that show a conserved cysteine pattern (CXXXCXXXCXXXCXXC). The minicollagen cysteine-rich domains (MCRD) are believed to function in a switch of the disulfide connectivity from intra- to intermolecular bonds during maturation of the capsule wall. The solution structure of the C-terminal fragment including a MCRD of minicollagen-1 was determined in two independent groups by ¹H NMR. The corresponding peptide comprising the last 24 residues of the molecule was produced synthetically and refolded by oxidation under low protein concentrations. Both presented structures are identical in their fold and disulfide connections (Cys2-Cys18, Cys6-Cys14, Cys10-Cys19) revealing a robust structural motif that is supposed to serve as the polymerization module of the nematocyst capsule.

Introduction

Minicollagens of nematocysts in *Hydra*, corals and other cnidaria are very unusual proteins with structural properties not shared by other invertebrate or vertebrate collagens. From both the N- and the C-terminus of the collagen triple helix emerge three polyproline-II-type helices, which consist of 5 to 23 proline or hydroxyproline residues (1-3). Each of the PPII-helices is terminated by a small Cys-rich domain, termed minicollagen Cys-rich domain (MCRD). The N- and the C-terminal MCRDs are homologous and share the cysteine pattern CXXXCXXXCXXXCXXC. A small propeptide region preceding the N-terminal MCRD is cleaved off during expression, and mature minicollagen has a rather symmetrical appearance with closely similar structural elements at both sides. This bipolar nature of minicollagen is unique among all other known collagens (4-7) and suggests a special function.

A unique function of minicollagen is also suggested by its restricted appearance in the capsule wall of nematocysts. Nematocysts are complex explosive organelles, which basically consist of a capsule, an inverted tubule armed with spines and an operculum. The tubule is connected to the capsule wall and is twisted in many turns inside the osmotically charged capsule matrix. Following stimulation, the internal tube is expelled, the osmotic pressure is released and capsule contents including toxins are released at the tubule end. This specialized form of exocytosis proceeds with ultra-fast rates and accelerations comparable to those of a fired bullet (8).

The capsule wall resists more than 150 atmospheres of osmotic pressure in the charged state. For *Hydra* nematocysts it consists mainly of two proteins: minicollagen and nematocyst outer wall antigen (NOWA) (9-11). The two proteins can be dissolved from capsule preparations only under reducing conditions. Already at a time at which the amino acid sequence of minicollagens was unknown it was found that these collagens formed disulfide cross-linked polymers that were insoluble in SDS but easily soluble in the presence of a reducing agent (12,13). Following the discovery of a family of minicollagens (3) and recombinant expression of minicollagen-1 (9) it was found that the proteins are expressed in a soluble precursor form present in the endoplasmatic reticulum and post-Golgi vacuoles in *Hydra*. They are converted to the disulfide linked assembly form of the nematocyst wall upon wall compaction, during which a dense and well-defined

capsule wall is formed (9). The morphological changes, a loss of accessibility to antibodies against minicollagen-1 and a parallel loss of solubility under non-reducing conditions suggested a close link between disulfide polymerization and the condensation of wall proteins. Both processes provide an explanation for the unusually high tensile strength of the mature nematocyst wall.

Minicollagen-1 of *Hydra* recombinantly expressed in mammalian cells contains internal disulfide bonds in its MCRDs but no interchain disulfide cross-links between chains (9). The trimeric collagen molecules dissociated into single chains when heated to 45°C under non-reducing conditions (10). Reduction did not influence this transition temperature indicating that only the collagen domain is responsible for trimerization. Recombinant minicollagen-1 was found to form aggregates in electron micrographs but no disulfide bridges were formed spontaneously under *in vitro* conditions (9). This material behaved like the precursor form *in vivo* and could be solubilized by SDS or other denaturants under non-reducing conditions. It was therefore concluded that disulfide isomerases or other external parameters are required for a disulfide reshuffling process by which internal disulfide bridges are converted to intermolecular links (14).

More recent results suggest, that the structural function of minicollagens in wall hardening is complemented by NOWA (11). Altogether ten domains were identified in this protein, namely a SCP-domain (smart00198), a C-type lectin domain (CTLD, smart00034) and 8 C-terminal domains with homology to the MCRDs. In particular, the pattern of six cysteines is shared by the corresponding domains in NOWA and minicollagen. The presence of homologous Cys-rich domains in both proteins suggested a joint function in disulfide-mediated polymerization. Supportive evidence was obtained by analysis of breakdown products of native nematocyst capsules after limited sonification without reduction (Özbek et al., in preparation). Minicollagen and NOWA formed disulfide cross-linked units that like the entire capsule were readily dissolved under even mild reducing conditions.

Disulfide reshuffling processes and formation of disulfide-linked complexes are common mechanisms in the extracellular space and some recently explored systems may be referenced (15-19). The minicollagen/NOWA system may stand as a prototype for the controlled formation of a highly stable matrix layer by disulfide linkage. To understand the assembly mechanism, the 3-dimensional

structure of the MCRDs involved is needed. The core of the MCRD consists of only 20 residues with 6 closely positioned Cys residues. At the start of this work it was not known whether the very small domains were autonomous or stable only as part of a larger structure. The disulfide connections were also not known and could not be explored by limited proteolysis because of the lack of suitable cleavage sites. These problems were approached by solving the structure of the C-terminal Cys-rich domain of minicollagen-1 by NMR spectroscopy. A new fold was found, with disulfide connections between Cys-2 and Cys-18, Cys-6 and Cys-14, and Cys-10 and Cys-19. Oxidative folding occurs at high rates in the presence of a GSSG/GSH redox buffer with formation of almost exclusively one single isomer. A highly conserved Pro residue located between Cys-10 and Cys-14 induces and probably directs correct disulfide connections. The presented structure proposes likely candidates for disulfide reshuffling supposed to be a key reaction during nematocyst morphogenesis.

Experimental Procedures

Peptide Synthesis and oxidation

Preparation 1

The 6xStBu protected peptide Ac-PCPPVCVAQCVPVTCPCQYCCPAKRK-NH₂ was synthesized on Fmoc-Rink-Amide PEGA resin by the Fmoc/tBu strategy using double couplings with Fmoc-Xaa-OH/HBTU/HOBt/DIEA (4:4:4:8), intermediate Fmoc cleavage with 20 % piperidine in DMF and acetic anhydride/DIEA (4:8) for N-terminal acetylation. After resin cleavage/deprotection with TFA/phenol/H₂O/thioanisole/1,2-ethanedithiol (82.5:5:5:5:2.5) the product was isolated by RP-HPLC; yield: 6 %; HPLC: t_R = 12.5 min (>98 %); ESI-MS: *m/z* = 1055.0 [M+3H]³⁺; 1581.8 [M+2H]²⁺; M_r = 3162.31 calculated for C₁₃₆H₂₃₀N₃₂O₂₉S₁₂. The Cys protecting groups were cleaved in TFE/H₂O with tributylphosphine (60 equiv) at RT for 5 h and the resulting fully deprotected peptide was oxidized at pH 8.0 in the presence of GSSG/GSH (9 equiv, 10:1) under air atmosphere at 7 °C. The crude product was purified by preparative size exclusion column chromatography; yield: 20 %; HPLC: t_R = 12.3 min (>98 %); ESI-MS: *m/z* = 1314.8 [M+2H]²⁺, 876.4 [M+3H]³⁺; M_r = 2627.23 calculated for C₁₁₂H₁₇₆N₃₂O₂₉S₆.

Preparation 2

The linear peptide was synthesized with an ABI 433A synthesizer. Couplings were carried out on a Fmoc-Lys(Boc)-PEG-PS resin (Perseptive Biosystems, 0.21 mmol/g) using Fmoc-amino acids (Fmoc-Arg(Pbf), Fmoc-Lys(Boc), Fmoc-Tyr(tBu), Fmoc-Cys(Trt), and Fmoc-Gln(Trt)) (Anaspec). HATU (O-(7-azabenzotriazol-1-yl)-1.1.3.3-tetramethyluronium hexafluorophosphate, (Perseptive Biosystems) (4.0 eq.) / Diisopropylethylamine mediated peptide couplings. The peptide was cleaved from the resin with trifluoroacetic acid, containing thioanisole (5 % v/v), ethanedithiol (3 % v/v), and anisole (2 % v/v). After precipitation in diethylether, the crude peptide was purified by preparative HPLC (Vydac[®] C18, 10-15 m, 300Å, 250 x 50 mm, W.R. Grace, MD, USA). The peptide was characterized by electrospray ionization/quadrupole/time-of-flight mass spectrometry and amino acid analysis. A mass of 2590.9 Da was determined and the expected amino acid composition was found.

The lyophilized purified peptide was dissolved in 25 mM Tris/HCl, pH 6.0, containing 100 mM NaCl at a concentration of 0.02 mM. Folding was allowed to proceed under N₂ for 72 to 96 hours at 4 °C. Oxidation was induced by changing the pH to 8.0-8.1 with saturated Tris, and the addition of reduced and oxidized glutathione (10:1 molar ratio) to a final concentration of 1 mM. The solution was exposed to air at 4 °C for four to ten days. Oxidation was stopped by the addition of trifluoroacetic acid to give a pH of 1.3. The oxidized peptide was purified by preparative HPLC. The yield of oxidized peptide was 103 mg (16 % of theoretical yield). Mass spectroscopy of the oxidized peptide showed a molecular mass of 2585.1 Da.

NMR Data Collection

Structure 1

NMR experiments for conformational analysis were carried out at 283 K on Bruker DRX500, DMX750 and DX900 spectrometers using a 3 mM sample of the peptide dissolved in H₂O/D₂O (9:1) mixture at pH 3.5. Resonance assignments were performed according to the method of Wüthrich (38). 173 experimental interproton distance constraints were extracted from 2D-NOESY (39) experiments with mixing times between 75 and 200 ms. Five hydrogen bonds were identified from temperature shifts and H/D exchange. Acceptor carbonyl groups were identified in initial structure calculations. The NOE intensities were converted into interproton distance constraints using the following classification: very strong (vs) 1.7-2.3 Å, strong (s) 2.2-2.8 Å, medium (m) 2.6-3.4 Å, weak (w) 3.0-4.0 Å, very weak (vw) 3.2-4.8 Å and the distances of pseudo atoms were corrected as described by Wüthrich (38). Distance geometry (DG) and molecular dynamics-simulated annealing (MD-SA) calculations were performed with the INSIGHTII 98.0 software package (Accelrys, San Diego, CA) on Silicon Graphics O2 R5000 computers (SGI, Mountain view, CA) as described recently (25). In brief, hundred structures were generated by distance geometry and refined with MD-SA steps. The experimental constraints were applied at every stage of the calculations. The coordinates and structural restraints have been deposited in the Brookhaven Protein Data Bank under accession number 1SOP.

Structure 2

Chemically synthesized C-terminal MCRD of minicollagen-1 was purified after oxidation according to purification procedure 2. The determination of the NMR structure (PDB accession number 1SP7) was carried out in 5 mM sodium phosphate buffer, pH 6.5 at 15°C by using homonuclear and heteronuclear techniques and information from weak alignment. Details of this structure determination will be published separately. Structure representations were generated with MOLMOL (43).

Analytical ultracentrifugation

Sedimentation equilibrium experiments were performed on a Beckman Optima XL-A analytical ultracentrifuge (Beckman Instruments) equipped with 12-mm Epon double-sector cells in an An-60 Ti rotor. The MCRD was analyzed in 5mM Tris buffer (pH 7) without salt or containing 100 mM NaCl at 20°C. The peptide concentrations were adjusted to 0.2-0.8 M. Sedimentation equilibrium scans were carried out at 48,000 rpm. Molecular masses were evaluated from $\ln A$ versus r^2 plots, where A is the absorbance at 277nm and r is the distance from the rotor center. A partial specific volume of 0.73 ml/g was used for all calculations.

Results

The MCRD constitutes a conserved sequence module in nematocyst minicollagens and in NOWA

The sequence of minicollagen-1 with domain indications and alignment of cysteine-rich domains from different minicollagens and NOWA are represented in Figure 1. Minicollagen-1 consists of an N-terminal MCRD, N-terminal polyproline region, a central collagen sequence, a shorter C-terminal polyproline stretch followed by a C-terminal MCRD (Fig. 1A). The preceding propeptide is cleaved off during recombinant expression of minicollagen-1 and probably also in *Hydra* (9). As already mentioned in the introduction the overall sequence homology of the Cys-rich domains is not very high but the cysteine pattern is identical for all minicollagens and for the eight C-terminal domains of NOWA with the only variation being in the number of residues spacing the first two Cys residues. The sequence of the C-terminal minicollagen-1 MCRD, which has been investigated in the present work, is underlined and the numbering of residues corresponds to the synthetic peptides used in this study. Beside the cysteines there is only one conserved residue, which is Pro12 (shown in purple in Fig. 1B).

Peptide synthesis and oxidation

As the MCRD occurs in different molecular contexts, at the N- and C-terminal extensions of minicollagen molecules as well as eight times repeated at the C-terminus of NOWA, we speculated that it might constitute an isolated domain with the capacity of independent folding. Peptide synthesis was carried out for the C-terminal MCRD of minicollagen-1 starting with the last proline residue of the C-terminal polyproline stretch and including the charged C-terminus of the full-length molecule. The formation of disulfide bonds occurs in the presence of redox buffer at 100 μ M peptide concentrations to avoid aggregation by intermolecular disulfide bonds (see Experimental Procedures). The final product showed a single peak in mass spectroscopic analysis with the reduced and oxidized MCRDs having a difference in molecular weight of 6 Da, thereby strongly indicating the formation of three intramolecular disulfide bonds (Table I). Disulfide bonds can be shown to be all-intramolecular in mass spectroscopic analysis. Analytical ultracentrifugation confirmed the absence of significant aggregation or multimerization in solutions

A

Minicollagen-1

propeptide N-Cys-rich poly-Pro
KTLHEMLKR**DAN****PCGSY****CPSV****CAPACAPV****CCY****PPPPPPPPPPPPPPPPPPPPPPPP****APLP**
collagenous poly-Pro C-Cys-rich basic tail
GNPGPPGRPGPPGAPGPPGLPGPPGPPGAPGQGLPGQP**A****PPPP****C****P****V****C****V****A****Q****C****V****P****T****C****P****Q****Y****C****C****P****A****K****R****K**

B

N- and C- terminal Cys-rich repeats of minicollagens (MCol) and NOWA (NW)

	1	10	20
MCOL1hN	DAN PCGS	Y CPSV CAPACAPV CCY PPPPPPPPPPPPPPPPPP	
MCOL2hN	SAQ ACGY	N CPAI CAPACTPI CC APPPPPPPPPPPPPPPPP	
MCOLadN	CGY	G CPSM CAPACEPT CC APPPPPPPPP	
MCOLapN	REAS PCGY	G CPSM CAPACEPT CC APPPPPPPPP	
MCOLacN	REAS PCGY	G CPSM CAPACEPT CC APPPPPPPPP	
MCOL1hC	PPPP CPP	<u>VCVAQCVPTCPQYCCPAKRK</u>	
MCOL2hC	PPPP CPP	I CPT Q C V P Y C P Q Y C C L K G P P G P P	
MCOLadC	PPPP CPP	I CIQH C IRI C PQP CC SPPPPP	
NOhREP1	QITGT CPS	G CSGD CY PE C KPG CC GQVNLNAPVQP	
NOhREP2	SGYTA CSQ	Y PN C GLS C QSS C SQS CC QQNPYQPSVMSGTIVIQP	
NOhREP3	NEQSV CPQ	H PG C SQH CAP R C SPQ CC QQSMNSLYQP	
NOhREP4	PQMSA CPQ	F PS C SPT CAP Q C SQ L CC QQSSMPLQM	
NOhREP5	PQMP S CPQ	F PS C SAS CAP Q C SQ CC QQPSMSIQP	
NOhREP6	LQISS CPQ	F PS C SP S CAPQ C SQ CC QQPSMPIQL	
NOhREP7	PLMGS CSQ	M PG C SAS CAP L C SQ CC QQQAMLQQSIMQQPMM	
NOhREP8	MAQNP CS LQQPG	C SSA CAP AR L S CC SLGRMNLGR	

Figure 1.

A, minicollagen-1 amino acid sequence and domain structure. Propeptide sequence is in blue, MCRDs in red, polyproline sequences in light green, collagen repeat in dark green. B, Alignment of MCRDs in minicollagen molecules from different cnidarians and in NOWA. MCol1h: minicollagen-1 *Hydra*, MCol2h: minicollagen-2 *Hydra* (3), MColad: minicollagen *Acropora donei* (2), MColac: minicollagen *Acropora cervicornus* (1), MColap: minicollagen *Acropora palmate* (1), N, C: N-, C- terminal, The sequence of the Cys-rich region of NOWA in *Hydra* (NWh) starts with repeat 1 and terminates with repeat 8. Residues in MCol1hC are numbered starting at proline preceding the first cysteine and the same numbering was used in the NMR structures. The highly conserved cysteine residues are marked in red. Proline in position 12, which is conserved with two exceptions, is marked in purple. The sequence of the synthesized and investigated peptide is underlined.

Table 1

Molar masses of the C-terminal MCRD peptide of minicollagen-I.

	molar mass UC (g/mol)	molar mass MS (g/mol)	molar mass calc. (g/mol)
MCol1hC reduced		2591	2592
MCol1hC oxidized	2700±300*	2586	2586

*concentrations were 0.5-2 mg/ml

from 0.2 to 0.8 mM total peptide concentration (Table I), which was further supported by NMR $^1\text{H}^{\text{N}}$ T_2 relaxation times of more than 100 ms at 25 °C, indicative of the prevalence of a monomeric state in solutions of 1.6 mM MCRD.

The NMR Structure of the MCRD

The solution structure of the MCRD was determined independently by a group in Basel and Munich (see affiliations in the author list) from two separate peptide preparations (see Experimental Procedures). Both structures show an identical tightly packed globular fold (Figures 2 and 3), which consists of a short N-terminal α -helix between Val5 and Gln9 followed by an inverse γ turn (Gln9-Val11), a type I β turn (Val11-Cys14) and a type III β turn (Pro15-Cys18). Thus cysteines 6, 10, 14 and 18 are directly located in turns whereas cysteine 2 is located in a proline-rich N-terminal sequence and cysteine 19 is oriented presumably by the β III turn and a C-terminal proline. All proline residues in the MCRD are in trans conformation as evidenced by specific NOEs.

The only conserved residue Pro12 (Fig. 1) imposes a β I turn topology on residues 11 to 14 due to its fixed φ angle of -60° . Hydrogen bonds are established in the turns between Val5 (O) and Gln9 (H^{N}), Gln9 (O) and Val11 (H^{N}), Val11 (O) and Cys14 (H^{N}), and Pro15 (O) and Cys18 (H^{N}) (Fig. 3), respectively, as derived both from the calculated structures and from the slow $^1\text{H}/\text{D}$ exchange upon lyophilization of MCRD and redissolving in $^2\text{H}_2\text{O}$. The positively charged C-terminus Lys22, Arg23, Lys24 is flexibly disordered and does not contribute to the MCRD structure (Fig. 2).

The first disulfide bond, Cys2-Cys18, clasps the N- and C-termini of the domain while the Cys6-Cys14 bond connects the N-terminal α -helix to the type I β turn starting with Val11, thus forming the core of the MCRD structure. The third disulfide bond Cys10-Cys19 is more exposed to the C-terminal surface of the domain and constrains the polypeptide backbone into two consecutive turns. The more surface-exposed N- and C-terminal disulfide bridges represent the most likely candidates for intermolecular disulfide exchange reactions. Complete reduction of the disulfide bonds with an excess of tris(2-carboxyethyl)-phosphine hydrochloride (TCEP) at pH 7.5 results in complete unfolding without retainment of local conformational preferences as well assessed by ^1H NMR.

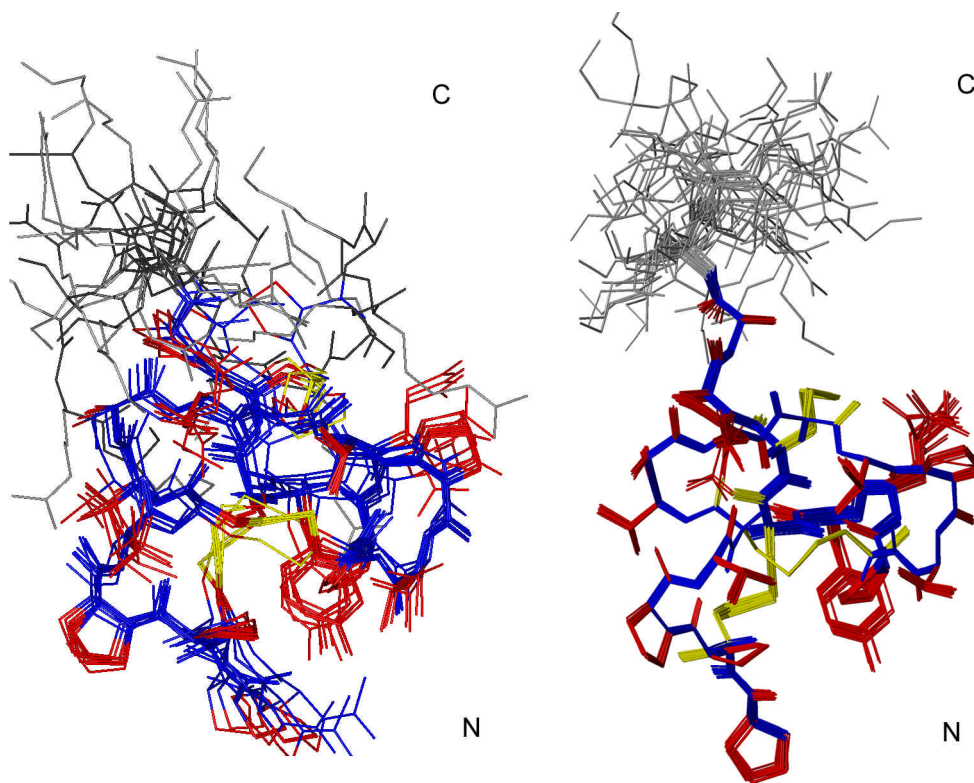


Figure 2.

NMR structures of the C-terminal MCRD of minicollagen-1. The backbone is displayed in blue, side chains in red except for cysteine side chains in yellow. *Structure 1* (left, accession number: 1SOP): the ten energy lowest structures are superimposed using the backbone atoms of residues 2-19 with an rmsd of 0.6 Å. Disordered residues 21-24 are depicted in grey. *Structure 2* (right, accession number: 1SP7), all-heavy-atom representation of the 20 lowest energy conformers of the minicollagen-1 C-terminal MCRD out of 100 structures calculated in CNS (42), with best fit for backbone heavy atoms of residues 2-21. The charged C-terminal sequence K²²R²³K²⁴ (grey) is disordered at pH 6.5 in the absence of additional salt.

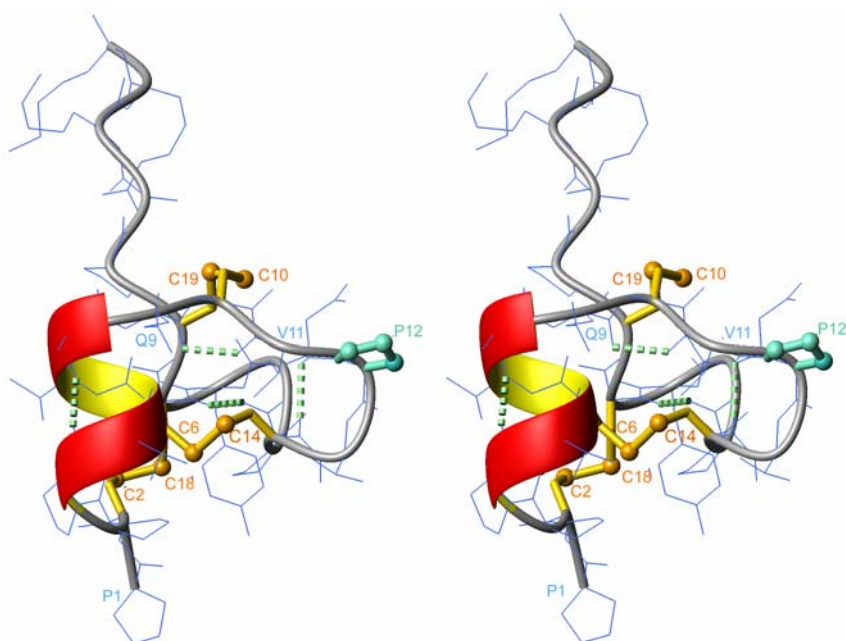


Figure 3.

Stereoview of the same conformer as in Figure 2 in ribbon presentation. Only structure 2 is shown. Cysteines and disulfide bonds are shown in yellow and Pro12 is in aquamarine. Disulfide bonds (Cys2-Cys18, Cys6-Cys14 and Cys10-Cys19) as well as the conserved Pro12 are indicated in ball and stick representation. Dashed lines indicate the hydrogen bonds identified by MOLMOL. These are bonds between Pro5 (O) and Gln9 (H^N); Val11 (O) and Cys14 (H^N); Pro15 (O) and Cys18 (H^N). The first two H-bonds belong to the α -helix, others belong to the three different turns. Pro12 induces a β I turn from residues 11 to 14. All proline residues in the structure can be shown to be in *trans* conformation from experimental NOE distance information.

Reoxidation of reduced MCRD with an excess of oxidized glutathione at pH 7.5 proceeds extremely fast and is completed within 2 hours as observed by ^1H NMR spectroscopy (Fig. 4). This is presumably due to the small domain size and the effect of Pro12 upon disulfide bridge formation (see discussion). Fluorescence spectroscopy allows monitoring of the refolding due to the quenching of Tyr17 fluorescence by a nearby disulfide bridge and yields a folding half time of 1.5 hours at pH 8 upon oxygen saturation of the solution in agreement with NMR data (not shown).

Model of trimeric minicollagen-1

It has already been mentioned that minicollagen-1 at native conditions appears to be a non-covalent trimer. A schematic representation of the trimeric minicollagen molecule including the connections of N- and C-terminal MCRDs to the polyproline type II helices is shown in Figure 5. A model of trimeric minicollagen-1 was proposed earlier (9) in which the MCRD was assumed to have a linear structure. After elucidation of the structure of the MCRD we are now able to draw a schematic model in scale with the known dimensions of the collagen triple helix and the polyproline-II helix (4). An open question is the geometry of the connections between the collagen and polyproline parts of the molecule and between MCRDs and polyprolines, respectively. The angles and flexibility at the junction sequence APLP in the N-terminus and the single Ala spacer in the C-terminus (Fig. 1, shown in black) or by any Pro residue that potentially can occur in *cis* conformation are not known. The lack of association between MCRDs even at relatively high concentrations would suggest that they also do not associate in minicollagen without the help of an isomerase or another catalytic system. Polyproline or polyhydroxyproline-II helices are also known to be monomeric. For these reasons the polyproline arms with their MCRD heads are displayed as non-interacting entities in Fig. 5. This is confirmed by previous biochemical data showing that minicollagen-1 trimers are not disulfide-crosslinked and the triple helix is stabilized solely by the collagen sequence composition (10).

The ways that MCRDs are linked to the main molecule are shown schematically (red arrows) in the upper (N-terminal) and the lower (C-terminal) part of Figure 5. The polyproline-II helices approach the MCRDs from the N-terminus for the C-terminal domain and from C-terminus for the N-terminal

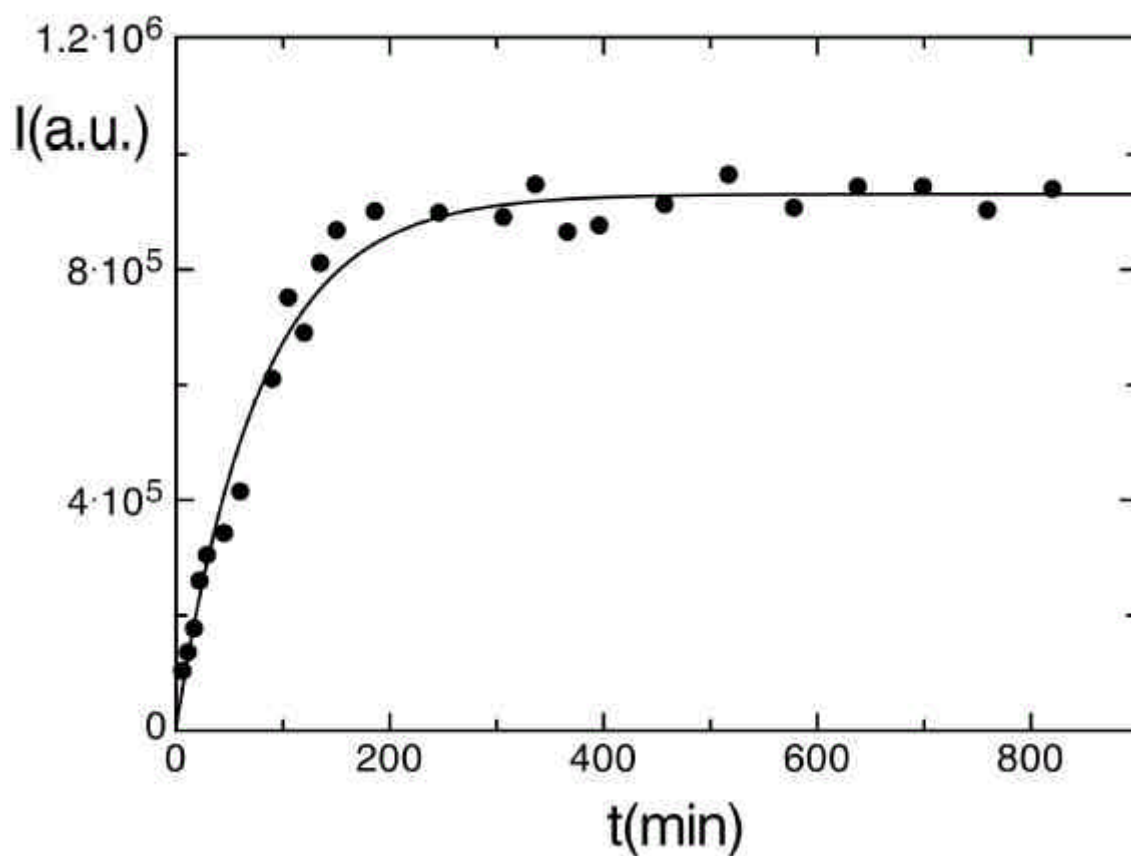


Figure 4.

Folding kinetics of the MCRD as monitored by NMR. The intensity of the amide resonance signal of Val5 in folded MCRD is shown upon reoxidizing fully reduced MCRD with an excess of oxidized glutathione. The reoxidation reaction is completed within 2 hours at pH 7.5 when catalyzed by the glutathione system. The unusually fast reoxidation is in agreement with data from fluorescence experiments (data not shown).

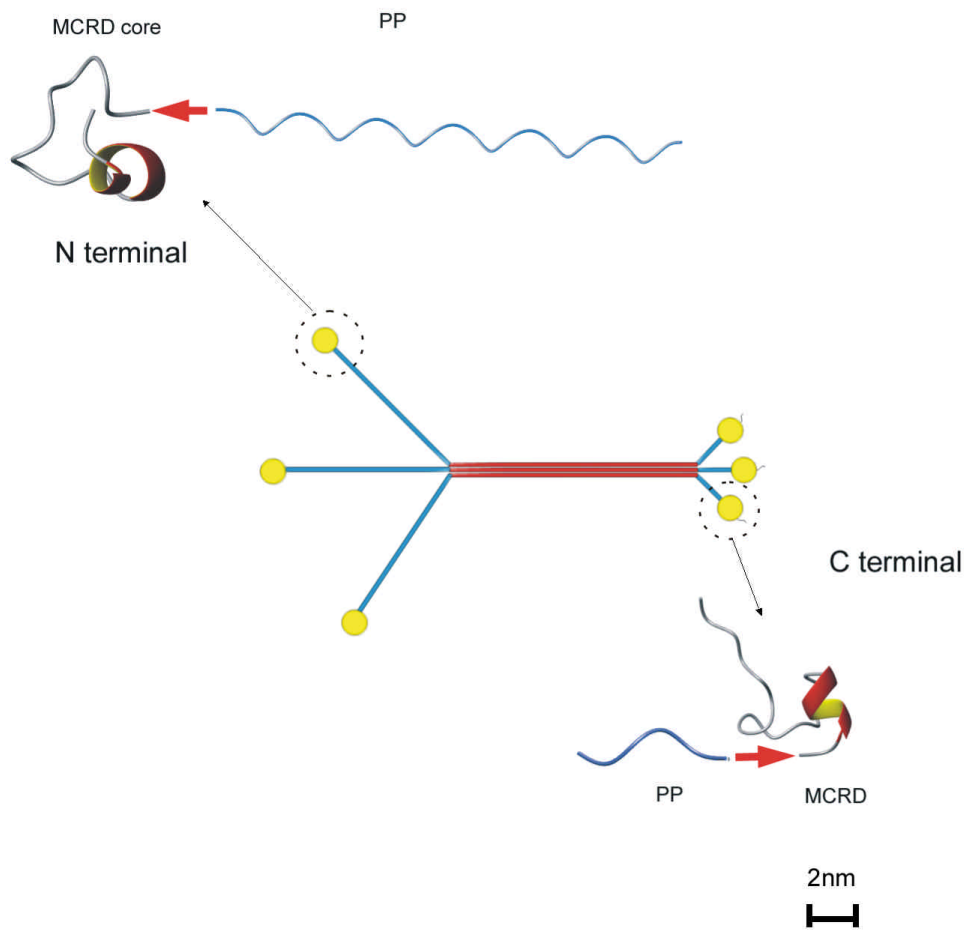


Figure 5.

Schematic presentation of the minicollagen-1 trimer. Full-length minicollagen-1 (central part of the figure) and connections of polyproline regions to MCRDs (upper and lower parts of the figure) are shown. Yellow circles and ribbon globular structures are MCRDs; blue lines and blue ribbons – polyproline type II helices (PP); red lines – collagen triple helix. Basic tails of the C-terminal MCRDs are represented in faint curves. In the upper part only the MCRD core (2-21 residues) is shown. The connection to the N-terminal 23 residue polyproline helix is indicated by a red arrow.

domain. The connections between the polyproline-II helices and the MCRD might alter the accessibility of particular disulfide bridges in the MCRD. As can be seen from comparison of Figures 3 and 5, in the N-terminal MCRD the Cys10 – Cys19 disulfide is less exposed. An opposite situation is observed in the C-terminus where the polyproline-II stretch hides the Cys2 - Cys18 bridge. Accordingly the suggested candidates for intermolecular disulfide exchange are Cys2-Cys18 for the N-terminal and Cys10-Cys19 for the C-terminal MCRD.

Discussion

Small Cys-rich domains are widely distributed building blocks of extracellular proteins in essentially all phyla including plants and bacteria. The most abundant domain type is the epidermal growth factor domain (EGF, smart00181). Including its variants EGFca (smart00179) and EGF-like (smart0001) several thousands of different EGF-domains are known in proteins of different functions (see Smart database, <http://smart.embl-heidelberg.de>). In most cases EGF-domains are arranged in arrays with other domains. Laminin (20) and fibrillin (21) are two out of very many examples. Many Cys-rich domains, however, also exist as single autonomous proteins and the epidermal growth factor domain is a well-known example. This fact provides a bridge to the numerous low-molar mass Cys-rich proteins, which are also products of larger precursor forms but express their function as toxins, antimicrobial peptides or other small bioactive agents. Variations of sequences, cysteine patterns and three-dimensional structures are however very large for this diverse class of small proteins and clear homologies exist for small groups only (22). Small Cys-rich peptides with antimicrobial or toxic functions are part of the innate immunity and defense system of invertebrate animals. They are often stored in secretory granules and released in response to parasites via exocytosis. Nematocyst discharge in cnidarians represents a specialized form of exocytosis from a giant post-Golgi vesicle. The appearance of a structural motif related to Cys-rich peptide toxins in proteins involved in the formation of a wall polymer, which is associated with the nematocyst membrane, might hint at a phylogenetic link between this group of defensive molecules and the evolution of the nematocyst.

The common feature of small Cys-rich domains is the prevalence of disulfide bridges in structure stabilization. This is already suggested by the large fraction of cysteines, which is 4/22 for gomesin (23), about 6/40 for EGF domains, 8/42 for crambin (24) and hellethionin (25) as compared to 6/20 for the Cys-rich domain of minicollagen-1. The later domain has one of the highest ratios of cysteines to total residues known so far. Comparably dense cysteine patterns are only described for small conotoxin peptides like PnIVA and PnIVB (26). The peptide whose structure was elucidated in the present work is 4 residues longer than the essential core. The structure shows that the first proline and the last three residues are randomly

oriented and probably not required for correct oxidative folding. The remaining structure is well defined and data demonstrate formation of a single topoisomer under optimized oxidative conditions.

In the reduced state no conformational preferences were found in MCRD by NMR. Similar observations were reported for many other Cys-rich domains underlining the importance of disulfide bonds for stabilization. As shown for tachyplesin mutational replacements of Cys- residues by alanine lead to a loss of structure (27). Interestingly the global fold of tachyplesin was rescued by hydrophobic interactions between pairs of tyrosines or phenylalanines if cysteines were replaced by these residues (27).

Although the equilibrium structure of MCRD is predominantly determined by the covalent interactions between Cys residues kinetic intermediates must be responsible for correct disulfide pairings. A folded-precursor mechanism (28,29,36) and a quasi-stochastic mechanism (30,31) were proposed for other monomeric proteins. True pathways are probably between these two extremes. For the Cys-rich domain of minicollagen formation of a type I turn by Pro12 and hydrogen bonding between Cys14 (H^N) and Val11 (O) is most likely a very important intermediate step. As can be seen from the structure (Figs. 2 and 3) this bend and the turn bring the cysteines into close vicinity for correct intramolecular disulfide bridging.

It is amazing that few non-covalent interactions in the MCRD of minicollagen and in many other short peptides lead to correct connectivities between several Cys residues, which statistically could also interact in very many different intra- and intermolecular modes. To establish the disulfide connections of MCRD pairwise bridges between adjacent Cys-residues have to be prevented. The three intervening amino acid residues found in MCRDs render pair-wise bridges unfavorable (32) and this feature is most likely essential for proper folding.

In small disulfide rich proteins identical folds are found in homologous domains in contrast to large variations in non-cysteine residues. A striking example are the about 200 solved structures of different EGF-domains, which exhibit the same fold although sequence identities of non-cysteine residues are difficult to detect (smart, key words EGF and structure). This high conservation of structure leads us to assume, that the related Cys-rich repeats in minicollagen of corals and in NOWA proteins have the same global fold as the MCRD of

minicollagen-1 of *Hydra*, which was investigated in the present work. Conservation of residues is low (Fig. 1) and would not allow the prediction of structure identities for conventional globular proteins (33)

Earlier data on the interaction of minicollagens and NOWA in the nematocyst wall conclusively demonstrated a switch from a soluble state of both proteins with all disulfides internally linked to an insoluble dense polymeric state with intermolecular disulfide bonds (see introduction). Analogous assembly processes involving disulfide reshuffling were reported for virus capsid proteins (19), collagen IV (34) and other systems (17,18). The only cysteines in minicollagen-1 are located in the MCRDs. Consequently a disulfide reshuffling interaction was proposed between these domains. The data also suggested corresponding interactions between the Cys-rich domains of minicollagen and NOWA. *In vivo* the situation may be rather complex because of possible interactions between N- and C-terminal domains of different minicollagens in the same organism. At each end of a minicollagen three MCRDs are present (Fig. 4). This opens the possibility of a simultaneous interaction between minicollagens and NOWA.

Extensive searches of the database failed to reveal MCRD-like domains in non-nematocyst proteins. The domain type seems to be highly specialized for disulfide mediated crosslinking of the nematocyst wall. For several organisms with nematocyst organelles minicollagen and NOWA genes have been found but sequencing of cnidaria genes is still too incomplete to allow a general conclusion. Interestingly in minicollagen of corals (AF507373.1) Cys-residues frequently occur after glycines in the collagenous part of the sequence. Cysteine residues, which interlink collagen chains of the same molecule are located at the ends of a triple helix to form a stable disulfide knot (35,36) or located in interruptions of the regular Gly-X-Y repeat (37). Cys-residues in X-position of collagens are highly unusual and are most likely used to link between collagen molecules. It may be speculated that the nematocyst walls of corals are cross-linked by disulfide bridges between collagen triple helices in addition to those between MCRDs thus providing a higher tensile strength.

Future work will focus on the mechanism of the disulfide reshuffling process using isolated Cys-rich domains of minicollagen and NOWA. A likely possibility is the interaction between N-and C-terminal domains of minicollagens. *In vivo*, the disulfide exchange reaction probably is catalyzed by disulfide isomerases or other

helper proteins, which have to be defined prior to *in vitro* studies. Our working hypothesis is that only one or two out of the three disulfide bonds will be reshuffled from intra to intermolecular. Likely candidates are the bonds Cys2-Cys18 and Cys10-Cys19, which are both surface exposed.

Acknowledgements

We thank Eric Steel for expert technical assistance.

This work was supported by SNF grant 31-61'757.00 to S.G.

References

1. Vollmer, S. V., and Palumbi, S. R. (2002) *Science* **296**, 2023-2025
2. Wang, W., Omori, M., Hayashibara, T., Shimoike, K., Hatta, M., Sugiyama, T., and Fujisawa, T. (1995) *Gene* **152**, 195-200.
3. Kurz, E. M., Holstein, T. W., Petri, B. M., Engel, J., and David, C. N. (1991) *J Cell Biol* **115**, 1159-1169.
4. Bateman, J. F., Lamande, S.R. and Ramshaw, J.A.M. (1996) *Collagen superfamily*. Extracellular Matrix. Molecular Components and Interactions (Comper, W. D., Ed.), 2, Harwood Academic Publisher, Amsterdam
5. Engel, J. (1997) *Science* **277**, 1785-1786
6. van der Rest, M., and Garrone, R. (1991) *Faseb J* **5**, 2814-2823
7. Ricard-Blum, S., Dublet, B., and van der Rest, M. (2000) *Unconventional Collagens*, Oxford University Press, New York
8. Holstein, T., and Tardent, P. (1984) *Science* **223**, 830-833.
9. Engel, U., Pertz, O., Fauser, C., Engel, J., David, C. N., and Holstein, T. W. (2001) *Embo J* **20**, 3063-3073.
10. Özbek, S., Pertz, O., Schwager, M., Lustig, A., Holstein, T., and Engel, J. (2002) *J Biol Chem* **277**, 49200-49204
11. Engel, U., Özbek, S., Engel, R., Petri, B., Lottspeich, F., and Holstein, T. W. (2002) *J. Cell Sci.* **115**
12. Lenhoff, H. M., Kline, E. S., and Hurley, R. (1957) *Biochim. Biophys. Acta* **26**, 204-205
13. Blanquet, R., and Lenhoff, H. M. (1966) *Science* **154**, 152-153.
14. Özbek, S., Engel, U., and Engel, J. (2002) *J Struct Biol* **137**, 11-14
15. Mullen, G. E., Kennedy, M. N., Visintin, A., Mazzoni, A., Leifer, C. A., Davies, D. R., and Segal, D. M. (2003) *Proc Natl Acad Sci U S A* **100**, 3919-3924
16. Wieringa, R., De Vries, A. A., Post, S. M., and Rottier, P. J. (2003) *J Virol* **77**, 12996-13004
17. Knaus, K. J., Morillas, M., Swietnicki, W., Malone, M., Surewicz, W. K., and Yee, V. C. (2001) *Nat Struct Biol* **8**, 770-774.
18. Wagner, D. D., Lawrence, S. O., Ohlsson-Wilhelm, B. M., Fay, P. J., and Marder, V. J. (1987) *Blood* **69**, 27-32.

19. Li, P. P., Nakanishi, A., Clark, S. W., and Kasamatsu, H. (2002) *Proc Natl Acad Sci U S A* **99**, 1353-1358
20. Engel, J. (1992) *Biochemistry* **31**, 10643-10651
21. Handford, P. A. (2000) *Biochim Biophys Acta* **1498**, 84-90
22. Tamaoki, H., Miura, R., Kusunoki, M., Kyogoku, Y., Kobayashi, Y., and Moroder, L. (1998) *Protein Eng* **11**, 649-659
23. Mandard, N., Bulet, P., Caille, A., Daffre, S., and Vovelle, F. (2002) *Eur J Biochem* **269**, 1190-1198
24. Housset, D., Benabicha, F., Pichon-Pesme, V., Jelsch, C., Maierhofer, A., David, S., Fontecilla-Camps, J. C., and Lecomte, C. (2000) *Acta Crystallogr D Biol Crystallogr* **56** (Pt 2), 151-160
25. Milbradt, A. G., Kerek, F., Moroder, L., and Renner, C. (2003) *Biochemistry* **42**, 2404-2411
26. Fainzilber, M., Nakamura, T., Gaathon, A., Lodder, J. C., Kits, K. S., Burlingame, A. L., and Zlotkin, E. (1995) *Biochemistry* **34**, 8649-8656
27. Laederach, A., Andreotti, A. H., and Fulton, D. B. (2002) *Biochemistry* **41**, 12359-12368
28. Boudko, S. P., and Engel, J. (2004) *J Mol Biol* **335**, 1289-1297
29. Welker, E., Wedemeyer, W. J., Narayan, M., and Scheraga, H. A. (2001) *Biochemistry* **40**, 9059-9064
30. Creighton, T. E. (1997) *Biol Chem* **378**, 731-744
31. Weissman, J. S., and Kim, P. S. (1991) *Science* **253**, 1386-1393
32. Zhang, R. M., and Snyder, G. H. (1989) *J Biol Chem* **264**, 18472-18479
33. Doolittle, R. F. (1995) *Annu Rev Biochem* **64**, 287-314
34. Gunwar, S., Ballester, F., Noelken, M. E., Sado, Y., Ninomiya, Y., and Hudson, B. G. (1998) *J Biol Chem* **273**, 8767-8775
35. Bruckner, P., Bächinger, H. P., Timpl, R., and Engel, J. (1978) *Eur J Biochem* **90**, 595-603
36. Barth, D., Kyrieleis, O., Frank, S., Renner, C., and Moroder, L. (2003) *Chemistry* **9**, 3703-3714
37. Kühn, K. (1995) *Matrix Biol* **14**, 439-445
38. Wüthrich, K. (1986) *NMR of proteins and nucleic acids*, Wiley, New York
39. Jeener, J., Meier, B. H., Bachman, P., and Ernst, R. R. J. (1979) *Chem. Phys.* **71**, 4546-4553

40. Delaglio, F., Grzesiek, S., Vuister, G.W., Zhu, G., Pfeifer, J., and Bax, A. (1995) *Journal of Biomolecular NMR* **6**, 277-293
41. Garrett, D. S., Powers, R., Gronenborn, A.M., and Clore, G.M. (1991) *Journal of Magnetic Resonance* **95**, 214-220
42. Brunger, A. T., Adams, P.D., Clore, G.M., DeLano, W.L., Gros, P., Grosse-Kunstleve, R.W., Jiang, J.S., Kuszewski, J., Nilges, M., Pannu, N.S., Read, R.J., Rice, L.M., Simonson, T., and Warren, G.L. (1998) *Acta Crystallographica Section D-Biological Crystallography* **54**, 905-921
43. Koradi, R., Billeter, M., and Wüthrich, K. (1996) *J Mol Graph* **14**, 51-55, 29-32

Chapter 4*

The structure of the first cysteine rich repeat of NOWA cysteine rich domain.

Fluorescence study of oxidative refolding.

* This work was performed in collaboration with Sebastian Meier.

Abstract

The solution structure of the first cysteine rich repeat of Hydra nematocyst wall protein NOWA (NCRD1) has been determined using homonuclear and heteronuclear NMR techniques at natural abundance. The domain consists of 25 amino acids with the cysteine pattern identical to that of the minicollagen-1 cysteine rich domains (MCRD). Except the cysteines and Pro12 overall amino acid composition of the investigated peptide has no homology to the MCRD. In the present study we demonstrate that NCRD1 has disulfide pattern identical to that of the MCRD. Moreover NOWA domain exhibits overall structure topology similar to the topology of minicollagen domain and therefore can be classified as the same fold. The C-terminal minicollagen-1 and the first NOWA cysteine rich domains both revealed the effect of tyrosine fluorescence quenching by disulfide bonds although the tyrosine positions are different within the domains. The oxidative refolding has been monitored using the fluorescence of single tyrosine residue for both peptides. Resulting kinetics could be fitted with single exponential suggesting a simple kinetic mechanism that arises from the quenching by only one particular disulfide bond. We propose that quenching occurs due to the Cys2-Cys18 bond in case of MCRD and Cys6-Cys14 in case of NCRD1. Oxidation and reduction rate constants differ in values according to the susceptibility of the disulfide bridge responsible for the fluorescence quenching.

Introduction.

Cysteine rich domain of NOWA exhibit the same structural fold as the C-terminal minicollagen-1 cysteine rich domain.

Two major proteins of nematocyst capsule wall, NOWA and minicollagen, share common cysteine rich domain (CRD) (1). This domain appears two times in minicollagen (see schematic representation of the minicollagen trimer on the figure 4 of chapter 3) and eight times in the NOWA protein (Fig. 1, sequence alignment). The 8-folded cysteine rich domain of NOWA termed ONCRD (octad NOWA cysteine rich domain) follows the C-type lectin domain of the protein and continues up to the basic C-terminal sequence. The structure of 24 amino acid peptide comprising C - terminal domain of minicollagen-1 has been recently solved (see chapter 3 for details). We have also proposed that regardless the low sequence homology among the cysteine rich repeats in the nematocyst proteins they all share identical disulfides connectivity and overall structural fold. Nonetheless there were no experimental evidences present for that. Here we report the structure of chemically synthesized first cysteine rich repeat of NOWA. Hereafter we refer to this peptide as NCRD1 (NOWA cysteine rich domain 1). This particular domain has very low homology to the previously solved MCRD peptide except the cysteines and the conserved Pro12 residue (Fig. 1). The Pro12 was discussed to be an important feature for the correct disulfide connectivity and overall structure formation of MCRD. According to the elucidated structure of NCRD1 cysteines connectivity found in C-terminal minicollagen cysteine rich domain are preserved. Furthermore both peptide structures have overall similar topology. These data strongly support the previous speculation that MCRD structure is a general fold for Hydra nematocyst wall proteins. Furthermore oxidative refolding of investigated peptides has been studied using intrinsic fluorescence of tyrosine in position 17 for MCRD and 11 for NCRD1.

Intrinsic tyrosine fluorescence quench as a tool to study oxidative protein folding.

Intrinsic fluorescence of the aromatic amino acids in proteins is a sensitive but at the same time very limited tool to study protein folding. Fluorescence changes arise from conformational and environmental changes. Sensitivity can

easily become a disadvantage. An enormous number of factors can influence protein fluorescence therefore making it impossible to understand what factor is the major player. Fortunately there are exceptions with simplified situations. Those are proteins containing single tryptophan or tyrosine with known structures. Considering the position of fluorescent amino acid within the protein one can more easily understand the origins of the fluorescence changes. Proteins with single Trp residue often extensively studied by fluorescence due to the higher fluorescence of Trp accomplished by the wavelength shifts depending on the degree of amino acid solvent exposition. The tyrosine fluorescence exhibits no wavelength shifts and has much lower intensity. Nevertheless the structural and folding studies of proteins containing single tyrosine residues and no tryptophanes can be possible in some cases. The C-terminal minicollagen cysteine rich domain (MCRD) and the first repeat of NOWA cysteine rich domain (NCRD1) are two fascinating examples of such fluorescent sensors. These domains are composed of only 24 and 25 amino acids accordingly. Both of them contain one tyrosine residue in position 17 for MCRD and position 11 for NCRD1. Here we applied fluorescence measurements to monitor the MCRD and NCRD1 oxidative refolding. Such monitoring is possible due to the quenching of tyrosines fluorescence by nearby disulfide bonds in both peptides.

The mechanism of fluorescence quenching by S – S bonds is not yet completely understood. Nevertheless several studies regarding this phenomenon have been performed over the last 40 years. First, Cowgill reported in 1967 that intrinsic fluorescence of tyrosine residue can be quenched by disulfide bonds (2). Already at that time Cowgill ascribed the diminished fluorescence to the vibrational dissipation of energy, not collisional quenching, hydrogen bond formation or FRET. Later studies (3) demonstrated the quenching of tyrosine containing peptides by oxidized dithiothreitol (DTT). Authors excluded collisional quenching mechanism based on the Stern - Volmer analysis and suggested the formation of complex between tyrosil and cysteine residues. Nevertheless Swadesh et.al. have not considered long range energy transfer as a quenching mechanism. Quenching mechanisms of tyrosine in polypeptides and proteins have been reviewed by Ross *et al.* in 1992 (4). Considerable effort to understand a mechanism of tyrosine fluorescence quenching by disulfides has been made in this work but still there

was no conclusive picture. Later investigators assigned the quenching of tyrosine by the disulfide bonds to the frequency resonance energy transfer (FRET) where tyrosine considered as a donor and disulfide bond as a weak acceptor (5). Most of the studies devoted to the understanding of this quenching mechanism were done with model peptides. There are only few examples of the described phenomenon among the real proteins such as oxytocin and vasopressin. The conformation of these peptides has been studied by different methods including fluorescence study of intrinsic tyrosine emission (6, 7). Similar quenching effect was observed for the tryptophan containing proteins such as DsbA protein (8). Overall the number of proteins exhibiting disulfide quenching of the intrinsic fluorescence is very limited. In this regard the MCRD and NCRD1 peptides investigated in this chapter can serve as a nice model systems for protein folding studies.

Materials and Methods.

Peptides synthesis and oxidation.

The NCRD1 peptide was synthesized chemically with an ABIMED economy peptide synthesizer EPS 221 (Abimed, Germany) using standard Fmoc chemistry (described above). Pre-coupled resin was purchased from Novabiochem, Switzerland. Amino acids were from Alexis Biochemicals, USA or from Iris Biotech, Marktredwitz, Germany. Solvents and other chemicals were from Fluka (Buchs, Switzerland). The protein was purified using HPLC with a C-8 reverse-phase preparative column (Hibar, LiChrosorb®100 RP-8 from Merck, Darmstadt, Germany). Protein purity was confirmed by nanospray mass spectrometry (2534.Da mass was found compared to calculated 2535.8 Da) and analytical HPLC.

Oxidation was carried out using the identical procedures. The lyophilized purified peptide was dissolved in 25 mM Tris/HCl, pH 6.0, containing 100 mM NaCl at a concentration of 0.05 mg/ml. Folding was allowed to proceed under N₂ for 72 to 96 hours at 4 °C. Oxidation was induced by changing the pH to 8.0-8.1 with saturated Tris, and the addition of reduced and oxidized glutathione (10:1 molar ratio) to a final concentration of 1 mM. The solution was exposed to air at 4 °C for four to ten days. Oxidation was stopped by the addition of trifluoroacetic acid to give a pH of 1.3. The oxidized peptide was purified by preparative HPLC. Mass spectroscopy of the oxidized peptide showed a molecular mass of 2528 Da. Theoretically calculated mass is 2529.8 Da.

NMR Data Collection

NMR samples of chemically synthesized first repeat of NOWA cysteine rich domain (NCRD1) purified after oxidation were prepared in 95 % ¹H₂O, 5 % ²H₂O and in 100 % ²H₂O, respectively. Samples had 1.5 mM concentration in a volume of 300 µl (Shigemi NMR microtubes) in 5 mM sodium phosphate buffer, pH 6.5 without further addition of salt. A set of standard homonuclear experiments similar to those described by Wüthrich (9) were recorded at 15°C with Bruker DRX 600 spectrometer. Data were processed with NMRPipe (10) and analysed with Sparky (11) to yield a complete proton assignment. Structure calculations were performed in CNS (12) with a standard simulated annealing

protocol. The coordinates and structural restraints have been deposited in the Brookhave Protein Data Bank under accession number XXX. Structure representations were generated with MOLMOL (13).

Fluorescence Measurements

Fluorescence spectra and kinetic measurements were recorded with an Aminco Bowman 2 spectrofluorimeter. All samples were temperature equilibrated at 25 ° C before measurements. Samples were prepared in 50 µM peptide concentration. For reduction kinetic measurements Tri (2-carboxyethyl) phosphine hydrochloride (Mr 286.64) TCEP was used. The TCEP was bought from Sigma–Aldrich. In order to monitor oxidation kinetics completely reduced peptides (those monitored for reduction kinetics) were dialyzed in a 1 kDa dialysis membrane against 10 mM phosphate buffer of pH 5.5 to remove TCEP and prevent spontaneous oxidation. After dialysis samples were enriched with molecular oxygen, initial buffers of pH 5.5 were adjusted to pH 8.1 to induce oxidation, samples were sealed and measurements started immediately. Excitation wavelength was 275 nm, emission was recorded at 304nm corresponding to a maximum of single Tyrosine fluorescence. All fluorescence spectra were corrected for according buffer solutions.

Partial reduction and alkylation

Partial reduction of MCRD and NCRD1 peptides was carried out with TCEP in 5mM Citrate buffer at pH 5. After various time of incubation either at room temperature or at 37 ° C reduction was stopped by direct injection of peptide solution on the analytical HPLC C18 or C8 columns. Intermediates as well as native and completely reduced fractions were collected and analysed with mass spectrometry. Desired intermediate fractions were alkylated by NEM (Sigma) for at least 1 hour at 37 ° C. Alkylated material was analysed with mass spectrometry again.

Foerster Theory for Frequency Resonance Energy Transfer (FRET).

Latest studies regarding the mechanism of the tyrosine fluorescence quenching by disulfide bonds revealed that FRET is the main player of the game (5). A quantitative theory for singlet-singlet energy transfer has been developed by Theodor Foerster which assumes that the transfer occurs through

dipole-dipole interactions of donor and acceptor. Multipole and electron exchange interactions can also result in energy transfer. To obtain useful structure information from energy transfer, the measured efficiency must be related to the distance between the two fluorophores. FRET efficiency, E can be obtained by measuring the fluorescence intensities of the donor with acceptor, F_{da} and without acceptor, F_d :

$$E = 1 - F_{da} / F_d$$

FRET efficiency can also be measured using the lifetime of the donor in presence, T_{da} and absence of the acceptor probe, T_d : These measurements were not done in the present study. The relationship between the transfer efficiency and the distance between the donor and acceptor, R is given by the equation:

$$E = R_0^6 / (R_0^6 + R^6)$$

or

$$R = R_0^6 (1/E - 1)^{1/6}$$

where R_0 is the Foerster distance, that is, the distance at which energy transfer is 50% efficient. In other words, it is the distance where 50% of excited donors are deactivated by FRET. At R_0 , there is an equal probability for resonance energy transfer and the radiative emission of a photon. The magnitude of R_0 is dependent of the spectral properties of the donor and acceptor:

$$R_0 = [8.8 \times 10^{-23} K^2 n^{-4} Q_d J]^{1/6} \text{ (Angstrom)}$$

where

- K^2 or *kappa square* = dipole orientation factor, a function of donor emission transition moment and the acceptor absorption transition moment (range 0 to 4, generally $K^2 = 2/3$ is assumed)
- Q_d = fluorescence quantum yield of the donor in the absence of acceptor
- n = refractive index of the medium which is generally assumed to be 1.4 (range 1.33-1.6) for proteins.

- J = spectral overlap integral which represents the degree of overlap between the donor fluorescence spectrum and the acceptor absorption spectrum.

The donor and acceptor must be within $0.5xR_0$ - $1.5xR_0$ from each other. These measurements give the *average* distance between the two fluorophores. When measuring a *change* in distance, the result is a scalar and gives no indications of which fluorophore (donor and/or acceptor) moves.

Results and Discussion

NMR structure of the first repeat of NOWA cysteine rich domain NCRD1

The solution structure of the synthesized NCRD1 peptide was determined by homo- and hetero-nuclear NMR techniques. The 25 amino acid peptide sequence is shown in bold and underlined on the figure 1 in comparison with the sequence of previously elucidated MCRD. Sequence specific 1H , ^{13}C , and ^{15}N assignments were obtained from TOCSY and NOESY as well as heteronuclear HSQC and HMBC spectra acquired at natural isotope abundance. All cysteine residues appeared to be bonded in disulfide bridges as evidenced by their ^{13}C shifts of 40 to 43.5 ppm (14). The disulfide pattern of the peptide was determined as Cys2 – Cys18; Cys6 – Cys 14 and Cys 10 – Cys19. This was derived from direct NOESY cross-peaks between $H\beta$ atoms of the cysteine residues plus overall structure calculation with no disulfide restraints applied. The structural fold determined in assumption of open cysteines (Fig. 2 lower ribbon) allowed the only possibility of disulfide bonds connectivity. Left upper part of the figure 2 represents all heavy atoms overlay of 10 lowest energy structures of NCRD1. All residues are displayed in dark green, except for cysteine side chains in yellow and proline 12 in red. Right part of the figure shows ribbon presentation in the same orientation. The structure of the NOWA cysteine rich domain is exclusively built up from a number of consecutive β -turns: Ser7 – Cys10, Tyr11-Cys14 and Pro15-Cys18. The Pro12 (Fig. 1) imposes a β -turn topology on residues 11 to 14 due to its fixed phi angle of -60° and subsequently positions Cys14 and Cys6 in the close contact to form S-S bridge. Formation of this disulfide bond is a central feature of the NCRD1

PCPPV	CVAQCVPTCPQYCCPAKRK	– C-terminal MCRD
2	6 10 14 1819	
TCPSG	CSGDCYPECKPGCCGQVNLN	APVQPSGYT
ACSQYPN	CGLSCQSSCSQSCC	QQNPYQPSVMSGTIVIQPNEQS
VCPQHFG	CSQHCAPRCSPQCC	QQSMNSLYQPPQMS
ACPQFPS	CSPTCAPQCSQLCC	QQSSMPLQMPQMP
SCPQFPS	CSASCAPQCSQQCC	QQPSMSIQPLQIS
SCPQFPS	CSPSCAPQCSQQCC	QQPSMPIQLPLMG
SCSQMPG	CSASCAPLCSQQCC	QQQSMLQQSIMQQPMMMAQN
PCSLQQPG	CSSACAPACRLSCC	SLGRMNLGR

Figure 1.

Sequence alignment of the C-terminal MCRD of minicollagen-1 and 8 NCRD domains of NOWA. The sequences of the MCRD with known structure (chapter 3) and NCRD1 are shown in bold. The sequence region of 8NCRD used for structure determination is underlined. Numbers indicate cysteine residues and correspond to the counting in the structures description.

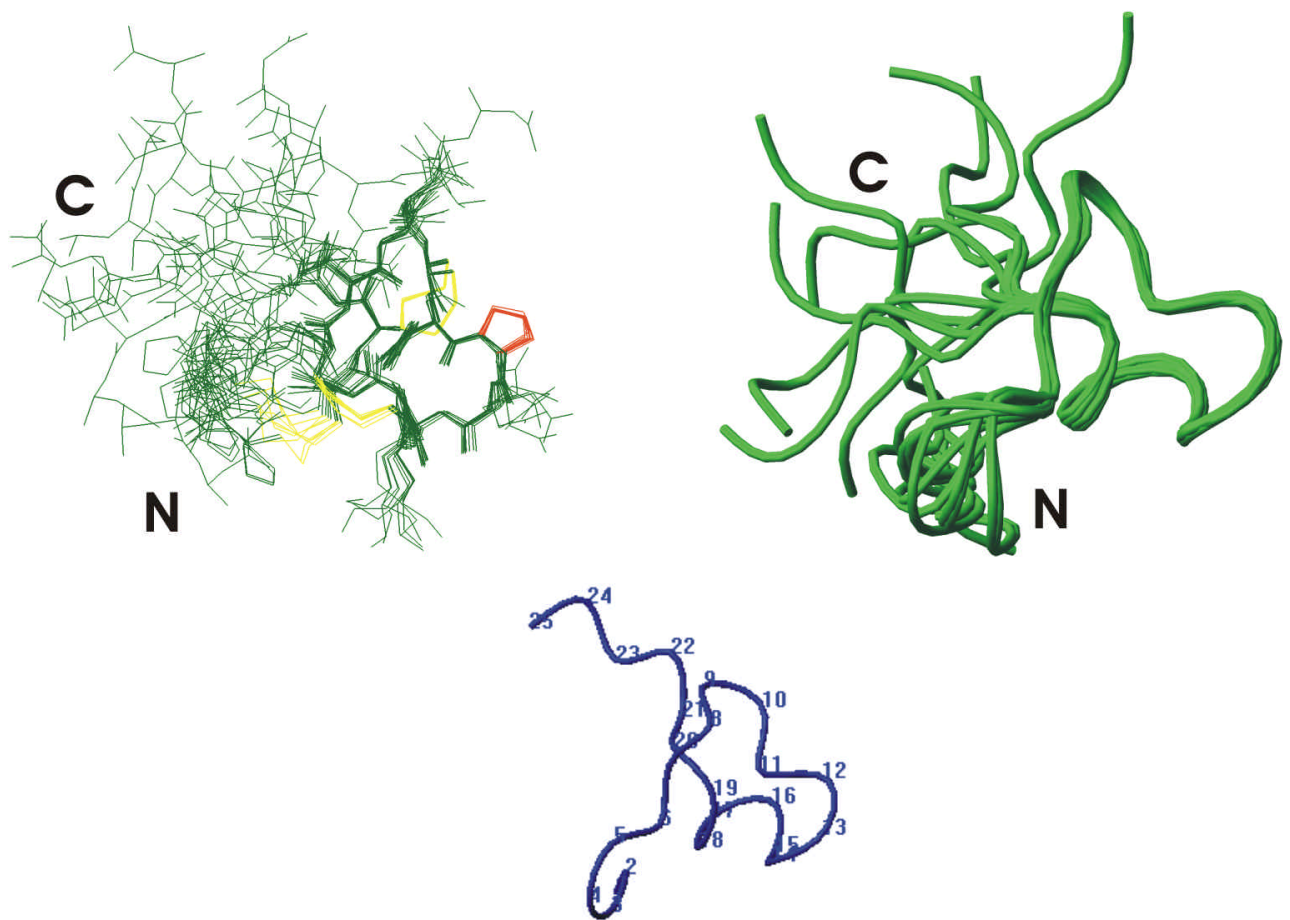


Figure 2.

NMR structures of the first cysteine rich repeat of NOWA. Left upper part of the figure represents all heavy atoms overlay of the 10 energy minimized structures. All residues are displayed in dark green, except for cysteine side chains in yellow and proline 12 in red. The ten energy lowest structures are superimposed using the backbone atoms of residues 6-20. Disordered residues are 1-5 from the N-terminus and 21-25 from C-terminus of the peptide. Most likely the N-terminus of the first cysteine rich repeat of NOWA continues the structural fold of the preceding protein domain. Right part of the figure shows the same view of the overlaid structures in ribbon representation. On the lower panel a ribbon presentation of the calculated structure without cysteine bridges is shown.

folding process. All prolines of the peptide are proved to be in trans conformation as evident from specific NOE distance information. In the full NOWA protein the NCRD1 follows the C-type lectin domain. All known CTLDs have conserved structural fold with a β -strand at the C-terminus. Proton chemical shifts of the Cys2 of NCRD1 adopt the characteristic β -strand values. Therefore N – terminus of the peptide is proposed to adopt the structure of preceding domain. In the isolated NCRD1 N-terminal structure is not stable. However the first disulfide bond Cys2-Cys18 is correctly formed. As it was discussed in the chapter 3 for the MCRD structure Cys2-Cys18 bond is formed later than Cys6-Cys14. Presumably in the NCRD1 it is the last one formed so that despite the flexibility of Cys2 the only possible partner Cys18 is found. This disulfide bond clasps the N- and C-termini of the NCRD1 structure. The third disulfide bond Cys10-Cys19 is more exposed to the C-terminal surface of the domains.

Comparison of the NCRD1 and MCRD structures.

Elucidated minicollagen and NOWA cysteine rich domains have 30 % sequence identity. The homology is restricted to the conserved cysteines and proline 12 residues. Pronounced structural similarity is observed for these peptides. In order to make common structural features of the NCRD1 and MCRD obvious the structures were superimposed on the C α atoms of the cysteines (Fig. 3B). The RMSD of such superposition was 1.5 Å. The disulfide pattern found for the NCRD1 is identical to that of the MCRD. Superimposed stereoview shows nicely colocalized disulfide bonds of two structures with the degree of solvent exposition comparable for each bond pair. Folding and disulfide pattern formation are often tightly coupled in cysteine rich peptides. The absence of significant secondary elements in the structural folds of both peptides indicates that folding and oxidation processes are almost synonymous here. The MCRD and NCRD1 structures built up from the turns with the only exception of the short α -helix in MCRD. Two turns are preserved: 11 – 14 and 15 – 18. Upon superimposition of the C α atoms of indicated residues the turns can be aligned at 0.2 Å (11-14) and 0.6 Å (15-18) RMSD accordingly. However orientation of these turns is slightly different in two structures (Fig 3B). Considering the goodness of the structural overlays 11-14 β -turn is the most

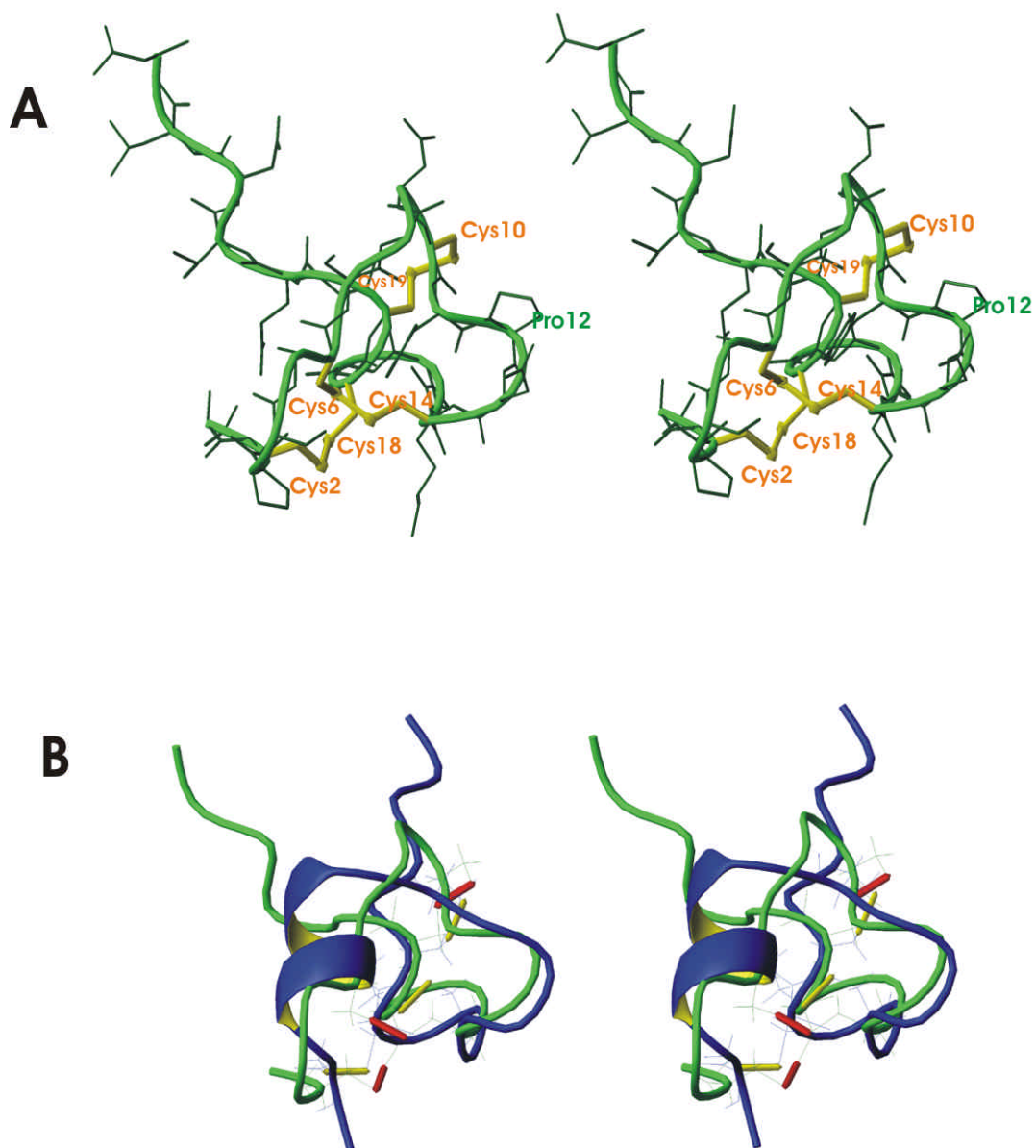


Figure 3.

A, Stereoview of the NCRD1 structure represented in the same orientation as on figure 2 in ribbon presentation. Cysteines and disulfide bonds are shown in yellow and Pro12 is indicated. Disulfide bonds are Cys2-Cys18, Cys6-Cys14 and Cys10-Cys19.

B, Stereoview of overlaid MCRD and NCRD1 structures. Blue ribbon is MCRD and green ribbon is NCRD1. Disulfide bonds indicated in yellow for MCRD and in red for NCRD1. Structures were superimposed on cysteines CA atoms. RMSD is 1.5 Å.

conserved feature of the fold. Formation of the central Cys6 – Cys14 bond is determined by this turn and induced by conserved Pro12 residue.

A major structural difference observed in the N-termini of the peptides. The N-terminal α -helix followed by inverse γ -turn of the MCRD are replaced by a flexible Thr1 - Gln5 sequence followed by a β -turn Ser7 – Cys10 of the NCRD1. This is proposed to be dependent on the preceding structural folds. In case of MCRD the preceding structure is polyhydroxyproline II helix while in case of NCRD1 it is presumably a β -strand. Remarkably in both peptide structures first residues adopt conformation of the corresponding preceding secondary structure. Therefore only conserved β -turns together with defined disulfide pattern must be considered as signatures of the new fold.

Partial reduction and alkylation of MCRD.

In order to approach the problem of minicollagen/NOWA intermolecular disulfide reshuffling we performed partial reduction experiments of the cysteine rich domains. Two equally accessible disulfide bonds Cys2 – Cys18 and Cys 10 – Cys19 can potentially undergo disulfide isomerisation. Partial reduction of MCRD peptide was performed with TCEP - a reducing agent which allows reduction to proceed at the low pH. Sample acidification prevents scrambling of disulfide bonds. MCRD peptide was incubated with different access ratios of the reducing agent for different times. Results (Fig. 4) revealed the presence of three peaks one of which was identified as native MCRD and the others represented completely reduced form and an intermediate. All fractions were collected and alkylated in order to distinguish between different intermediates. Alkylated material was characterized by mass spectroscopy and identified an intermediate peak as the one containing two intact disulfide bonds (2S-S). It has to be mentioned that reduction of MCRD peptide was rather slow process although completely reduced form appeared already at the time when 2S-S intermediate did. This fact led to the insufficient peaks separation. Native, reduced and intermediate peptide were simultaneously presented in all collected fractions. Variations of the reduction time, HPLC run parameters or columns (C8 or C18) did not yield a satisfactory result. Therefore further determination of the particular reduced disulfide bond in the 2S-S intermediate

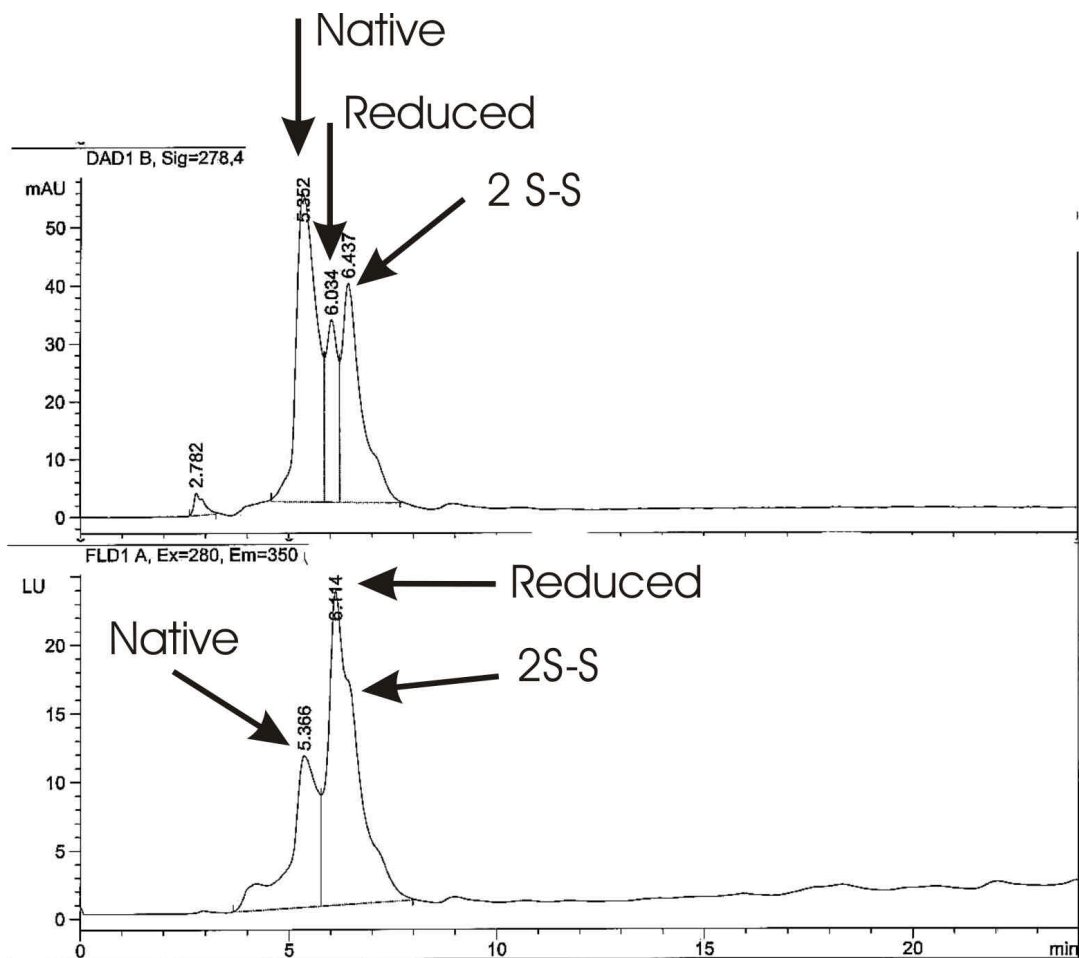


Figure 4

High pressure liquid chromatography run of the partially reduced MCRD peptide. There are native, completely reduced and 2S-S intermediate identified which indicated by arrows. Upper panel represents absorption at 280 nm, lower panel is monitoring of the fluorescence signal at 350 nm.

is possible but complicated. There are two possibilities in this direction: LC/MS/MS study and the introduction of charges via alkylation with Iodoacetamide with subsequent fraction separation on the ion exchange column. The alkylation process with Iodoacetamide requires pH 8 or higher that can lead to disulfide reshuffling and complicated picture of the intermediates as a result. However following one of these approaches should reveal the most susceptible disulfide bond *i. e.* the most prominent for intermolecular isomerization.

Interestingly comparison of the fluorescence and absorption signals from the HPLC peaks is not conclusive on the first glance. The most pronounced absorption peak at 280 nm corresponding to the native peptide is at the same time the least pronounced among the fluorescence peaks. The opposite is true for the reduced peptide peaks. The absorbance of this fraction is the least when fluorescence is the most. As concerned the 2S-S intermediate peak it is the only one exhibiting comparable absorption and fluorescence signal (Fig.4). Similar effect was observed for the partial reduction of NCRD1 peptide (data not shown). These observations were completely reproducible therefore we excluded an artefact interpretation. Further measurements clearly demonstrated that observed phenomenon is due to the quenching of the tyrosine fluorescence by the intact disulfide bond.

Quenching of tyrosine fluorescence by disulfide bond. Kinetics of reduction and oxidation

Fluorescence spectroscopy was utilized to investigate the reductive unfolding and oxidative refolding of the MCRD and NCRD1. The solvent environment of single tyrosine in these peptides was probed in the native and reduced forms. Figure 5 shows the results of the addition of 10 mM TCEP to a 50 μ M solution of MCRD and NCRD1 followed by incubation during 2 hours at 37 °C. Before measurements all samples were equilibrated in temperature to 25 °C. The fluorescence spectra of MCRD and NCRD1 alone were low in intensity and maximum were observed at 304 nm for both peptides as expected for Tyr – containing proteins. Addition of TCEP to the MCRD and NCRD1 resulted in a large and significant increase in the fluorescence intensity in both cases (~3-fold for MCRD and ~2 – fold for NCRD1). Quantum yields of the peptide fluorescence were determined by comparison with the fluorescence of

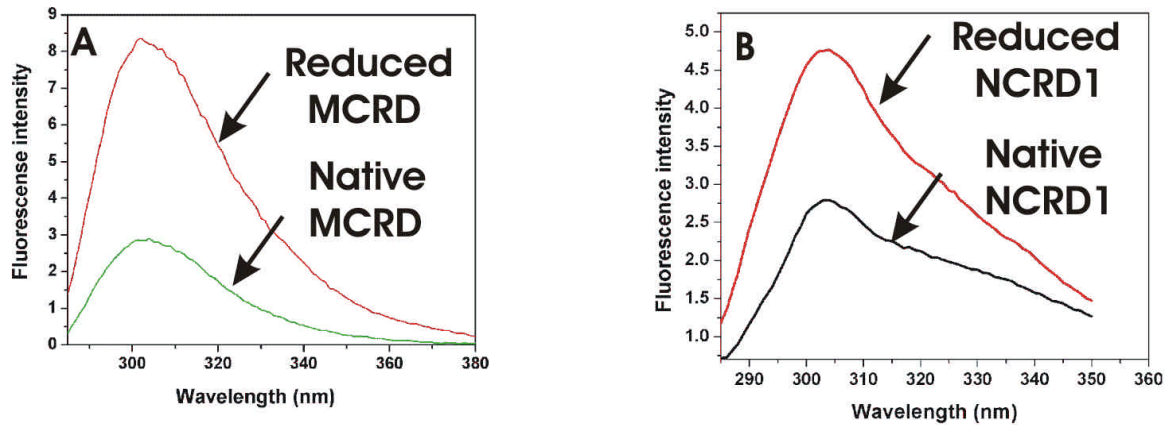


Figure 5

Effect of Tri (2-carboxyethyl) phosphine hydrochloride (TCEP) on the fluorescence of single tyrosine in MCRD (A) and NCRD1 (B) peptides. Fluorescence spectra of minicollagen cysteine rich domain (MCRD) in 50 μ M in the presence and absence of 10 mM TCEP shown on figure A. The same for the first repeat of NOWA cysteine rich domain (NCRD1) represented on figure B. The native peptides have very low fluorescence intensity (0.05 and 0.04 quantum yield for MCRD and NCRD1 accordingly) due to quenching of the Tyr residue by the neighboring disulfide, an effect removed upon reduction by TCEP.

tyrosine solution in the same molar concentration. Quantum yield of the MCRD revealed 0.052 and 0.13 in native and reducing conditions accordingly. The tyrosine fluorescence of NCRD1 exhibited even lower quantum yields of 0.042 in the native form and 0.087 in the reduced form. Reduced fluorescence of NCRD1 compare to MCRD indicates the presence of additional quenching mechanism unrelated to the reduction process. However quenching of Tyr 17 in the MCRD peptide is more effective ($E_{\text{MCRD}} = 0.67$) than quenching of Tyr 11 in the NCRD1 ($E_{\text{NCRD1}} = 0.44$). Indicated efficiencies of the fluorescence quenching were determined in terms of frequency resonance energy transfer using Foerster theory described in materials and methods section of this chapter. Implying that quenching of tyrosine fluorescence by disulfides governed by frequency resonance energy transfer (FRET) one can speculate that quenching effect is dependent on the distances separating according tyrosines and disulfides and on the mutual dipole orientation of donors (tyrosines) and acceptors (disulfide). The shortest distances from the tyrosine residues to the disulfide bonds are indicated in the stereo view for MCRD and NCRD1 structures on the figure 6 and figure 7 accordingly. Potential donor/acceptor pairs are Tyr17/Cys2 – Cys18 in MCRD and Tyr11/Cys6-Cys14 in NCRD1 although other disulfides may also participate.

Kinetics of reductive unfolding and oxidative refolding of both peptides were studied by tyrosine fluorescence quenching. Figure 8 summarized the results of these experiments. Reduction and oxidation kinetics of MCRD and NCRD1 were fitted with mono-exponentials. This fact suggests a simple quenching mechanism most probably controlled by a single disulfide bond in both cases. The NCRD1 revealed slower reduction rate constant $3.4 * 10^{-4} \text{ s}^{-1}$ compare to $4.3 * 10^{-4} \text{ s}^{-1}$ for the MCRD. On the other hand oxidation had happened faster in the NOWA domain ($3.9 * 10^{-4} \text{ s}^{-1}$) compare to the minicollagen peptide ($1.7 * 10^{-4} \text{ s}^{-1}$). In the other words half oxidation time of the MCRD was 90 minutes when that of the NCRD1 was only 40 minutes. The values calculated for the MCRD peptide are in good agreement with 80 minutes of half oxidation time measured by monitoring of NMR signal of Tyr17 and Val5 amide protons (chapter 3) (15). Oxidative folding of the NCRD1 was not studied with NMR. However the following question has to be answered: “Where the two times difference in the oxidation rates of the peptides with similar structures arises from?” A simple answer is proposed. Assuming that tyrosine quenching

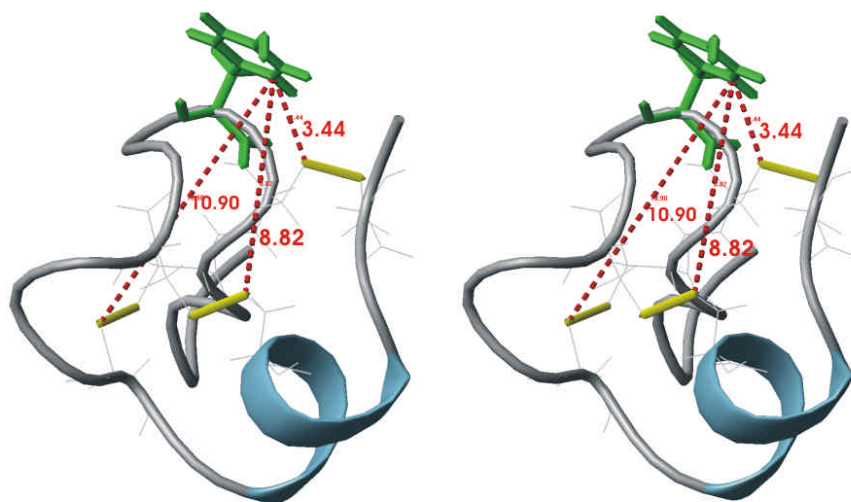


Figure 6

Stereo view of the MCRD structure in ribbon presentation with the indicated shortest distances between tyrosine 17 shown in green and disulfide bonds shown in yellow. Distances are shown in red by dashed lines. Following distances correspond to: 3.44 Å – Tyr17/Cys2-Cys18; 8.82 Å - Tyr17/Cys6-Cys14; 10.90 Å - Tyr17/Cys10-Cys19.

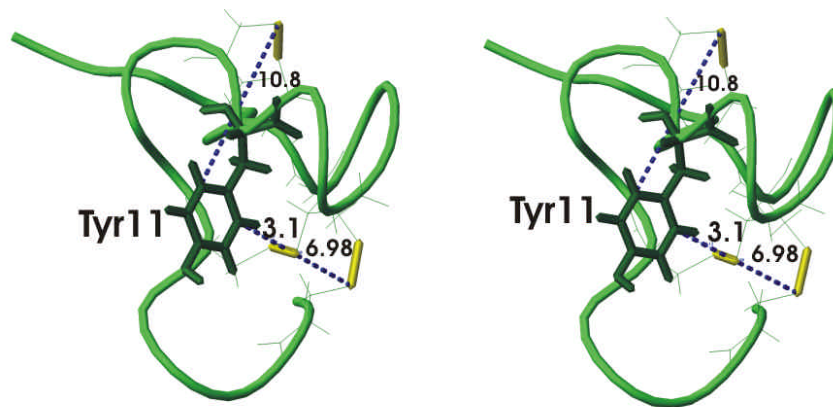


Figure 7

Stereo view of the NCRD1 structure in ribbon presentation with the indicated shortest distances between tyrosine 11 shown by dashed lines and disulfide bonds shown in yellow. Following distances correspond to:

- 3.13 Å – Tyr11/ Cys6-Cys14;
- 6.98 Å - Tyr11/ Cys2-Cys18;
- 10.8 Å - Tyr17/Cys10-Cys19.

is controlled by single disulfide bond we consider pairs of Tyr17/Cys2 – Cys18 in MCRD and Tyr11/Cys6-Cys14 in NCRD1. It was discussed several times that Cys2 – Cys18 bond is more susceptible for reduction than Cys6 – Cys14. Subsequently this bond opens first during unfolding and closes last during folding of the peptides. This assumption immediately explains the observed rate constants of quenching kinetics. Represented reduction and oxidation kinetics reflect the rates of reduction and oxidation of the Cys2-Cys18 bond in MCRD and the Cys6–Cys14 bond in the NCRD1. The difference in the kinetic rates is therefore due to the fact that central disulfide bridge opens later and forms earlier than two others. Two other potential donor/acceptor pairs Tyr17/Cys6-Cys14 in MCRD and Tyr11/ Cys2-Cys18 in NCRD1 would exhibit exactly the opposite behaviour.

To study the peptides oxidative folding in details one should analyse the intermediates isolated at the certain times of the oxidation and (or) reduction kinetics. However oxidative refolding of both peptides is fast process leading to the formation of the correct structure at the high yield as evident from the NMR data (15). Moreover the MCRD peptide showed no unfolding transition neither for temperature heating up to 120 °C nor for the titration with chemical chaotropes up to 8M of urea or 6M of guanidine chloride. The MCRD unfolding has been monitored using CD and Calorimetry measurements (data not shown). In the 8M urea the peptide exhibited native 1D NMR spectrum (15).

In summary, folding of the investigated peptides is completely determined by disulfides formation and follows a certain direction without populating the wrong intermediates. The MCRD and NCRD1 are interesting models for general protein folding studies due to the disulfide quenching of tyrosine fluorescence controlled by two different S-S bridges.

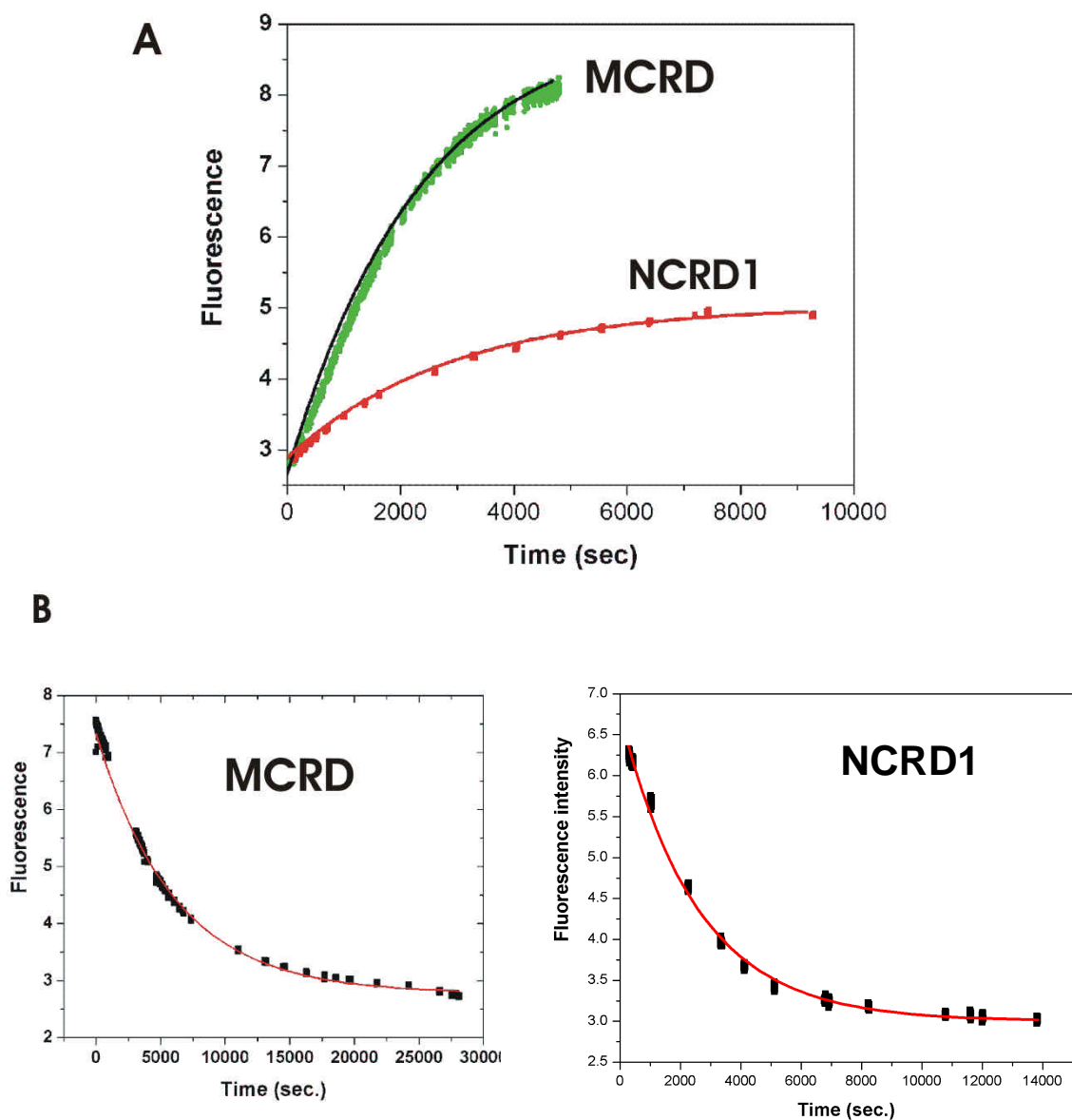


Figure 8.

Fluorescence quenching effect applied for reduction (A) and reoxidation (B,C) kinetics measurements of the MCRD and NCRD1. Measured fluorescence data shown by symbols. Lines correspond to the kinetics fit with single exponentials.

Reduction rate constants from the according fitting curves are:

$3.4 \cdot 10^{-4} \text{ s}^{-1}$ for the NCRD1 (red)

$4.3 \cdot 10^{-4} \text{ s}^{-1}$ for the MCRD (green).

Oxidation rate constants are:

$1.7 \cdot 10^{-4} \text{ s}^{-1}$ for the MCRD

$3.8 \cdot 10^{-4} \text{ s}^{-1}$ for the NCRD1

References.

1. U. Engel *et al.*, *J Cell Sci* **115**, 3923-34 (Oct 15, 2002).
2. R. W. Cowgill, *Biochim Biophys Acta* **140**, 37-44 (1967).
3. J. K. Swadesh, P. W. Mui, H. A. Scheraga, *Biochemistry* **26**, 5761-9 (Sep 8, 1987).
4. J. Ross, W. Laws, K. Rousslang, H. Wyssbrod, in *Topics in Fluorescence Spectroscopy; Biochemical Applications*. L. JR, Ed. (Plenum Press, New York, 1992), vol. Vol. 3, pp. 1-63.
5. H. Szmecinski *et al.*, *Eur Biophys J* **24**, 185-93 (1996).
6. W. Laws *et al.*, *Biochemistry* **25**, 599-607 (1986).
7. J. Ross, W. Laws, A. Buku, J. Sutherland, H. Wyssbrod, *Biochemistry* **25**, 607-612 (1986).
8. J. Hennecke, A. Sillen, M. Huber-Wunderlich, Y. Engelborghs, R. Glockshuber, *Biochemistry* **36**, 6391-400 (May 27, 1997).
9. K. Wüthrich, *NMR of proteins and nucleic acids* (Wiley, New York, 1986).
10. F. Delaglio *et al.*, *Journal of Biomolecular NMR* **6**, 277-293 (1995).
11. T. Goddard, D. Kneller.
12. A. Brunger *et al.*, *Acta Crystallographica Section D-Biological Crystallography* **54**, 905-921 (1998).
13. R. Koradi, M. Billeter, K. Wuthrich, *J Mol Graph* **14**, 51-55, 29-32 (1996).
14. D. S. Wishart *et al.*, *J Biomol NMR* **6**, 135-40 (Sep, 1995).
15. S. Meier, D. Haussinger, E. Pokidysheva, H. Bachinger, S. Grzesiek, *FEBS Letters* **accepted** (2004).

Acknowledgements:

I am very grateful to Jürgen Engel for giving me the opportunity to work in his group, useful advices and helpful discussions.

I thank Suat Özbek for his help and bright ideas.

I thank Sebastian Meier and Daniel Haussinger for introducing me in the NMR field.

I am grateful to Florian Krieger for his help in peptide synthesis.

I thank Thomas Holstein for interesting discussions and his interest in the project.

I thank all the group: Thomas Ahrens, Sergei Boudko, Sabine Frank, Simon Hellstern, Ruth Landwehr, Joseph B. D. Mascarenhas, Suat Özbek, Therese Schulthess, Martine Schwager, Joerg Stetefeld for their help and nice atmosphere.

I am very grateful to my family and all my friends for general support.

CURRICULUM VITAE

Name: Elena N. Pokidysheva.

Address: Department of Biophysical Chemistry, Biozentrum,
University of Basel, CH 4056 Basel, Switzerland

e-mail: elena.pokidysheva@unibas.ch

Date of Birth: March 25, 1976

Place of Birth: Nalchik, Russia

Citizenship: Russian

EDUCATION

July 1993 - June 1999 - Moscow Institute of Physics and Technology (MIPT),
Department of Molecular and Biological Physics.
Cathedra of Living Systems Physics
(Chairman-Academician V. I. Shumakov)

B.S. June 1997, MIPT

M.S. in Applied Mathematics and Physics June 1999, MIPT

July 2000 – November 2001 - Graduate student at the Materials Department of
University of California Santa Barbara (UCSB)

January 2002 – present time - PhD student at the Department of Biophysical
Chemistry, Biozentrum, University of Basel

SCIENTIFIC EXPERIENCE

February 1995 – June 2000

Diploma work: “Biocompatibility of Intraocular lenses (IOL)”

Research advisor: Prof. Sevastianov V.I.

Center for Blood Compatible Biomaterials

Research Institute of Transplantology and Artificial Organs.

July 2000 – November 2001

Project: “Actin structures induced by different cross-linkers: from simple peptides (OligoLysine) to cross-linker proteins (Alfa-actinin). ”

Research advisor: Prof. Cyrus Safinya

Materials Department,

University of California Santa Barbara (UCSB).

January 2002 – Present time

Project: “Assembly of Hydra nematocyst capsule wall.”

Research advisor: Prof. Jurgen Engel

Biozentrum, University of Basel

Skills:

Molecular biology techniques: cloning, expression in E.coli and eukaryotic cell lines and purification of proteins, preparation of lipid mono/bilayers, interaction of proteins with lipid membranes. Solution NMR for protein structure calculation.

Methods:

Total Internal Reflection Fluorescence (TIRF), Small angle X-ray scattering (SAXS), Confocal Microscopy, Transmission Electron Microscopy (TEM), Surface Plasmon Resonance (Biacore), UV, CD and Fluorescence spectroscopies.

PUBLICATIONS:

1. **E. Pokidysheva**; S. Meier; S. Grzesiek; J. Engel.

„The solution structure of NOWA cysteine-rich domain. Fluorescence study of oxidative folding.“

In preparation

2. **E. Pokidysheva**; S. Ozbek; J. Engel.

„NOWA (Nematocyst outer wall protein) self-assembles into pseudo capsulomers and binds to the model charged lipid membrane.“

In preparation

3. S. Ozbek; **E. Pokidysheva**; M. Schwager; T. Schulthess; N. Tariq; D. Barth; A. Milbradt; L. Moroder; J. Engel and T. Holstein

“The formation of the *cnidarian* nematocyst reflects a viral assembly process”

Submitted

4. **Elena Pokidysheva**^{3*}, Alexander Milbradt^{1*}, Sebastian Meier^{2*}, Christian Renner¹, Daniel Häussinger², Hans Peter Bächinger⁴, Luis Moroder¹, Stefan Grzesiek², Thomas W. Holstein⁵, Suat Özbek³, Jürgen Engel³

“The structure of the Cys-rich terminal domains of *Hydra* minicollagen, which are involved in disulfide networks of the nematocyst wall.”

Accepted in JBC.

5. Sebastian Meier ^a, Daniel Häussinger ^a, **Elena Pokidysheva** ^b, Hans Peter Bächinger ^c and Stephan Grzesiek

“Determination of a high-precision NMR structure of the minicollagen cysteine rich domain from *Hydra* and characterization of its disulfide bond formation”

Accepted in FEBS Letters.

6. O. Pelltier, **E. Pokidysheva**, L.S. Hirst, N. Bouxsein, Y. Li, and C. R. Safinya

"Structure of actin cross-linked with alpha-actinin: a network of bundles"

Phys. Rev. Letters 91, 148102 Sept 2003

7. **E.N. Pokidysheva**; I.A. Maklakova; Z.M. Belomestnaya; N.V. Perova; S.N. Bagrov; V.I. Sevastianov.

“Comparative analysis of human serum albumin adsorption and complement activation for hydrophobic and hydrophilic intraocular lenses.”

Artif Organs. 2001 Jun;25(6):453-8.

8. S. Petrash, T. Cregger, B. Zhao, **E. Pokidysheva**, M. D. Foster, W. J. Brittain, V. Sevastianov and C. F. Majkrzak

“Changes in Protein Adsorption on Self-Assembled Monolayers with Monolayer Order: Comparison of Human Serum Albumin and Human Gamma Globulin, “

Langmuir 2001, 17, 7645-7651.

9. Titushkin, IA; Vasin, SL; Rozanova, IB; **Pokidysheva, EN**; Alekhin, AP; Sevastianov, VI.

“Carbon coated polyethylene: Effect of surface energetics and topography on human platelet adhesion.”

ASAIO Journal, Jan-Feb, 2001, V47(N1):11-17.

10. **Pokidysheva, EN**; Nemets, EA; Tremsina, YS; Sevast'yanov, VI.

“Competitive adsorption of human fibrinogen on the surface of amorphous quartz.”

Biofizika, Sep-Oct, 2000, V45(N5):809-815. Russian

11. V.I. Sevastianov; **E.N. Pokidysheva**; I.A. Maklakova; S.N. Bagrov.

“Use of the fluorescence method in the study of protein adsorption onto the surface of intraocular lenses.”

Medical Engineering, 1998 Sep-Oct,(5):3-6.

Conferences

Posters:

1. *Biozentrum Symposium 17 of October 2003*

“Binding of NOWA to the model lipid membrane.”

E. Pokidysheva; S. Ozbek; J. Engel.

“Capsulomers are the structural building blocks of the Hydra nematocyst wall ”

S. Ozbek; **E. Pokidysheva**; M. Schwager; T. Schulthess; N. Tariq; D. Barth; A. Milbradt; L. Moroder; J. Engel and T. Holstein.

2. *Materials Research Outreach Symposium. January 31-February 2 2001.*

“Self-assembled structures of cell cytoskeletal actin filaments by actin-crosslinking proteins.”

Olivier Pelletier, **Elena Pokidysheva**, Allison Lin, Youli Li, Cyrus Safinya

3. *American Physical Society annual meeting, 2001. Session A18-Biopolymers.*

“Self-assembled structures of cell cytoskeletal actin filaments by actin-crosslinking proteins.”

Olivier Pelletier, **Elena Pokidysheva**, Allison Lin, Youli Li, Cyrus Safinya